NUREG/CR-1652
LA-8477-MS

TRAC-P1A Independent Assessment—1979

University of California

LOS ALAMOS SCIENTIFIC LABORATORY
Post Office Box 1663 Los Alamos, New Mexico 87545

Edited by

Nancy Sheheen
Group Q-DO/RS

NUREG/CR-1652
LA-8477-MS

R4

TRAC-P1A Independent Assessment—1979

Compiled and Edited by

T. D. Knight

Contributors

T. D. Knight
A. C. Peterson*
J. J. Pyun
S. T. Smith
J. C. Vigil
G. J. E. Willcutt, Jr.
K. A. Williams

Manuscript submitted: January 1981
Date published: January 1981

Prepared for
Division of Reactor Safety Research
Office of Nuclear Regulatory Research
US Nuclear Regulatory Commission
Washington, DC 20555

NRC FIN No. A7053

*EG&G Idaho, Inc., P.O. Box 1625, Idaho Falls, ID 83401.

UNITED STATES
DEPARTMENT OF ENERGY
CONTRACT W-7405-ENG. 36

CONTENTS

TABLES

TRAC-P1A INDEPENDENT ASSESSMENT--1979

Compiled and Edited by

T. D. Knight

Contributors: T. D. Knight, A. C. Peterson, J. J. Pyun,

S. T. Smith, J. C. Vigil, G. J. E. Willcutt, Jr., and K. A. Williams

ABSTRACT

The Transient Reactor Analysis Code (TRAC) is being developed at the Los Alamos Scientific Laboratory (LASL) to provide an advanced best-estimate predictive capability for the analysis of postulated accidents in light-water reactors. TRAC-P1A provides this analysis capability for pressurized water reactors and for a wide variety of thermal-hydraulic experimental facilities. The code is intended primarily for large-break loss-of-coolant accident (LOCA) analysis. TRAC-P1A features a three-dimensional treatment of the pressure vessel and associated internals, two-phase nonequilibrium hydrodynamics models, flow-regime-dependent constitutive relations, reflood tracking capability for both bottom reflood and falling-film quench fronts, and a consistent treatment of the entire accident sequence from the steady-state conditions through reflood. Detailed descriptions of the thermal-hydraulic models, numerical solution methods, user information, and programming features are given in a separate LASL report, "TRAC-P1A: An Advanced Best-Estimate Computer Program for PWR LOCA Analysis," LA-7777-MS (NUREG/CR-0665).

This report presents the results of the TRAC-P1A independent assessment analyses performed during calendar year 1979. These calculations were performed with the publicly released version of the code and include separate-effects tests for vessel level swell and large-scale critical flow, integral-effects tests for the blowdown/refill/reflood phases of the large-break LOCAs, and integral-effects tests for small-break LOCAs. Although the independent assessment analyses do not represent an exhaustive study of the full range of available facilities and tests, they do represent a rigorous test of the capabilities of the code. The results indicate that the code is directly applicable to LOCA analyses; several areas have been identified for improvement in future code development.

I. INTRODUCTION

The Transient Reactor Analysis Code (TRAC) is an advanced best-estimate systems code for analyzing light-water reactor (LWR) accidents. It is being developed at the Los Alamos Scientific Laboratory (LASL) under the sponsorship of the Reactor Safety Research Division of the U.S. Nuclear Regulatory Commission. TRAC-P1A (Ref. 1) was completed in March, 1979, and is the second in a series of publicly released codes intended primarily for the analysis of large-break loss-of-coolant accidents (LOCAs) in pressurized water reactors (PWRs). However, because of the generality incorporated into the thermal-hydraulic modeling, TRAC-P1A can be applied directly to a large variety of analyses ranging from blowdowns in simple pipes to integral LOCA tests in multiloop test facilities to separate-effects tests. Models specifically required to treat boiling water reactors (BWRs) and other accident types (such as anticipated transients without scram (ATWS), reactivity insertion accidents (RIAs), and small-break LOCAs) will be incorporated into future versions of the code. TRAC-P1A has improved hydrodynamic and heat-transfer models, is more efficient, and should be more easily implemented on various computers than the previous versions of TRAC.

TRAC assessment is a two-stage process. The first stage is the developmental assessment and is closely coupled to the code development process. Developmental assessment principally involves posttest analyses of a variety of thermal-hydraulic experiments. The primary objectives of developmental assessment are to define the limits of validity of the methods, models, and correlations in the developmental version of the code and to establish values for various empirical parameters; these objectives are achieved by comparing the calculated results with the experimental measurements. Other objectives include the determination of code sensitivity to input data, model assumptions, and solution techniques; recommendation of standard calculational procedures for various classes of problems; and identification of code and model improvements or additional experiments needed to assess the advanced TRAC models.

Independent assessment is the second stage of the assessment process. This second stage begins following the release of the code for external use. Independent assessment uses publicly available and documented versions of TRAC. The process relies heavily on pretest and posttest predictions of tests in

designated facilities, although posttest analyses also are utilized. The primary objective is to determine the predictive capability of the code when applied to new tests involving different scales and experimental configurations. All of the developmental assessment objectives also apply to independent assessment; however, in independent assessment, the results are factored into the future code development without updating the current, released code. Discrepancies between the calculations and data are resolved by performing additional posttest analyses as required. Guidance for future code development and recommendations for future experiments also are provided.

The developmental assessment results are reported in Ref. 2. These TRAC-P1A analyses represent the initial set of independent assessment analyses. Table I summarizes the experiments analyzed and the areas of the code that were tested. The first five analyses involved only the one-dimensional capability of TRAC-P1A, and the remaining four analyses invoked the three-dimensional vessel module in addition to the one-dimensional components. The developmental assessment analyses included separate-effects tests that involved generally one type of component, systems-effects tests that coupled several components in a single LOCA transient phase (either blowdown or reflood), and an integral test that involved several components through the blowdown and refill phases. The developmental assessment results are not discussed in this report; however, the conclusions reached in Ref. 2 still apply and have been factored into the independent assessment results.

The independent assessment calculations for calendar year 1979 are summarized in Table II. These calculations were made with TRAC-P1A. The table reflects the order in which the results are discussed in this report. The first two sets of calculations are for separate-effects tests. The Battelle-Frankfurt level-swell experiment was analyzed to investigate the phase separation and mixture level swell resulting from the depressurization of a liquid pool, phenomena not investigated directly in the developmental assessment process. The analyses of the Marviken critical flow tests continued the separate-effects investigation of the TRAC-P1A critical flow calculation. The third set of calculations was for Semiscale Mod-3 test S-07-6. This test represented basically a new (reconfigured) facility and provided synergistic effects throughout the entire LOCA transient.

TABLE I

TRAC-P1A DEVELOPMENTAL ASSESSMENT ANALYSES

No.	Experiment	Thermal-Hydraulic Effects
1	Edwards Horizontal Pipe Blowdown (Standard Problem 1)	Separate effects, one-dimensional critical flow, phase change, slip, and wall friction
2	CISE Unheated Pipe Blowdown (Test 4)	Same as (1) plus pipe wall heat transfer, flow area changes, and gravitational effects
3	CISE Heated Pipe Blowdown (Test R)	Same as (2) plus critical heat flux (CHF)
4	Marviken Full-Scale Vessel Blowdown (Test 4)	Same as (1) plus full-scale effects
5	Semiscale 1-1/2 Loop Isothermal Blowdown (Test 1011, Standard Problem 2)	Synergistic and systems effects, one-dimensional flow, phase change, slip, wall friction, and critical nozzle flow
6	Semiscale Mod-1 Heated Loop Blowdown (Test S-02-8, Standard Problem 5)	Same as (5) plus three-dimensional vessel model with rod heat transfer including nucleate boiling, departure from nucleate boiling (DNB), and post-DNB
7	Creare Countercurrent Flow Experiments	Separate effects, countercurrent flow, interfacial drag and heat transfer, and condensation
8	FLECHT Forced Flooding Tests	Separate effects, reflood heat transfer, quench front propagation, and liquid entrainment and carryover
9	Nonnuclear LOFT Blowdown with Cold-Leg Injection (Test L1-4, Standard Problem 7)	Integral effects during blowdown and refill, scale midway between Semiscale and full-scale PWR

TABLE II

TRAC-P1A INDEPENDENT ASSESSMENT ANALYSES

No.	Experiment	Thermal-Hydraulic Effects
1	Battelle-Frankfurt Level-Swell Experiment (Test SWR-2R, OECD Standard Problem No. 6)	Vessel level swell, phase separation, and two-phase flow
2	Marviken Critical Flow Tests (several)	Large-scale critical flow; phase change; slip; wall friction, diameter, and length/diameter (L/D) effects; and subcooling effect
3	Semiscale Mod-3 Large-Break LOCA Test (Test S-07-6)	A new facility; integral systems effects, including one-dimensional pipe flow, three-dimensional vessel with rod heat transfer, emergency core cooling (ECC), critical flow, and downcomer wall heat transfer
4	Dartmouth Countercurrent Flow Flooding Tests	Air/water countercurrent flow flooding tests in a vertical tube
5	LOFT Large-Break LOCA Tests (Tests L1-5, L2-2, L2-3)	Same as (3) with larger scale and nuclear core, power level effects
6	LOFT Small-Break LOCA Tests (Tests L3-0, L3-1)	Same as (5) except small-break simulation

The analysis of the Dartmouth countercurrent flow flooding tests was prompted by the difficulties experienced in calculating the downcomer behavior exhibited in the Semiscale test. The Loss-of-Fluid Test (LOFT) Facility large-break tests represented a new series conducted in a reconfigured facility (with the nuclear core installed), and the calculations were blind pretest predictions, conducted before the test using anticipated initial and boundary conditions. The blind pretest prediction is a stringent test of the predictive capability of the code because the opportunity to adjust the code and the input

model to the test data does not exist. The LOFT reactor provides data on synergistic effects through the entire LOCA transient. The three large-break LOFT tests also provide a check on the sensitivity of the code to core power. The analyses for LOFT small-break LOCA tests also were conducted in the blind pretest prediction mode and represent the application of the code to a type of accident simulation for which the code was not originally intended. In particular, the small-break LOCA emphasizes mixture level tracking and/or critical flow with subcooled stagnation conditions.

Two additional calculations were completed during calendar year 1979 as a part of the TRAC-P1A independent assessment and were submitted to the U.S. Nuclear Regulatory Commission as part of the standard problem analyses. The first calculation was for Semiscale Mod-3 test S-07-10B, a communicative small-break test. The second calculation was for Influence of PWR Primary Loops on Blowdown (LOBI) test A1-04, a large-break blowdown simulation. The Semiscale test represents a new type of test in a relatively new facility; the LOBI test is a new facility for code assessment. The Semiscale calculation was made after the test with measured initial and boundary conditions but without knowledge of the transient data (a blind posttest prediction). The LOBI calculation was made before the test using anticipated initial and boundary conditions (a blind pretest prediction). The data for these two tests were not released during 1979, and the results of the data comparisons will be reported at a future date.

Each of the six analyses listed in Table II is discussed separately. Brief descriptions of the facility, the test, and the TRAC-P1A input model are given. Then, the calculation is compared to pertinent data, and the results and conclusions are discussed. The final section summarizes all conclusions.

II. INDEPENDENT ASSESSMENT CALCULATIONS

A. Battelle-Frankfurt Level-Swell Experiment

The Battelle-Frankfurt level-swell experiment was a series of vessel blowdown tests performed at the Battelle Institute, Frankfurt, Federal Republic of Germany. The test analyzed was SWR-2R, the Organization for Economic Cooperation and Development -- Committee on the Safety of Nuclear Installations (OECD-CSNI) Standard Problem No. 6 (Ref. 3). This test was a separate-effects simulation of a steam-line rupture in a BWR (without loops and without most vessel internals). The objective was to calculate the mass flow at the break, the vessel pressure, and the fluid temperature for the initial 3 s of the blowdown. The data for this test were available before the analysis.

1. Facility and Test Descriptions

The physical system consisted of a vertically oriented pressure vessel, 11.9 m high, 0.77 m inside diameter, and 5.2-m^3 volume. The only vessel internal structures were resistance heaters located between 2.69 and 5.19 m above the vessel bottom. The vessel material was ferritic steel, plated with Futaloy. A horizontal pipe with a 1.43-mm inside diameter was attached to the vessel at the 10.05-m elevation. The effective length of the pipe from the vessel to the outlet orifice was 0.472 m. The outlet orifice was square edged with a 64-mm diameter and a 15-mm thickness. Downstream of the orifice was a rupture disk assembly.

The test was conducted by filling the vessel to the 7.07-m elevation and using the electric heaters to obtain the desired fluid-temperature distribution (see Table III). The vessel pressure was adjusted to the initial value of 71.1 MPa. The initial flows were zero. Before the test, the heaters were turned off. The test was initiated by triggering the rupture disk assembly and allowing the system to blow down to atmospheric pressure.

2. TRAC-P1A Input Model Description

The facility initially was modeled with the three-dimensional vessel component, a pipe component, and a break component as shown in Fig. 1. The vessel component consisted of 10 axial levels, 2 radial rings, and 4 azimuthal segments. The axial level heights varied from 0.49-1.88 m; the radial and azimuthal nodings were uniform. The pipe component was attached to the vessel at level 10 and consisted of 20 cells. The orifice was modeled with two cells

TABLE III

INITIAL TEMPERATURE DISTRIBUTION FOR
OECD STANDARD PROBLEM NO. 6

Height (m)	Temperature (K)
0.6	548.65
1.7	562.55
3.8	562.65
6.4	561.15
7.07	558.15

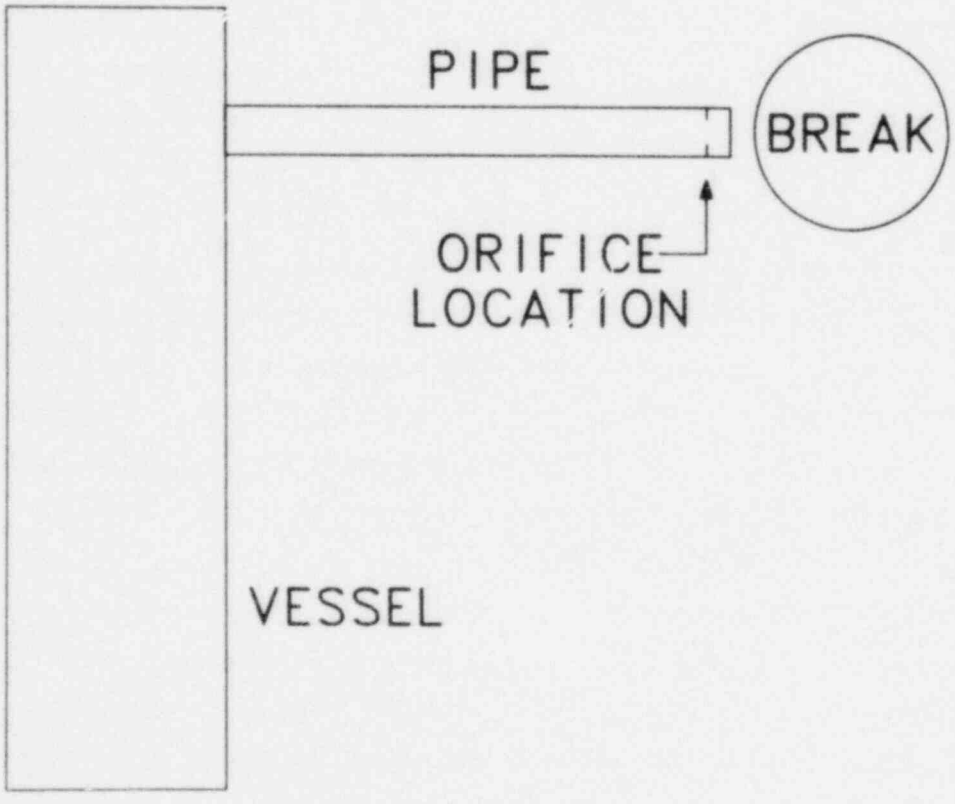

Fig. 1. TRAC-P1A component schematic for OECD Standard Problem No. 6.

and included the flow area restriction. Additive friction (the FRIC array) was used to obtain the proper hydraulic loss at the entrance to the orifice. The fully implicit hydrodynamics were used in the pipe, and the vessel numerics were semi-implicit. The back pressure boundary condition was represented by the break component.

A second input model also was developed. This second model used a tee component to represent the vessel and pipe components in the original model. The primary leg of the tee component replaced the vessel component, and the axial noding was maintained. The ends of the primary leg of the tee were terminated with zero-velocity fill components. The pipe component in the original model became the side leg of the tee.

3. Comparisons Between the Calculations and the Data

Several cases were run with both models in which the additive friction loss coefficient at the junction of the pipe and the main vessel was varied to account both for the sudden flow contraction and the 90° change in flow direction. The results from both models agreed reasonably well with the experimental data for temperatures and pressures; the temperature and pressure comparisons indicated very little sensitivity to the variation of the additive friction at the vessel/pipe junction. Figures 2 and 3 show the pressure and temperature comparisons at the junction level (10.05-m elevation) of the vessel. However, for the mass-flow comparisons at the break (Fig. 4), the tee model yielded better results when the additive friction at the pipe connection was set to a value of 8.0. The sharp rise in the experimental mass flow between 2.2-2.4 s resulted from the arrival of the two-phase mixture at the break.

4. Conclusions and Observations

The TRAC-P1A code has the capability to calculate pool level swell caused by depressurization. The calculation was sensitive to the frictional losses that control the flow from the system. Figure 4 indicates that the code permitted the swelling to occur more rapidly than the test; the interface between the vapor space and the two-phase mixture was not as sharp as in the test. The sharpness of the interface during the experiment was demonstrated by the approximate step change in the mass flow of the break at 2.4 s, whereas the calculation showed a gradual rise to the final flow at 3.0 s. The step change in the mass-flow data was caused by pure vapor entering the pipe during the initial 2.2 s, and then by relatively low-void-fraction fluid entering later.

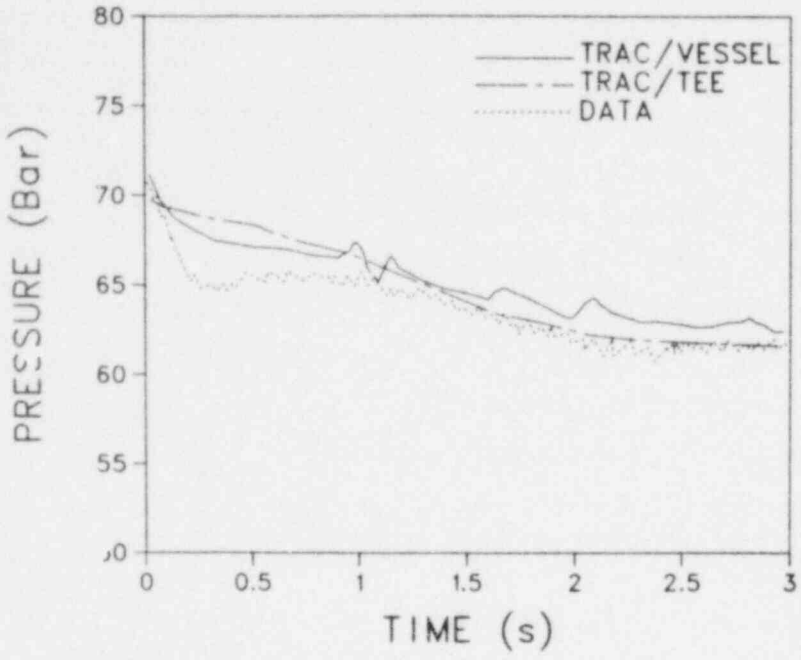

Fig. 2. OECD Standard Problem 6 pressure comparisons at the 10.05-m elevation in the vessel. The data uncertainty is ~1%.

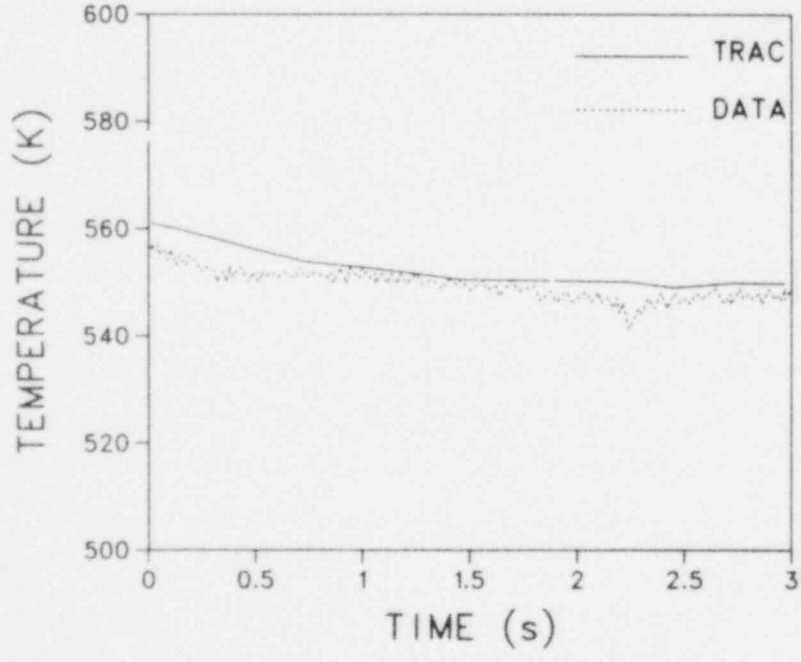

Fig. 3. OECD Standard Problem 6 fluid-temperature comparisons at the 10.05-m elevation in the vessel. The data uncertainty is ~2 K.

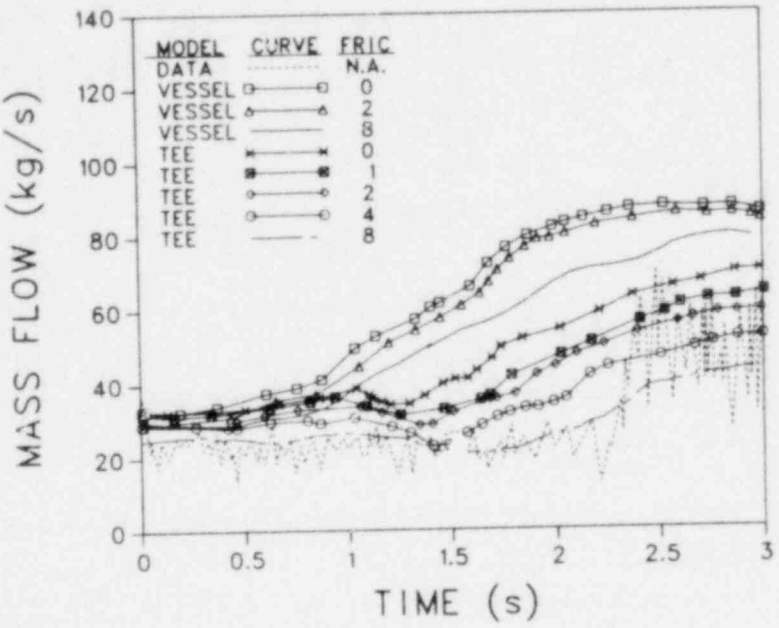

Fig. 4. OECD Standard Problem 6 break mass-flow comparisons. The data uncertainty is 10 to 15%.

In the calculation the void fraction of the fluid entering the pipe varied smoothly from the initial vapor to the final two-phase mixture. This calculated behavior, manifested in a lack of sharpness in the mixture level, was the result of numerical diffusion of the liquid and vapor phases.

The discrepancy between the calculated and measured pressure (Fig. 2) during the initial 0.5 s was the result of near-equilibrium vapor generation in the liquid region in response to the initial depressurization. Experimentally, the vapor generation was driven initially by a pressure (or temperature) offset from saturation and, therefore, occurred after the initial depressurization (delayed nucleation).

The tee component appeared to produce superior results; however, the comparisons were based on the same value of additive friction at the pipe junction. The implied loss coefficient (K factor) was lower for the vessel model than for the tee model. Both the tee and the vessel components appear to calculate properly level swell when the loss coefficients are set correctly. The loss coefficient is ideally based on data but may be found in reference tables.

B. Marviken Critical Flow Experiments

The Marviken facility[4] in Sweden was originally designed as a BWR power plant. After construction began, however, the facility was modified to be a test facility. The facility consisted principally of the containment structure and the reactor pressure vessel. The initial two series of tests investigated the transient response of various containment features. The third series of tests provided large-scale critical flow data. These data were obtained by blowing down the pressure vessel through nozzles of varying diameters and lengths. The critical flow tests provided data to assess the capability of thermal-hydraulic codes to predict large pressure vessel blowdowns with an emphasis on the critical flow calculation; selected tests have been analyzed with TRAC-P1A.

1. Facility and Test Descriptions

The four major components of the Marviken facility important to the critical flow tests were the pressure vessel, the discharge pipe, the test nozzle with the minimum flow area in the system, and the rupture disk assembly. The vessel, which was 24.55-m high, included part of the original core superstructure and moderator tank; three gratings were installed in the vessel to inhibit the formation of vortices. The discharge pipe extended vertically downward 5.568 m from the vessel bottom to the nozzle entrance; the entrance to the discharge pipe was rounded and 0.74 m above the vessel bottom. The nozzle also was oriented vertically downward and had a rounded entrance. The rupture disk assembly was located downstream (and below) the nozzle; in later tests the rupture disk assembly formed the last section of the nozzle. During the tests the system vented directly into the containment building and ultimately to the atmosphere.

Before a test the vessel was partially filled with deionized water; the water was preheated by removing water from the bottom of the vessel, circulating it through an external electrical heater, and injecting the water back into the steam dome at the top of the vessel. The preheating procedure produced a nonuniform temperature distribution in the vessel liquid before the test began. The steam-filled region above the vessel liquid was at saturation. The water at the nozzle inlet was substantially subcooled. The test was initiated by

releasing the rupture disks and terminated by closing a ball valve in the discharge pipe.

Tests 1, 2, 4, 7, 13, 22, and 24 were analyzed. Table IV summarizes the nozzle geometries for the tests analyzed, and Table V summarizes the initial conditions for the tests.

2. TRAC-P1A Input Model Description

The TRAC-P1A input model for the Marviken critical flow tests consisted of four components. The vessel above the 2.6-m elevation, which included the maximum diameter region and the top cupola, was represented as a semi-implicit pipe component; this component consisted of 15 hydraulic cells. The lower section of the vessel, the discharge pipe, and the nozzle were represented as a single, fully implicit pipe component; the number of cells in this second component varied with the length of the nozzle. The cell lengths near the

TABLE IV

MARVIKEN CRITICAL FLOW TEST NOZZLES

Test	Nozzle Straight-Section Length (m)	Nozzle Diameter (m)	L/D
1	0.895	0.300	2.98
2	0.895	0.300	2.98
4	1.520	0.509	2.99
7	0.290	0.300	0.97
13	0.580	0.200	2.90
22	0.727	0.500	1.45
24	0.166	0.500	0.33

TABLE V

MARVIKEN CRITICAL FLOW TEST CONDITIONS

Test	Initial Subcooling Near Vessel Bottom (K)	Initial Subcooling At Nozzle Inlet (K)	Water Level (m)	Initial Pressure (MPa)	End Time (s)
1	27	39	17.84	4.94	112
2	38	54	17.41	4.98	95
4	36	60	17.6	4.94	48
7	19	37	17.86	5.01	89
13	35	98	17.52	5.10	148
22	52	95	19.64	4.93	58
24	33	76	19.88	4.96	60

discharge end of the nozzle were 0.03 m. Figure 5 shows the noding for the vessel and discharge pipe. Figure 6 shows the noding for the nozzle and rupture disk assembly for test 4. A zero-velocity fill component provided the vessel upper boundary condition, and a break component provided the pressure boundary condition downstream of the rupture disk assembly.

Because the vessel included some internal structure, the model diameter was reduced slightly (from 5.220 to 5.136 m) to maintain the correct initial water mass and net internal volume. The discharge pipe was modeled as starting at the vessel bottom, and a loss coefficient accounted for the inlet projecting into the vessel. The annular flow friction factor correlation option (NFF = 4) was specified.

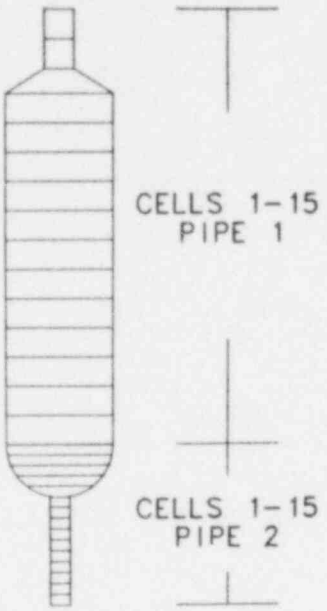

Fig. 5. Marviken critical flow test facility vessel and discharge pipe noding.

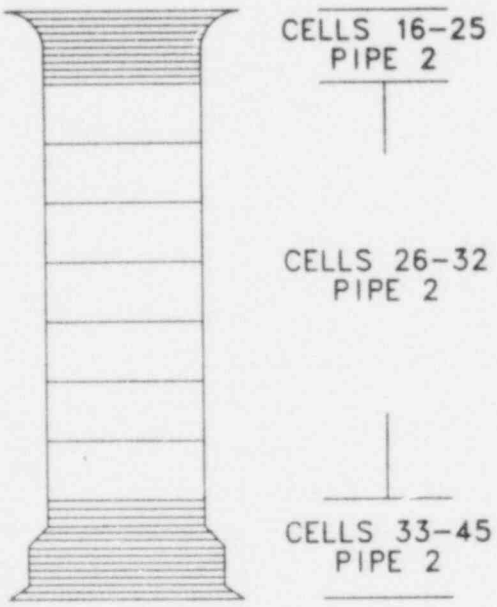

Fig. 6. Marviken critical flow test facility nozzle and rupture disk assembly noding.

3. Comparisons Between the Calculations and the Data

Of the seven tests analyzed, test 4 was analyzed and compared to data as a part of the TRAC-P1A developmental assessment; the results of test 4 are discussed in Ref. 2 and are not repeated here. All of the results for the various tests were qualitatively the same; therefore, only the results for test 22 are discussed in detail. The results for the remaining tests are then summarized. The calculations for tests 22 and 24 were posttest blind predictions. The test data were obtained from Refs. 4-10.

Figure 7 compares the calculated and measured mass flux histories for test 22. The Pitot-static data curve was valid throughout the transient, whereas the vessel differential pressure curve was valid only after ~5 s. The code calculated the initial peak mass flux well but subsequently underpredicted slightly the mass flux during the remaining subcooled part of the blowdown. After the flow saturated at the break (~35 s), the comparison is very good. The

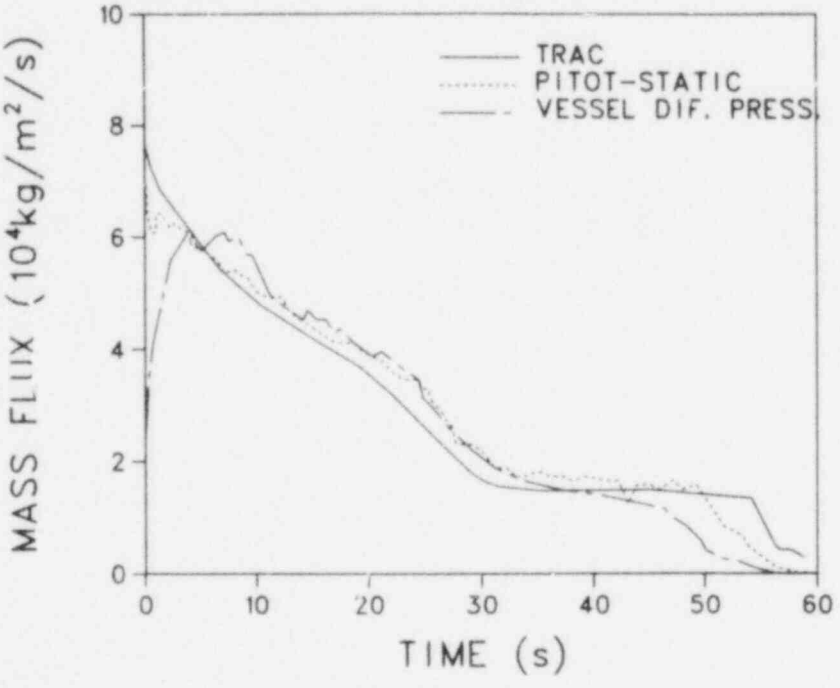

Fig. 7. Marviken critical flow test 22 mass flux comparisons. The Pitot-static data uncertainty is 7%; the vessel differential pressure data uncertainty is 15% after 5 s.

differences between the calculation and the data after 50 s resulted from a small difference in the emptying times.

The test 22 pressure comparisons for the upper and lower vessel and the discharge pipe are shown in Figs. 8-10. During the first 3 s there is a dip in the experimental data that was not calculated by the code because the constitutive relations do not permit delayed nucleation. After the dip the code slightly underpredicted the pressure at all three locations during the subcooled depressurization. After the system saturated, the pressure comparisons were very good. Again, the discrepancies after 50 s reflected small differences in the emptying times.

Figures 11-15 show the fluid-temperature comparisons for test 22 at three elevations in the vessel and two locations in the discharge pipe. Figure 11 shows the vapor temperature above the liquid, and the early dip in the data followed the dip in the pressure data. At this elevation the comparison was the same as the pressure comparison. In Figs. 12-15 the temperature rise from the initial subcooling was caused by the warm liquid near the top of the mixture

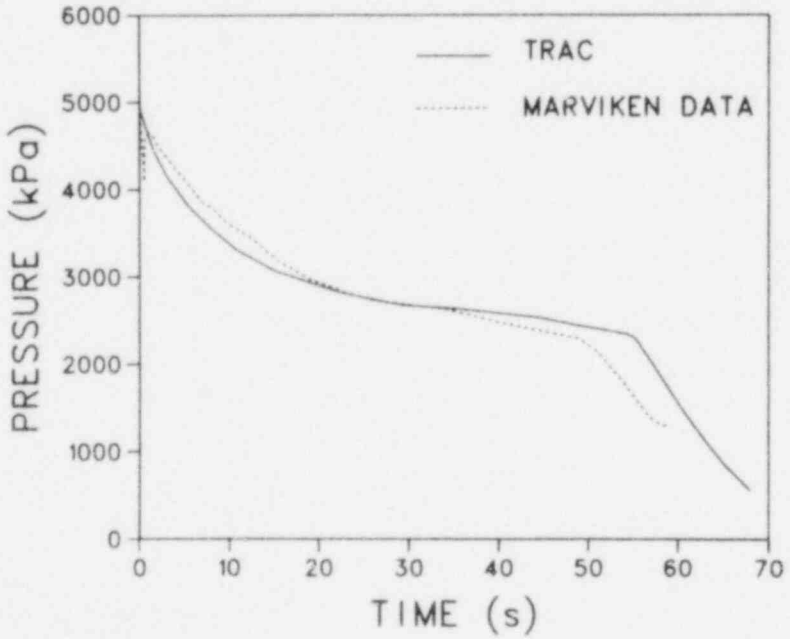

Fig. 8. Marviken critical flow test 22 pressure comparison at the 23.13-m vessel elevation. The data uncertainty is ~50 kPa.

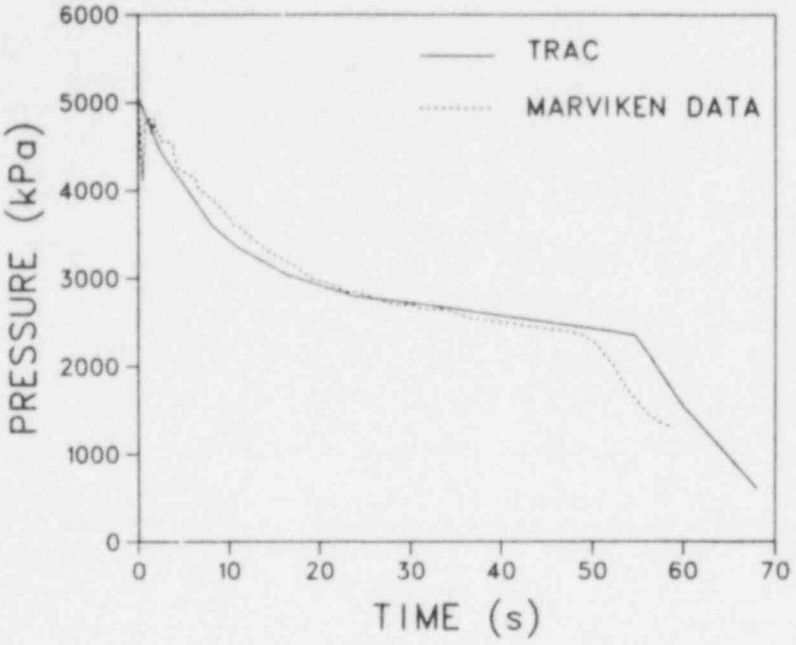

Fig. 9. Marviken critical flow test 22 pressure comparison at the 0.525-m vessel elevation. The data uncertainty is ~60 kPa.

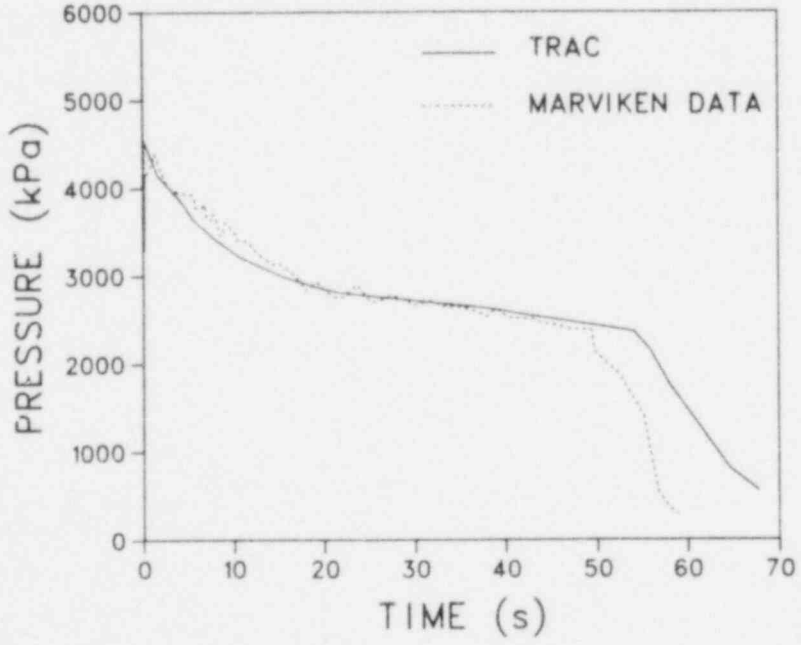

Fig. 10. Marviken critical flow test 22 pressure comparison in the discharge pipe 4.868 m below the vessel. The data uncertainty is ~60 kPa.

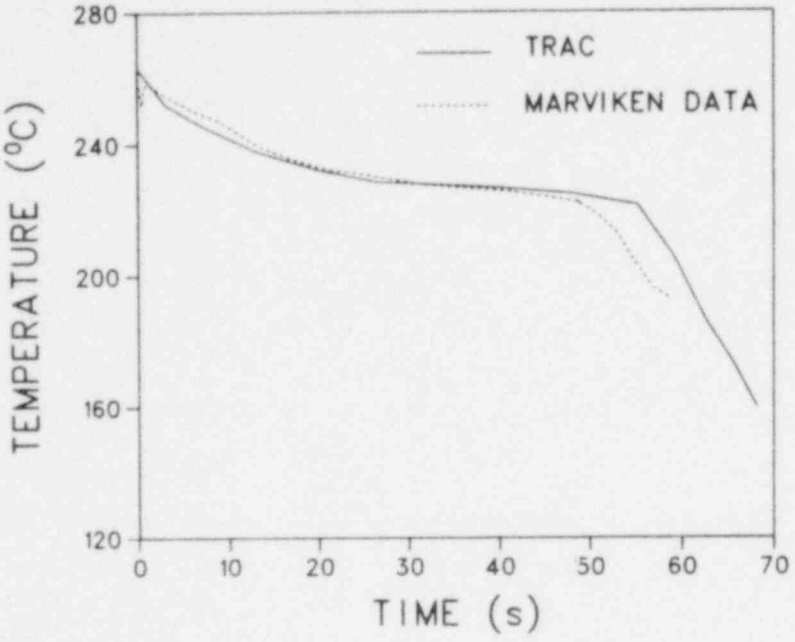

Fig. 11. Marviken critical flow test 22 fluid-temperature comparison at the 20.543-m vessel elevation. The data uncertainty is 2 K.

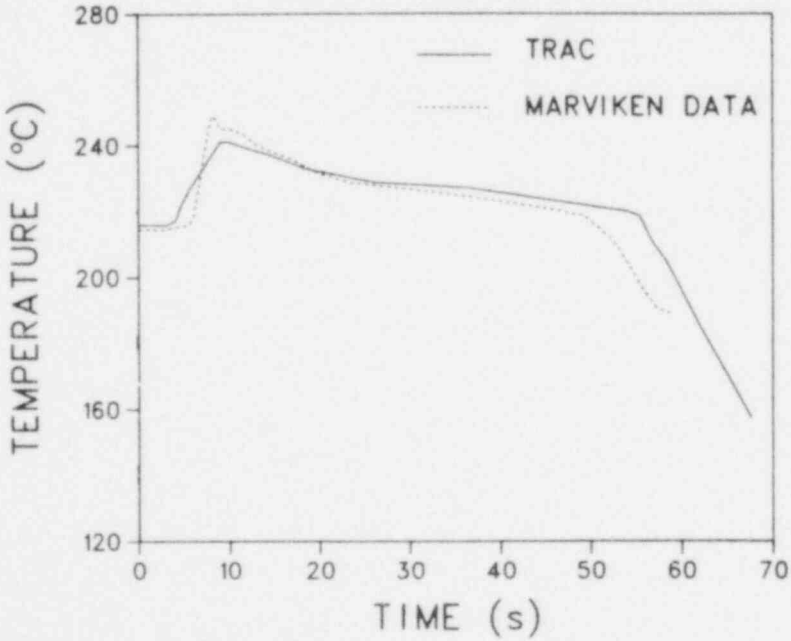

Fig. 12. Marviken critical flow test 22 fluid-temperature comparison at the 10.836-m vessel elevation. The data uncertainty is 2 K.

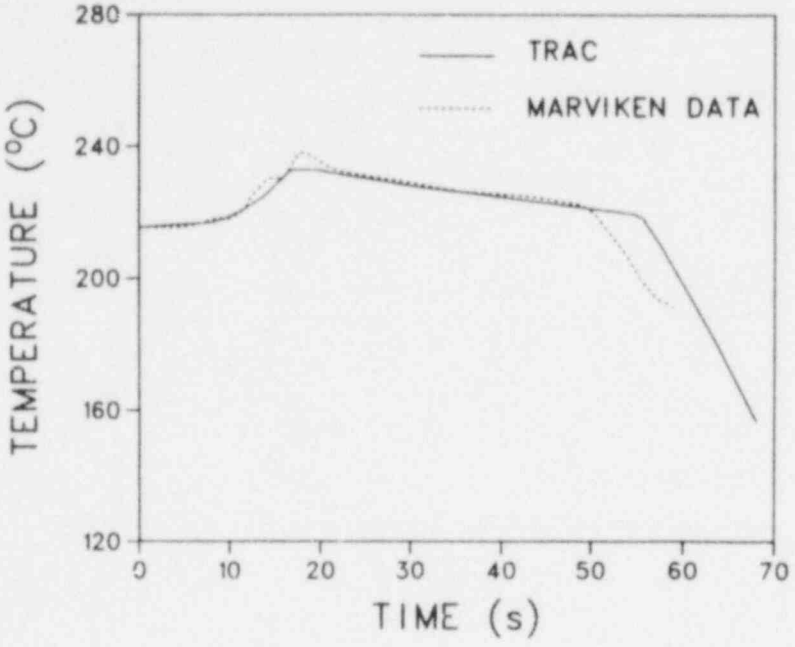

Fig. 13. Marviken critical flow test 22 fluid-temperature comparison at the 5.970-m vessel elevation. The data uncertainty is 2 K.

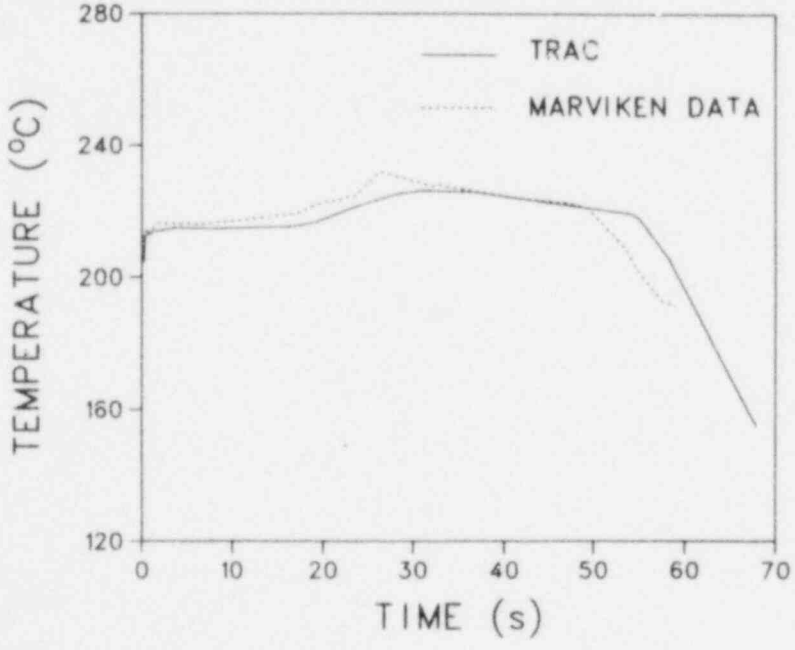

Fig. 14. Marviken critical flow test 22 fluid-temperature comparison in the discharge pipe 0.630 m below the vessel. The data uncertainty is 2 K.

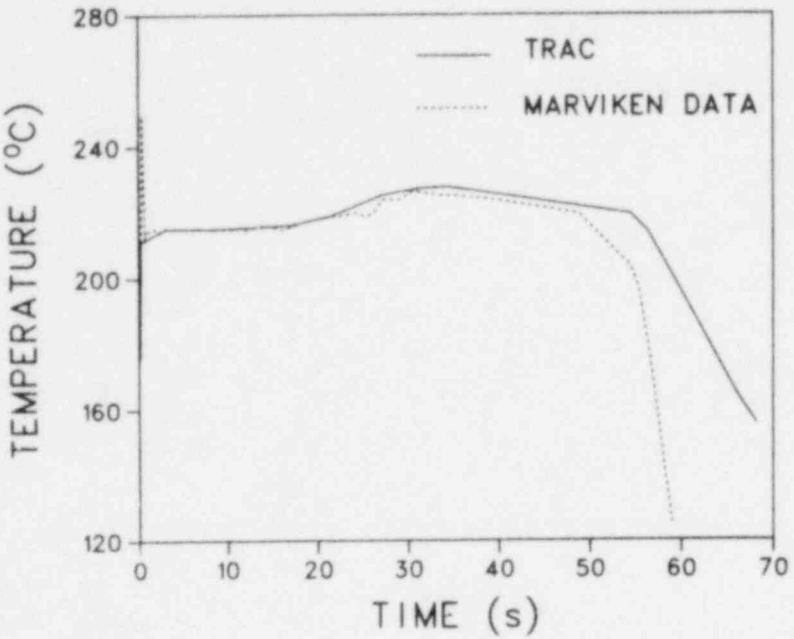

Fig. 15. Marviken critical flow test 22 fluid-temperature comparison in the discharge pipe 4.868 m below the vessel. The data uncertainty is 2 K.

level moving down the vessel and the discharge pipe as the vessel emptied. The code did not calculate as sharp a rise in the temperature as the data exhibited because of the averaging of the fluid conditions within a hydraulic cell as warm liquid mixed with the cooler liquid. The mixing process within a cell tended to diffuse the thermal stratification within the liquid. After the peak temperature was reached, the temperatures followed saturation.

The fluid density comparison in the discharge pipe below the vessel is shown in Fig. 16. The comparison was good to 33 s, when the calculation clearly showed the presence of vapor.

Figures 17-21 show the mass flux comparisons for tests 1, 2, 7, 13, and 24. These mass flux comparisons were qualitatively similar to the mass flux comparison for test 22 (Fig. 7). Relating these figures to the information in Table IV revealed that the quality of the comparisons degraded with decreasing length-to-diameter ratio. The discrepancy in emptying times increased as the underprediction of the mass flux became more severe. The quality of the comparisons for other parameters such as temperature, pressure, and density was directly related to the quality of the mass flux comparisons.

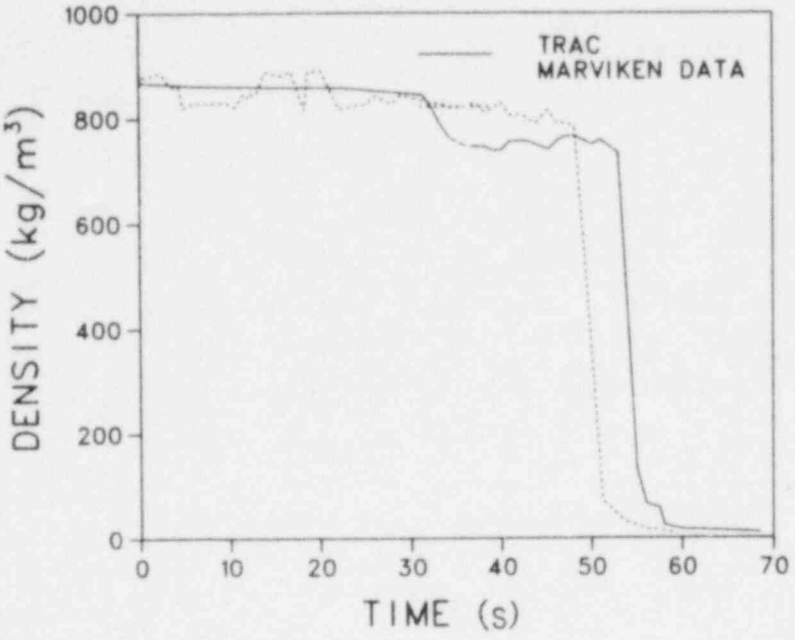

Fig. 16. Marviken critical flow test 22 fluid density comparison in the discharge pipe 2.390 m below the vessel. The data uncertainty is ~40 kg/m^3.

4. Conclusions and Observations

Table VI summarizes the mass flux data comparisons for all seven tests during the subcooled portion of the blowdown. The integrated calculated mass flow during the subcooled period was within 15% of the data for all of the blowdowns except for the very short nozzle cases: test 24, which was 20% below the data, and test 7, which was 25% below the data. The results indicated that when the upstream conditions were subcooled and the critical flow was controlled by nonequilibrium effects, the code underpredicted the flow and did not calculate properly the nonequilibrium effects (underprediction inferred that the error was toward equilibrium). The longer nozzles, because of the frictional effects, tended to drive the flow toward equilibrium and thus accounted for the improved comparisons at the larger length-to-diameter ratios. Once the system saturated, the code generally calculated the correct critical flows. The results were sensitive to the initial temperature distribution in the system.

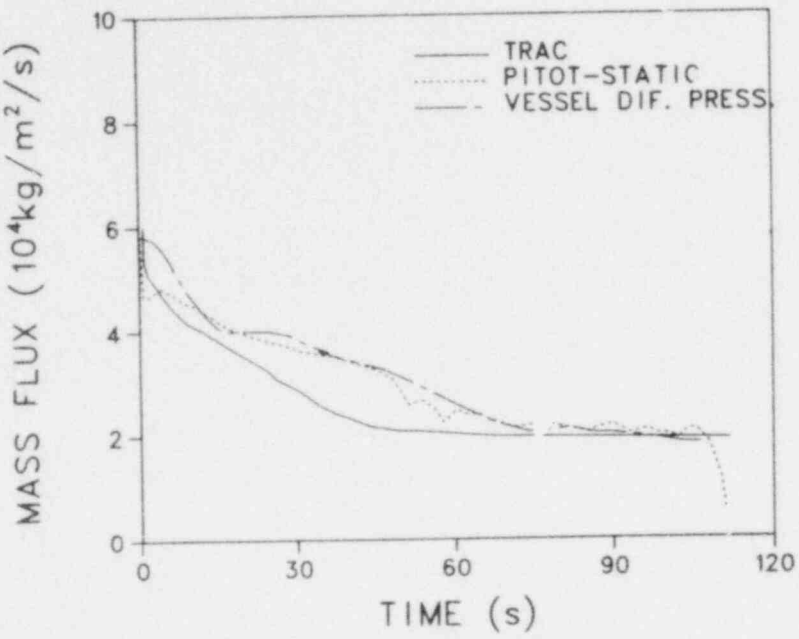

Fig. 17. Marviken critical flow test 1 mass flux comparisons. The Pitot-static data uncertainty is 7%; the vessel differential pressure data uncertainty is 15% after 15 s.

The discrete nature of the hydraulic cells led to the artificial mixing of the hotter liquid near the top of the liquid region with the colder liquid further down in the vessel and, ultimately, propagated the higher enthalpy fluid to the break earlier than observed in the tests. The constitutive relations in TRAC-P1A did not permit delayed nucleation; this problem prevented the code from calculating the initial dip in the pressure at the beginning of the tests and forced the critical flow calculation toward equilibrium, resulting in an underprediction of flow.

C. Semiscale Mod-3 Test S-07-6

Semiscale test S-07-6 was the sixth test in the initial test series (Semiscale test series 7) in the new Mod-3 facility configuration. The test provided data to evaluate the integral blowdown and reflood behavior during a 200% cold-leg break with emergency core coolant (ECC) injected into the intact-loop cold leg only. The TRAC-P1A analysis determined the ability of the

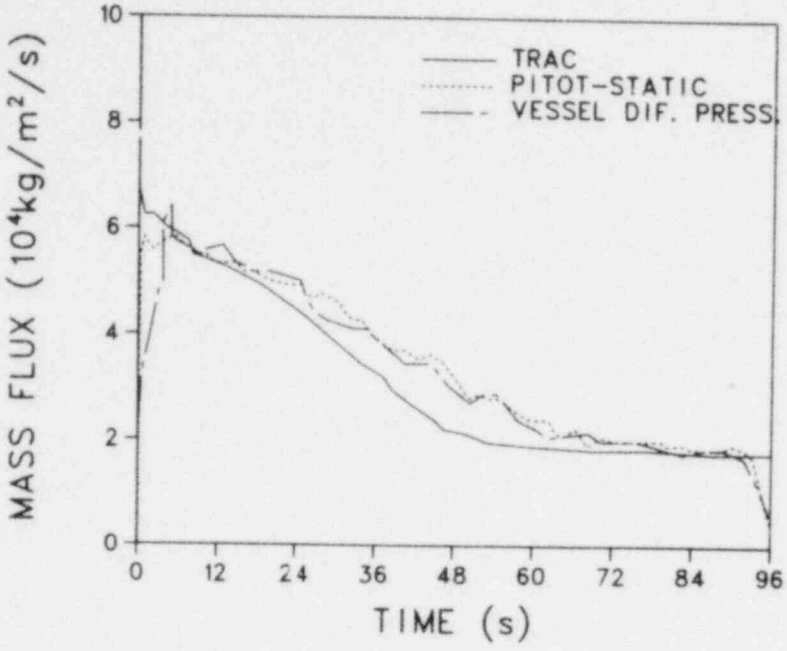

Fig. 18. Marviken critical flow test 2 mass flux comparisons. The Pitot-static data uncertainty is 7%; the vessel differential pressure data uncertainty is 15% after 5 s.

code to calculate the long-term oscillations that were observed in the downcomer and core liquid levels during the reflood phase of the test.

1. Facility and Test Descriptions

The Mod-3 facility[11] simulated a PWR with an upper head injection ECC system. The scaling rationale was based on maintaining the relative volume distribution and the core-power-to-system-volume ratio for the reference PWR.

The core consisted of a 5-by-5 bundle of 3.66-m-long electrical heater rods. The central nine rods were peaked 13% above the outer ring of rods. A liquid level probe was installed in one corner rod position. To maintain symmetry, the corner rod opposite the liquid level probe was not powered. The core simulator was installed in a 10-m-high vessel. The lower portion of the vessel contained the lower plenum, core, and upper plenum; the upper portion of the vessel represented the upper head. Guide tube and core support tube simulators connected the two vessel regions. The inlet distribution annulus and downcomer were external to the main vessel, and the downcomer was represented by

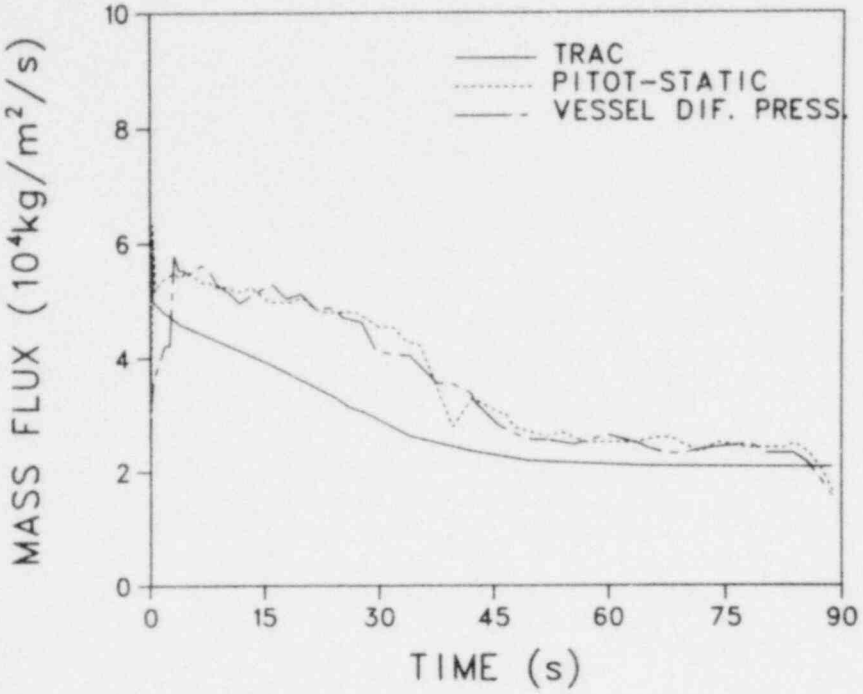

Fig. 19. Marviken critical flow test 7 mass flux comparisons. The Pitot-static data uncertainty is 7%; the vessel differential pressure data uncertainty is 15% after 5 s.

a pipe. A tube connected the inlet annulus to the upper head of the vessel to simulate the bypass flow between the two components.

The intact loop was scaled to represent three loops of the reference PWR; most of the components were taken from the intact loop of the Mod-1 facility. The intact loop contained an active steam generator and primary coolant pump and a complete ECC injection system connected to the cold leg. The pressurizer was attached to the hot leg.

The broken loop was scaled to a single loop of the reference plant. Like the intact loop, the broken loop contained an active steam generator and pump. An ECC injection system was provided, although it was valved out for test S-07-6. A noncommunicative break simulator was installed in the cold leg to represent a 200% double-ended break.

Table VII summarizes the initial conditions[12] for test S-07-6. The ECC fluid temperature was 312 K. The high-pressure injection system (HPIS) and the low-pressure injection system (LPIS) actuation pressures were, respectively, 15.2 and 1.0 MPa. Accumulator injection began at 4.28 MPa. The transient was

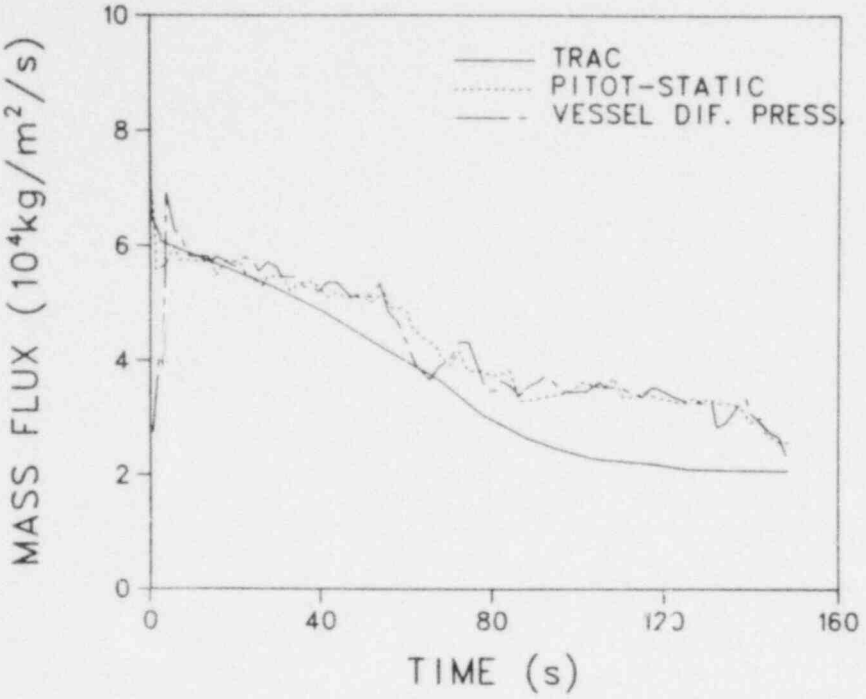

Fig. 20. Marviken critical flow test 13 mass flux comparisons. The Pitot-static data uncertainty is 7%; the vessel differential pressure data uncertainty is 15% after 5 s.

initiated by triggering the rupture disk assembly to begin the blowdown. The core power was controlled to simulate decay heat.

2. TRAC-P1A Input Model Description

The TRAC-P1A input model for test S-07-6 consisted of 36 components and 38 junctions; there were 307 hydraulic cells. Figure 22 is the noding diagram. The lower region of the vessel (upper and lower plenums and core), the inlet annulus, and the downcomer pipe were combined into a single vessel component; this vessel component incorporated 14 axial levels, 3 radial rings, and 2 azimuthal segments. The inlet annulus was located in the outermost ring, and the downcomer pipe was represented by a single vertical stack of cells in the outer ring connecting the inlet annulus and the lower plenum (the vertical stack of cells in the outer ring opposite the downcomer pipe stack were blocked off).

The upper head region of the vessel was modeled as a separate vessel component and is labeled HEADER in Fig. 22. This vessel consisted of three axial levels, one radial ring, and one azimuthal segment. Three pipe components connected the upper head vessel to the main vessel; these pipe components

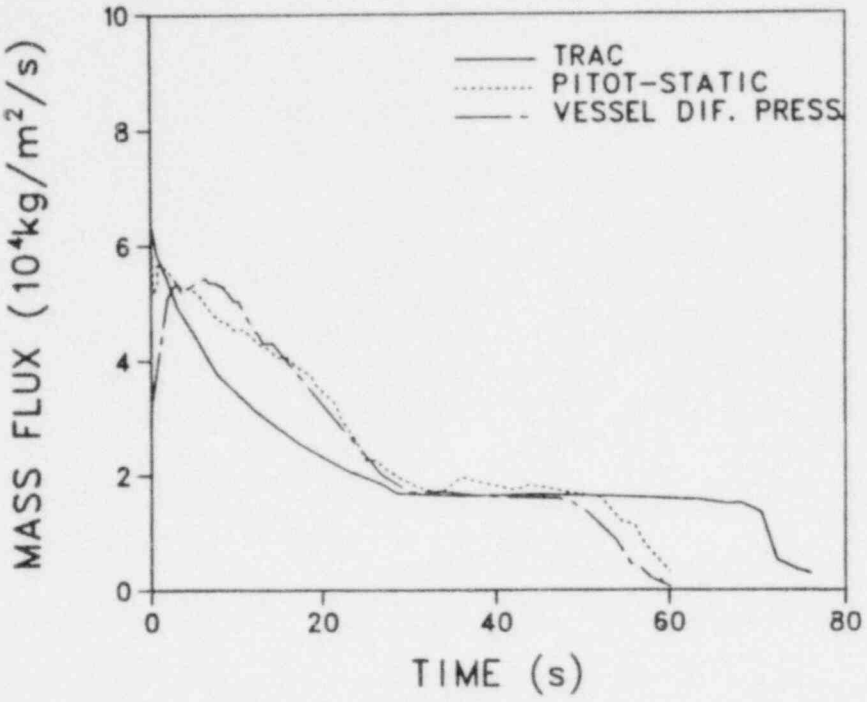

Fig. 21. Marviken critical flow test 24 mass flux comparisons. The Pitot-static data uncertainty is 7%; the vessel differential pressure data uncertainty is 15% after 5 s.

represented the guide tube and core support tube simulators and the inlet-annulus-to-upper-head bypass.

The one-dimensional hydraulic cell lengths varied between 2.0-10.0 m except near the breaks. The cell lengths for the component representing the break (component 6 in Fig. 22) varied from 0.01-0.1 m. The semi-implicit numerics were used for all components except component 6, where the fully implicit numerics were required to represent the choking phenomena.

Test S-07-6 data[13] showed multiple downcomer and core liquid mass depletions with a period of ~125 s. Because of these oscillations and the implied slow reflood, the peak power zone did not quench axially until after the test was terminated. An investigation[14] of this depletion phenomenon identified several possible causes: (1) unusually high heat transfer to the downcomer fluid from the hot downcomer metal structures through the insulator between the bulk material of the pipe and the inner liner, (2) backflow of steam from the core into the downcomer, and (3) the one-dimensional nature of the Mod-3 downcomer. Because the lumped-parameter heat slabs in the TRAC-P1A vessel component do not

TABLE VI

COMPARISON OF TRAC-P1A AND MARVIKEN FLOWS DURING THE SUBCOOLED PERIOD

Test	End of Subcooled Period (s)	Minimum TRAC-P1A/Marviken Flow Rate Ratio During Subcooled Period	TRAC-P1A/Marviken Mass Removed Ratio by End of Subcooled Period
1	67	0.687	0.850
2	56	0.682	0.893
4	17	0.778	0.919
7	38	0.616	0.750
13	65	0.830	0.951
22	33	0.759	0.954
24	25	0.664	0.798

adequately model composite, distributed heat structures like the Mod-3 downcomer pipe, the heat-transfer rates from the downcomer outer pipe to the downcomer fluid were specified based on the measured temperatures[12] of the downcomer metal structures. The specified heat fluxes were

1. for the downcomer inlet annulus region

$$Q = 0 \quad , \quad 0 \leq t < 20$$

$$= 30 \text{ kW/m}^2 \quad , \quad 20 \leq t < 460$$

$$= 0 \quad , \quad t \geq 460$$

and

TABLE VII

SEMISCALE MOD-3 TEST S-07-6
STEADY-STATE INITIAL CONDITIONS

	Experiment	TRAC-P1A
Initial core power (MW)	1.97	1.97
Primary system pressure (MPa)	15.2	15.0
Suppression system pressure (MPa)	0.25	0.25
Cold-leg fluid temperature (K)	559	560
Hot-leg fluid temperature (K)	594	595
Coolant temperature rise (K)	35	35
Core mass flow (kg/s)	9.5	9.5
Clad temperature (K) high-powered rod	687	670
Clad temperature (K) low-powered rod	585	584
Pump differential pressure (MPa)		
intact loop	0.48	0.46
broken loop	0.34	0.32
Vessel differential pressure (MPa)	0.11	0.10

2. for the downcomer pipe region

$$Q = 25.0\ kW/m^2 , \quad 0 \leq t < 90$$

$$= 12.4\ kW/m^2 , \quad 90 \leq t < 100$$

$$= 6.20\ kW/m^2 , \quad 100 \leq t < 120$$

$$= 2.20\ kW/m^2 , \quad 120 \leq t < 460$$

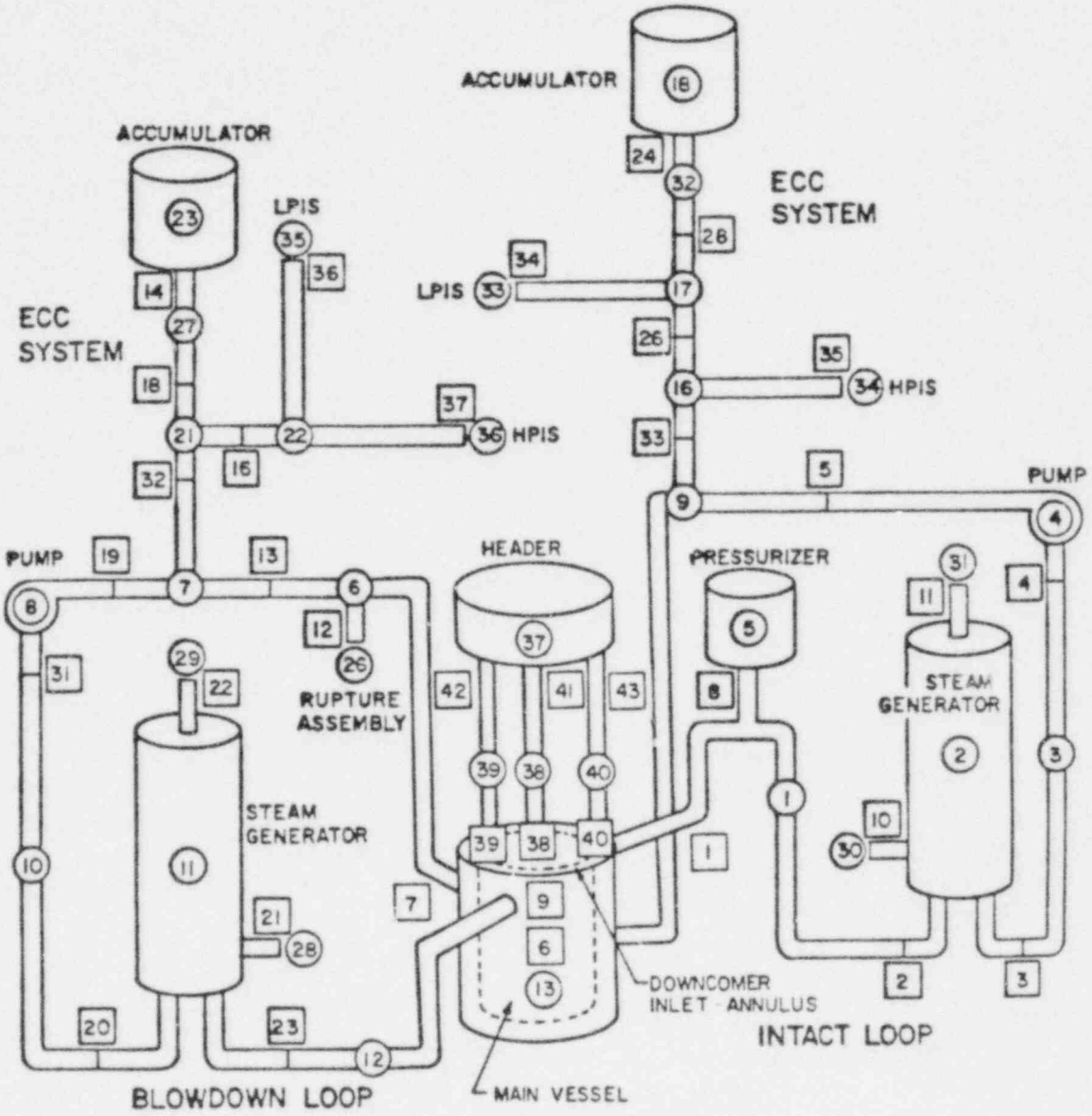

Fig. 22. Semiscale Mod-3 test S-07-6 component schematic.

where Q is heat flux and t is transient time (s). These heat-transfer rates were incorporated into the TRAC-P1A calculation for test S-07-6.

The steady-state calculation was initiated from conditions of zero velocity and uniform temperatures and pressures. The system conditions approached steady-state values after ~33 s of real time. Table VII compares the calculated initial conditions with the test data; all calculated values were within 10% of the measured values. The transient calculation was restarted from the final dump of the steady-state calculation and was terminated at 430 s.

3. Comparisons Between the Calculations and the Data

Typical comparisons of the calculated results with experimental data[12,13] are shown in Figs. 23-32. In addition to the base calculation made with the specified inlet annulus and downcomer heat flux discussed above, a calculation was made without that heat flux. The code sensitivity to the downcomer heat transfer also is discussed.

Figure 23 shows the downcomer- and core-collapsed liquid levels. The data show vividly the downcomer and core liquid level oscillations, which began at

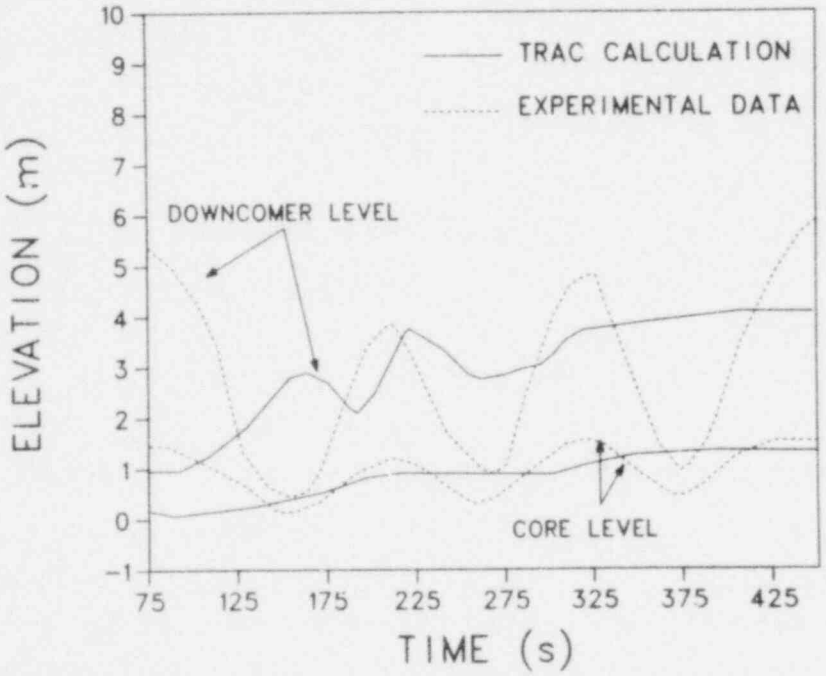

Fig. 23. Semiscale Mod-3 test S-07-6 downcomer- and core-collapsed liquid levels. The data uncertainty is ~5% of full scale.

75 s. The period of the oscillations is ~125 s. The oscillations began at ~75 s after the intact-loop accumulator had emptied and was beginning to inject nitrogen into the primary system. However, the initiating phenomenon[14] involved the high heat flux from the downcomer metal structures to the downcomer liquid. As the flow in the downcomer stagnated, the liquid heated to saturation and began to boil. The voiding in the downcomer produced a pressure imbalance between the downcomer and the core. This pressure differential drove the initial cycle of the liquid level oscillations. Subsequent cycles were driven by steam backflow from the core. The TRAC-P1A calculation did produce a few oscillations, but the period and magnitude of the oscillations did not reflect the data. In particular, the code did not predict the almost complete voiding of the downcomer, and the code results were out of phase with the data at 75 s when the oscillations began. Also, the calculated oscillations were more damped than in the data, and they had damped by 300 s; whereas, the data oscillations continued throughout the test. One obvious problem with the calculation was that the code did not calculate the initial filling of the downcomer at the correct time.

The specified downcomer wall heat transfer affected the lower plenum filling behavior. Figure 24 indicates that without downcomer heat transfer the lower plenum filled at 80 s. With the specified downcomer heat flux, the initial filling of the lower plenum was delayed until 150 s. This sensitivity of the lower plenum filling behavior to heat transfer is a direct result of the code not calculating the initial filling of the downcomer properly and suggests potential problems with the specified heat flux. In particular, the heat-flux specification incorporated no dependence on fluid conditions in the downcomer, and the method for developing the specification ignored external heat losses.

Figure 25 shows a comparison of measured and calculated cladding temperatures near the bottom of the core (0.0 to 0.61-m elevation) for the high-powered rods. The calculated results agreed qualitatively with the data, but TRAC-P1A underpredicted the measured peak temperature. A comparison of the calculated high-powered rod cladding temperature to data near the core midplane (1.52 to 2.13-m core elevation) is shown in Fig. 26. TRAC-P1A underpredicted the peak cladding temperature during blowdown and overpredicted the reflood peak. The calculated quench occurred at 230 s, but the test did not quench (during the time frame of the test). Figure 27 shows a comparison of the

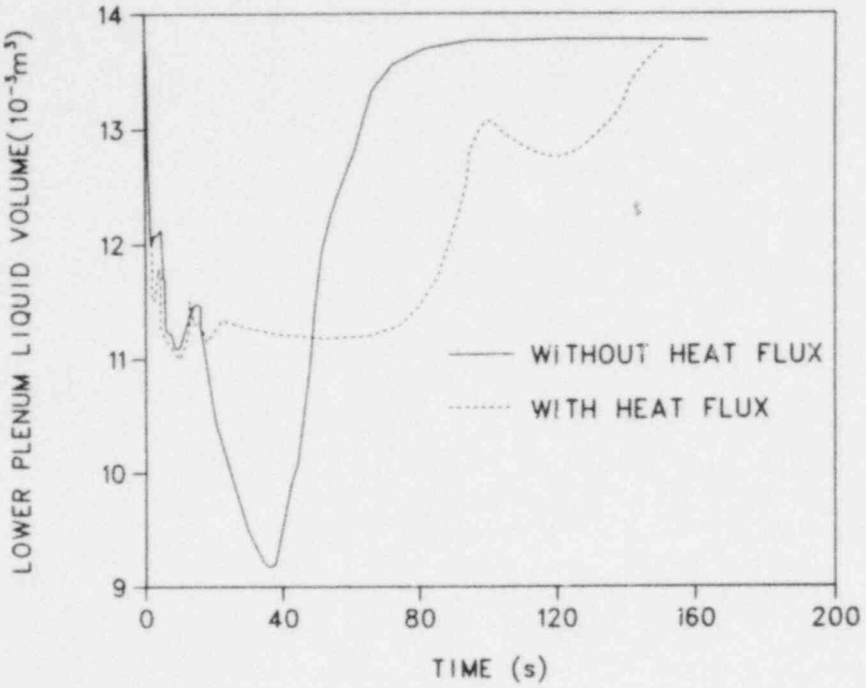

Fig. 24. Semiscale Mod-3 test S-07-6 calculated lower-plenum filling behavior.

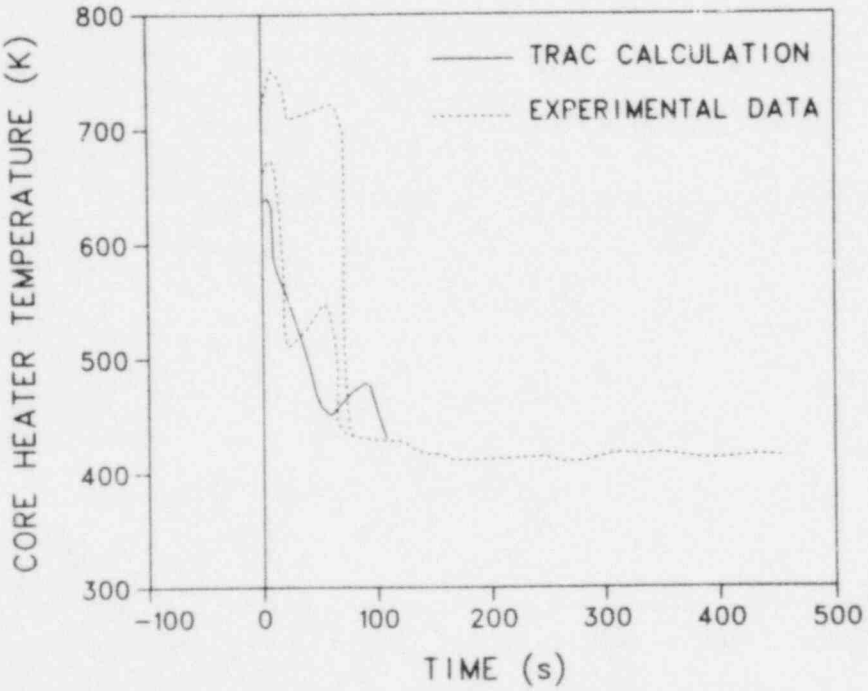

Fig. 25. Semiscale Mod-3 test S-07-6 high-powered rod cladding temperature comparisons, 0.0 to 0.61-m elevation. The data uncertainty is 5 K.

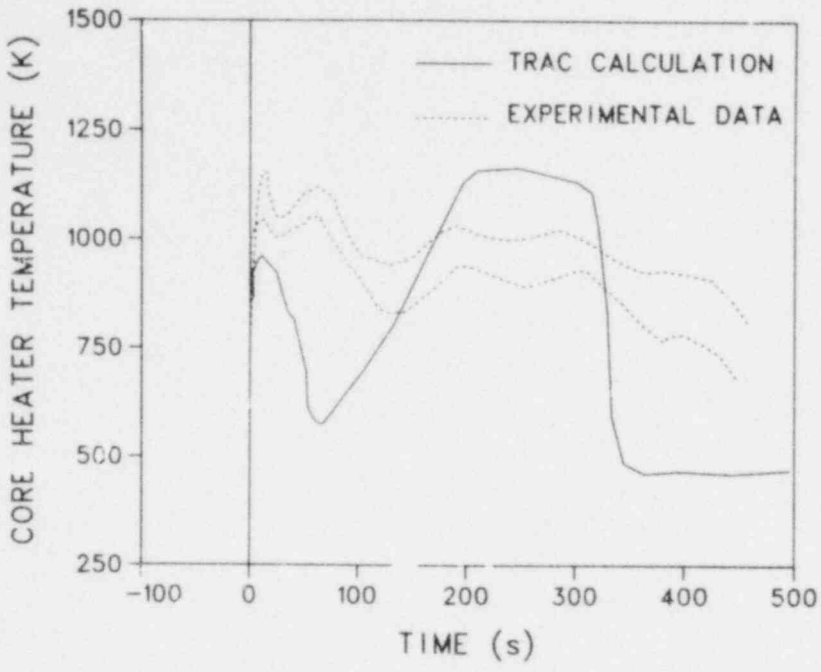

Fig. 26. Semiscale Mod-3 test S-07-6 high-powered rod cladding temperature comparisons, 1.52 to 2.13-m core elevation. The data uncertainty is 5 K.

calculated low-powered rod cladding temperatures to data near the top of the core (3.05 to 3.66-m core elevation). The calculation compared reasonably well, but a higher peak clad temperature during reflood was predicted. Figures 28 and 29 compare the calculated mass flow to data from the pump side and from the vessel side of the break, respectively. The calculated results agreed very well with the experimental data; the short duration of the subcooled blowdown and the extended period of saturated blowdown result in the good agreement. Figure 30 shows a comparison of the mixture density at the intact-loop hot leg. The three data traces correspond to the three beams of the gamma densitometer. The calculated density was greater than the data and indicated that the intact-loop hot leg did not void properly.

Figures 31 and 32 show a comparison of calculated and measured pressures in the pressurizer and vessel upper plenum, respectively. The base-case calculation with the specified downcomer heat flux depressurized more slowly than the data. However, when the downcomer heat flux was zero, the comparison improved.

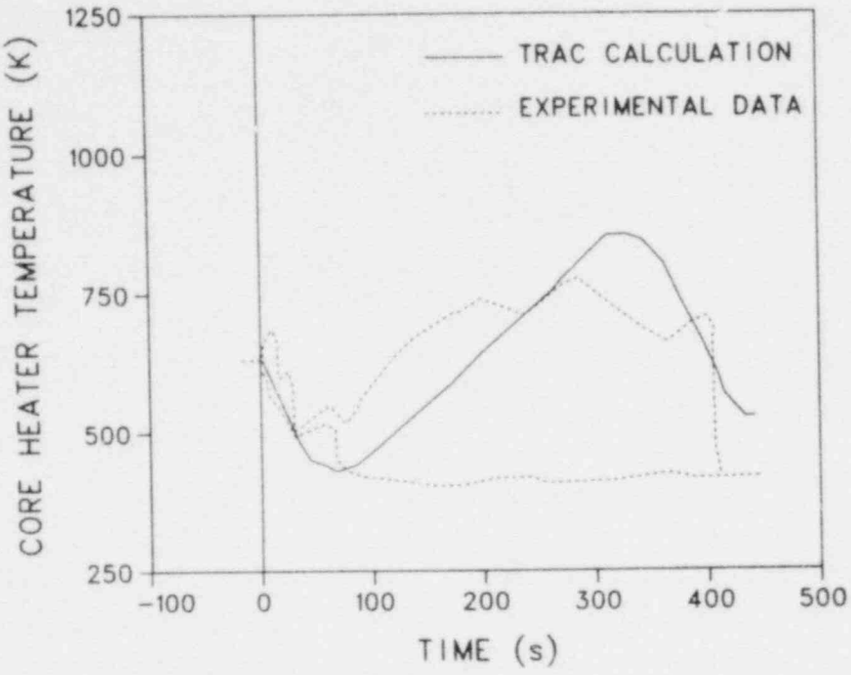

Fig. 27. Semiscale Mod-3 test S-07-6 low-powered rod cladding temperature comparisons, 3.05 to 3.66-m core elevation. The data uncertainty is 5 K.

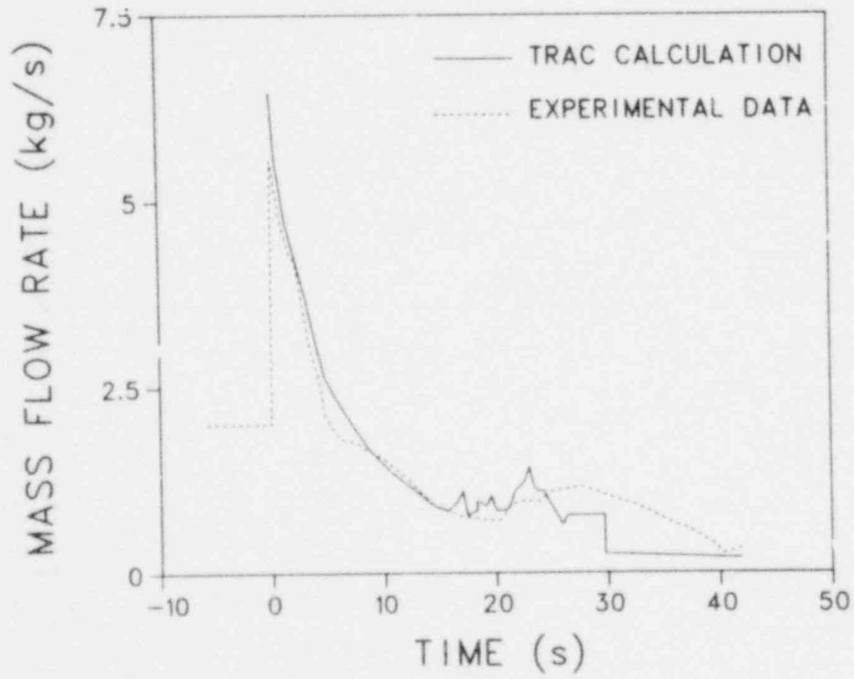

Fig. 28. Semiscale Mod-3 test S-07-6 mass flow from the pump side of the break.

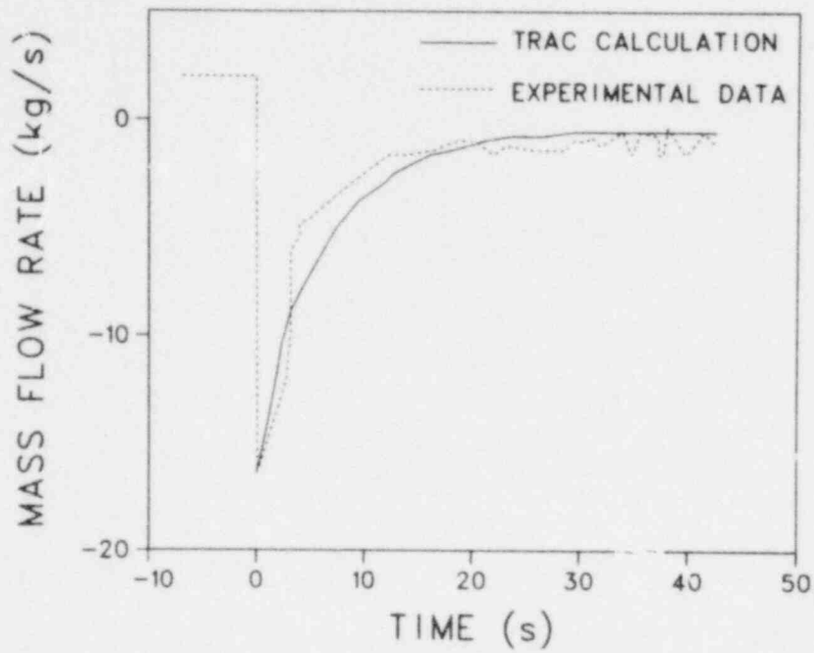

Fig. 29. Semiscale Mod-3 test S-07-6 mass flow from the vessel side of the break.

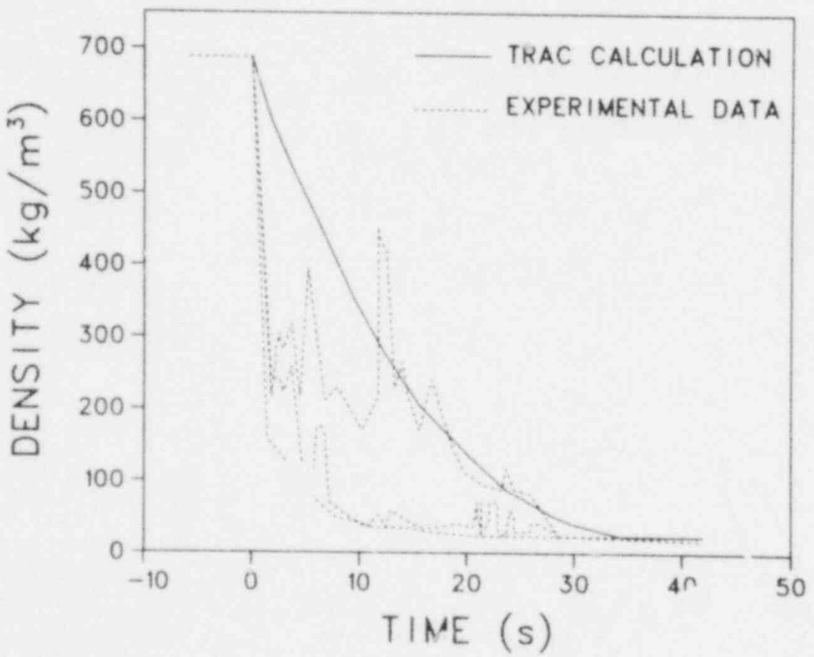

Fig. 30. Semiscale Mod-3 test S-07-6 mixture density in the intact-loop hot leg.

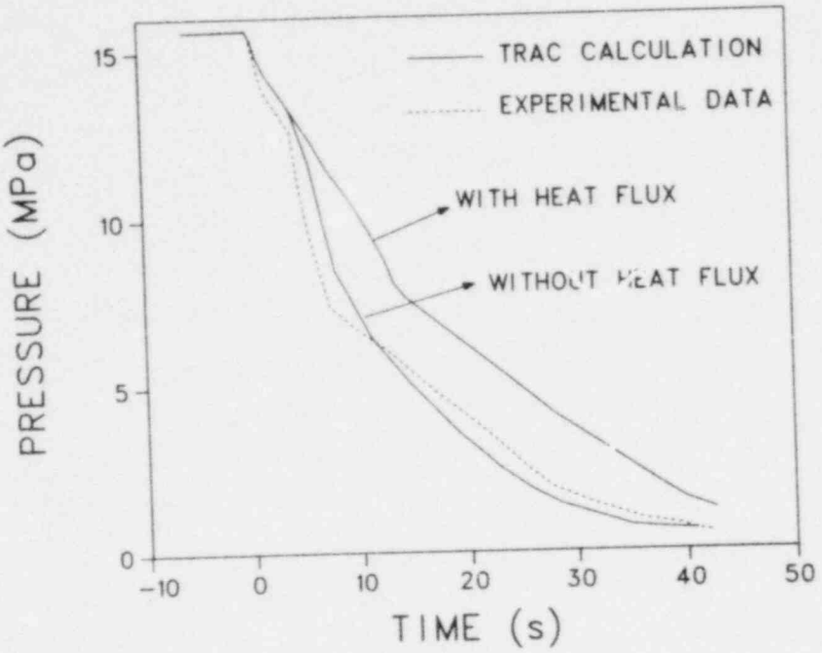

Fig. 31. Semiscale Mod-3 test S-07-6 pressurizer pressure. The data uncertainty is 2% of full scale.

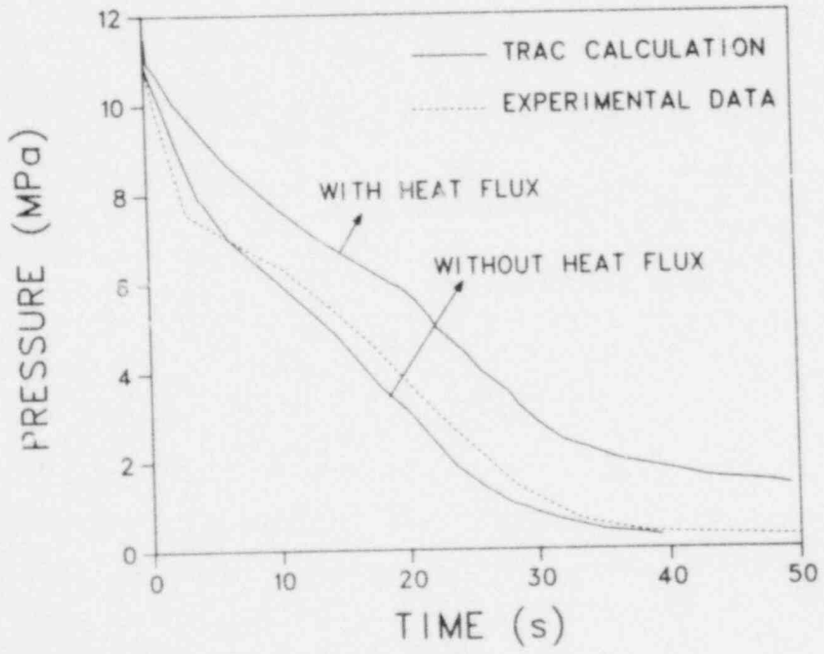

Fig. 32. Semiscale Mod-3 test S-07-6 vessel upper-plenum pressure. The data uncertainty is 2% of full scale.

4. Conclusions and Observations

In summary, the agreement between the TRAC-P1A calculation without the specified downcomer heat flux and experimental data for Semiscale Mod-3 test S-07-6 was good for the steady-state calculation and the blowdown portion of the transient. However, the agreement during the refill and reflood portions of the transient was not good. In particular, TRAC-P1A did not predict the long-term downcomer and core liquid level oscillations and overpredicted peak cladding temperatures during reflood. The specification of downcomer wall heat flux resulted in worse comparisons during blowdown and did not improve the comparisons to data during refill and reflood.

A careful study of the problem indicated that the following factors were involved in the disagreement between the code results and the data:

1. Insufficient downcomer liquid penetration.
2. Uncertainties in the amount of heat transfer from structural metal to the fluid.
3. Reflood heat-transfer and entrainment model deficiencies.
4. Effect of accumulator nitrogen on heat transfer and vapor generation.

In the one-dimensional downcomer pipe of the Semiscale Mod-3 facility, TRAC-P1A underpredicted the liquid penetration rate both in the one-dimensional drift-flux formulation (early calculations not discussed here) and in the two-fluid hydrodynamics of the vessel component. Auxiliary TRAC-P1A analyses of countercurrent air-water flow in vertical pipes were performed to investigate further the problem (see Sec. II.D). These analyses indicated that in vertical pipes the interfacial shear coefficient was too high at low countercurrent gas velocities.

The downcomer depletions in test S-07-6 began when the ECC water in the downcomer reached saturation temperature. The time when saturation was achieved was sensitive to the downcomer wall-to-fluid heat transfer, which was estimated from the measurements of pipe interior wall temperatures. A composite, distributed heat slab model in TRAC-P1A would eliminate the need for a heat flux boundary condition.

The vapor generation rate in the core appeared to be one of the controlling mechanisms for the long-term oscillations in the test. TRAC-P1A analyses[2] of Full-Length Emergency Cooling Heat Transfer (FLECHT) forced flooding tests indicated that the reflood heat-transfer models were insufficient for predicting the low reflood rate phenomena in those tests. In particular, the quench front propagation, liquid entrainment, and transition and film boiling heat-transfer models require further development. (Reflood modeling improvements are scheduled for TRAC-PD2.)

Injection of nitrogen from the accumulator into the loops and vessel could have had a significant effect on interfacial heat and mass transfer and wall heat transfer. Because TRAC-P1A cannot treat the simultaneous presence of a noncondensable gas and water vapor, the effect of nitrogen on the system response was not evaluated.

D. Dartmouth Countercurrent Flow Flooding Tests

The Dartmouth College air-water countercurrent flow flooding tests[15] investigated the liquid penetration rate during air-water countercurrent flow in a simple vertical tube. The analyses were initiated because TRAC-P1A calculated less ECC downcomer penetration for Semiscale Mod-3 test S-07-6 than was evident in the data, and further testing was needed against simple separate-effects tests involving countercurrent flow in vertical pipes.

1. Facility and Test Descriptions

The test facility consisted of a vertical transparent tube 1.12 m long connecting upper and lower plenums (see Fig. 33). The plenums were 0.21-m^3 drums. Water entered through a 0.05-m pipe into the upper plenum at rates up to 0.016 m^3/s. An overflow vent was cut out of the side of the upper plenum and excess water was drained away. Air was supplied by an air compressor and entered the side of the lower plenum through a 0.25-m pipe. While the inside diameter of the vertical tube was varied from 0.05-0.25 m, only the 0.05-m tube was modeled. The air velocity was varied from 0.9-6.1 m/s.

The tests were performed from initial conditions of 300 K and 101 kPa. The air supply was first adjusted to a level that would prevent all liquid penetration, and then the water supply to the upper plenum was turned on. Subsequently, the air supply was reduced to permit water to penetrate the

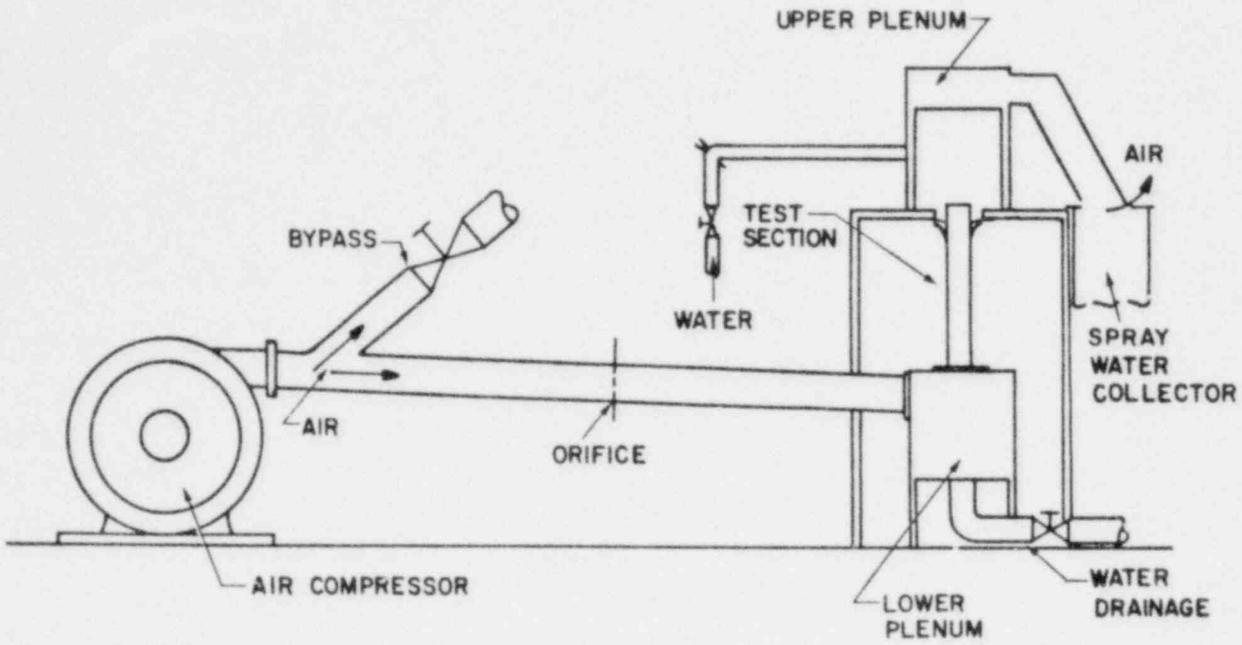

Fig. 33. Dartmouth countercurrent flow test facility.

vertical tube. The water accumulation in the lower plenum was measured as a function of time.

2. TRAC-P1A Input Model Description

Figure 34 shows a detailed noding diagram for the Dartmouth facility. The system was modeled with 7 components and 6 junctions; a total of 16 fluid cells was incorporated. The air and water were injected by fill components 7 and 5, respectively, through pipe components 1 and 8 to the plenums. The vertical tube and the plenums were represented with a vessel component (component 2, 10 axial levels, 1 radial ring, and 1 azimuthal segment). Pipe component 3 vented the liquid overflow to break component 4. The air-water option in TRAC-P1A was selected by setting IEOS (second field of the first main control data card) to 1. The steady-state calculation was run to initialize the air flow through the system before initiating the water flow. The transient calculations were then run for various water injection rates.

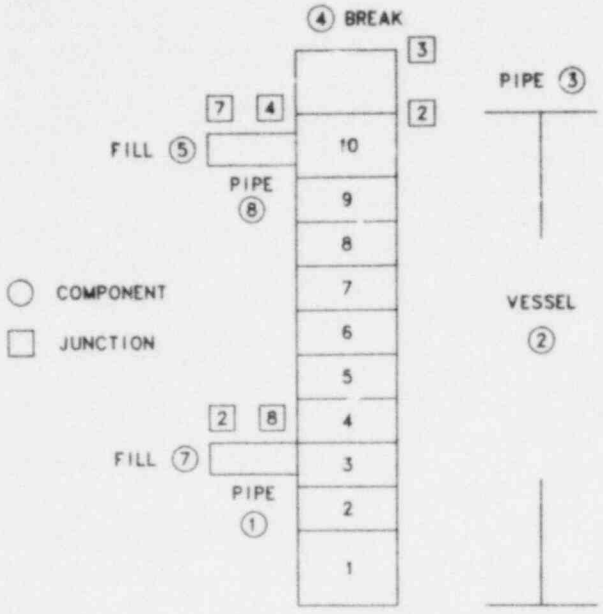

Fig. 34. Dartmouth countercurrent flow facility noding diagram.

3. Comparisons Between the Calculations and the Data

Figure 35 shows the comparison of TRAC-P1A calculations with experimental data. Case I represented the calculation with the standard TRAC-P1A code. The experimental data in Fig. 35 matches the Wallis flooding correlation[16]

$$(J_g^*)^{0.5} + (J_\ell^*)^{0.5} = 0.7 \qquad (1)$$

where

$$J_g^* = j_g \times \left(\frac{\rho_g}{gD(\rho_\ell - \rho_g)}\right)^{0.5},$$

$$J_\ell^* = j_\ell \times \left(\frac{\rho_\ell}{gD(\rho_\ell - \rho_g)}\right)^{0.5},$$

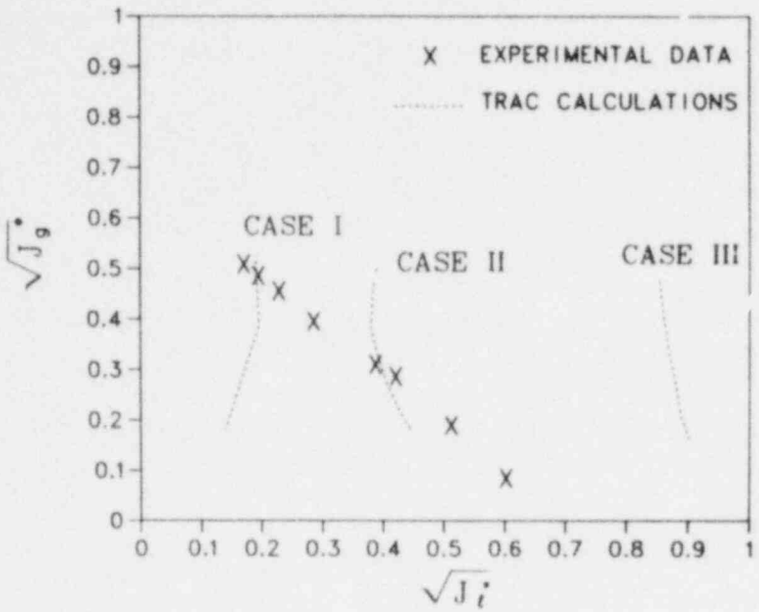

Fig. 35. Dartmouth countercurrent flow flooding curve.

ρ_g = density of vapor phase,

ρ_ℓ = density of liquid phase,

j_g = superficial vapor velocity,

j_ℓ = superficial liquid velocity,

g = gravitational force constant,

= 9.8 m/s^2, and

D = hydraulic diameter of tube.

This correlation is generally valid if the tube inside diameter is less than or equal to 0.05 m. As shown in Eq. (1), the higher the superficial vapor velocity, the smaller the liquid penetration rate under isothermal conditions.

However, the TRAC-P1A results did not show this dependence of liquid penetration rate on the superficial vapor velocity.

A detailed examination of this problem showed that the TRAC-calculated void fraction in the flooding tube varied from 30-70%. For this flow regime the interfacial shear coefficient was calculated mainly based on the assumption that the continuous liquid was flowing over a rigid bubble (or vapor flowing over a droplet). The Wallis wavy film interfacial shear coefficient is always small compared with the interfacial shear coefficient based on the droplet model. The interfacial shear coefficient in TRAC-P1A did not explicitly depend on the superficial vapor velocity. However, the agreement between the TRAC-P1A calculations and the data was good at a particular superficial gas velocity as shown in Fig. 35. The deviation between the code and the data became large as the superficial gas velocity decreased below (or increased above) this particular superficial gas velocity. This trend was consistent with that reported by Giles.[17]

Case II was the TRAC-P1A calculation of the liquid penetration rate using the following modifications to the interfacial shear formulation:

1. The bubble Weber number was set to 1.0.
2. The droplet Weber number was set to 2.0.
3. The minimum values of relative velocity and liquid velocity were limited to 0.001 m/s.

As shown in Fig. 35, these code modifications improved slightly the agreement between the code and the data. More importantly, these modifications did result in the correct trend for the liquid penetration rate.

Case III was the TRAC-P1A calculation of liquid penetration rate with the following modifications to the interfacial shear formulation:

1. If the void fraction was less than or equal to 0.3, then the TRAC-P1A interfacial shear coefficient was used.
2. If the void fraction was larger than 0.3 and less than 0.5, the interfacial shear coefficient was calculated by interpolating the values of interfacial shear coefficients at 0.3 and 0.5 void fractions.

3. If the void fraction was equal to or larger than 0.5, the interfacial shear coefficient was calculated based on the assumptions that the annular flow regime only existed under countercurrent flow conditions (Ref. 18) and the fraction of entrained droplets was negligibly small compared with the fraction of liquid in falling film form. Then, the interfacial shear coefficient, C_{iz}, can be written

$$C_{iz} = 1.26 \times 10^{-2} \left(1.0 + \frac{300\ \delta}{D}\right) \alpha^{-1.7} \qquad (2)$$

where

δ = liquid film thickness,

D = flooding tube diameter, and

α = void fraction.

Equation (2) has the form of a Wallis wavy film interfacial shear coefficient for a void fraction close to 1.0. However, these modifications to the interfacial shear coefficient did not improve the agreement between the calculations and the data. The code consistently overestimated the liquid penetration rate for a gas velocity range of 0.9-6.1 m/s.

4. Conclusions and Observations

Whereas the comparisons for the Dartmouth countercurrent flow air-water tests were not particularly good, the TRAC-P1A calculations agreed very well with experimental data in both the Idaho National Engineering Laboratory (INEL) air-water tests[17] and the Creare downcomer penetration tests.[19] The average gas velocity was ~3 m/s for the Dartmouth tests and ~90 m/s for the INEL and Creare tests. It is possible that the dispersed flow regime dominated in the INEL and Creare tests because of the high gas velocity, whereas separated flow dominated in the Dartmouth tests. The flow regime was not determined experimentally during the Dartmouth tests. The flow regime map used in TRAC-P1A to determine the interfacial shear coefficient was based on the simplified combinations of

cocurrent vertical and horizontal flow regime maps, and the resulting composite flow regime map may not be applicable to countercurrent flow conditions.

The manner in which the Dartmouth tests were simulated also may have contributed to the poor comparisons to data. The tests were conducted by establishing a high air flow up the tube to prevent liquid penetration until a stable liquid pool had formed in the upper plenum. The air flow was then reduced to the test value. However, in the calculation the air flow was first set to the specified value for that test, and then the liquid flow was initiated. Hysteretic effects may have affected the results adversely. Also, pool depth and entrance effects to the vertical tube were not accounted for properly and may have affected the outcome.

E. LOFT Large-Break LOCA Tests

The LOFT (Loss-of-Fluid-Test) facility[20] is a volume-to-power scaled model of a PWR; the system maintains the same relative volume distribution as the PWR. The facility was designed to simulate LOCAs and has the flexibility to simulate a large variety of transients that have been hypothesized to occur in a full-scale PWR. LOFT has a nuclear core and all other equipment to enable the facility to simulate in detail a PWR performance. LOFT has a maximum core power of 50 MW_t (megawatts thermal), which makes the facility ~1/60 scale.

The initial two test series conducted at LOFT were large-break simulations. The first series consisted of isothermal (zero core power) blowdowns. The nuclear core was installed just before test L1-5, the final isothermal test. The second test series, the power ascension series, required successive facility power increases. Tests L2-2 and L2-3 were the initial tests in the second series. Analyses for L1-5, L2-2, and L2-3 are compared to the data.

The LOFT system configuration was the same for these three tests. The principal parameter varied was the steady-state core power. The initial and boundary conditions for each test reflected the differences in core power. Each test produced data on integral systems effects through the entire LOCA sequence. The three tests investigated the sensitivity of the code to differences in core power.

1. Facility and Test Descriptions

LOFT simulates noncommunicating breaks in the primary coolant system. To provide this simulation, the system consists of the pressure vessel and two coolant loops. The vessel is 6.6 m high and has an inside diameter of 1.5 m. The vessel contains the inlet distribution annulus, an annular downcomer, upper and lower plenums, and the nuclear core. The core contains 1300 fuel pins that are 1.68 m long and are arranged into 9 bundles. The bundles represent a 15-by-15 rod array spacing.

The broken loop was configured to represent a 200% double-ended, noncommunicating, cold-leg break. As such, the broken loop did not form a circulating loop for the vessel. The pump and steam generator in the broken loop were represented as hydraulic resistances (through two sets of orifice plates). The break simulation was achieved through quick-opening blowdown valves installed in the broken-loop cold and hot legs; these valves opened in ~20 ms. The break areas were scaled to maintain prototypical transient times; the scaling produced break diameters of 10.32 cm.

The intact loop consisted of two active pumps and an active steam generator. Scaled to represent three PWR loops during the transient, an intact loop had to carry the entire thermal load during steady-state operation because of the passive steam generator in the broken loop. The two pumps were connected in parallel. The pressurizer was connected to the hot leg of the intact loop. For the three tests under consideration, the ECC system, consisting of a LPIS, a HPIS, and an accumulator system, was valved into the intact-loop cold leg.

Before each test the desired steady-state conditions were achieved. For tests L2-2 and L2-3, these included operation of the reactor at power for sufficient time to establish equilibrium fission product concentrations for proper decay heat during the transient. For all three tests the pump speeds were controlled to a constant value for the portion of the transient analyzed. At time zero the quick-opening blowdown valves were opened, and the system began to depressurize. Reactor scram and steam generator shutdown were accomplished on normal trips. The ECC system also functioned based on usual set points.

2. TRAC-P1A Input Model Description

The input models used to analyze the three tests were effectively the same; the information regarding initial and boundary conditions was test specific. Certain minor modifications were made to the input as new or updated information

became available. Also, slight differences existed because of selective changes in the calculational sequence. The following discussion is specifically applicable to the L2-3 input and generally applicable to L1-5 and L2-2.

The input model consisted of 27 components with a total of 322 hydraulic cells. The component noding scheme is shown in Fig. 36. The reactor vessel was modeled with the vessel component and consisted of 12 axial levels, 4 radial rings, and 4 azimuthal segments (192 cells). The core, a subset of the vessel component, had 5 axial levels, 3 radial rings, and 60 cells. The reflood fine-mesh noding was activated 10 s after the initiation of accumulator injection. Five uniform fine nodes were used in the rods for each core level, totaling 25 fine nodes over the entire length of the fuel rod. The numerics were semi-implicit throughout the model except at the break, where fine nodes were used to represent the nozzles.

Steady-state calculations were made for all three tests to initialize the steady-state conditions before running the transient calculation. Sufficient iterations were made on the steady-state calculations to achieve the desired set of initial conditions. The transient calculations were initiated from the final steady-state dumps.

3. Comparisons Between the Calculations and the Data

The comparisons for each of the three tests are discussed separately. The results for all three tests were qualitatively similar; therefore, the discussion for L1-5 and L2-2 are relatively brief, and the discussion for L2-3 is expanded. Test L1-5 is discussed first, followed by L2-2 and L2-3. The discussion follows the sequence and severity of the test performance and analyses. For those figures in which a calculated temperature is compared to two or three data traces, the data curves approximately correspond to the minimum, maximum, and mean (if there are three curves) of the data.

3.1. LOFT Test L1-5 Data Comparisons

The L1-5 (Ref. 21) calculation was made after the test and used the measured initial conditions. Those conditions are briefly summarized in Table VIII. The initial conditions calculated by TRAC-P1A were within the data uncertainties of the measured initial conditions.

Figure 37 shows the system depresurization for test L1-5. The calculated depressurization agrees well with the test data.

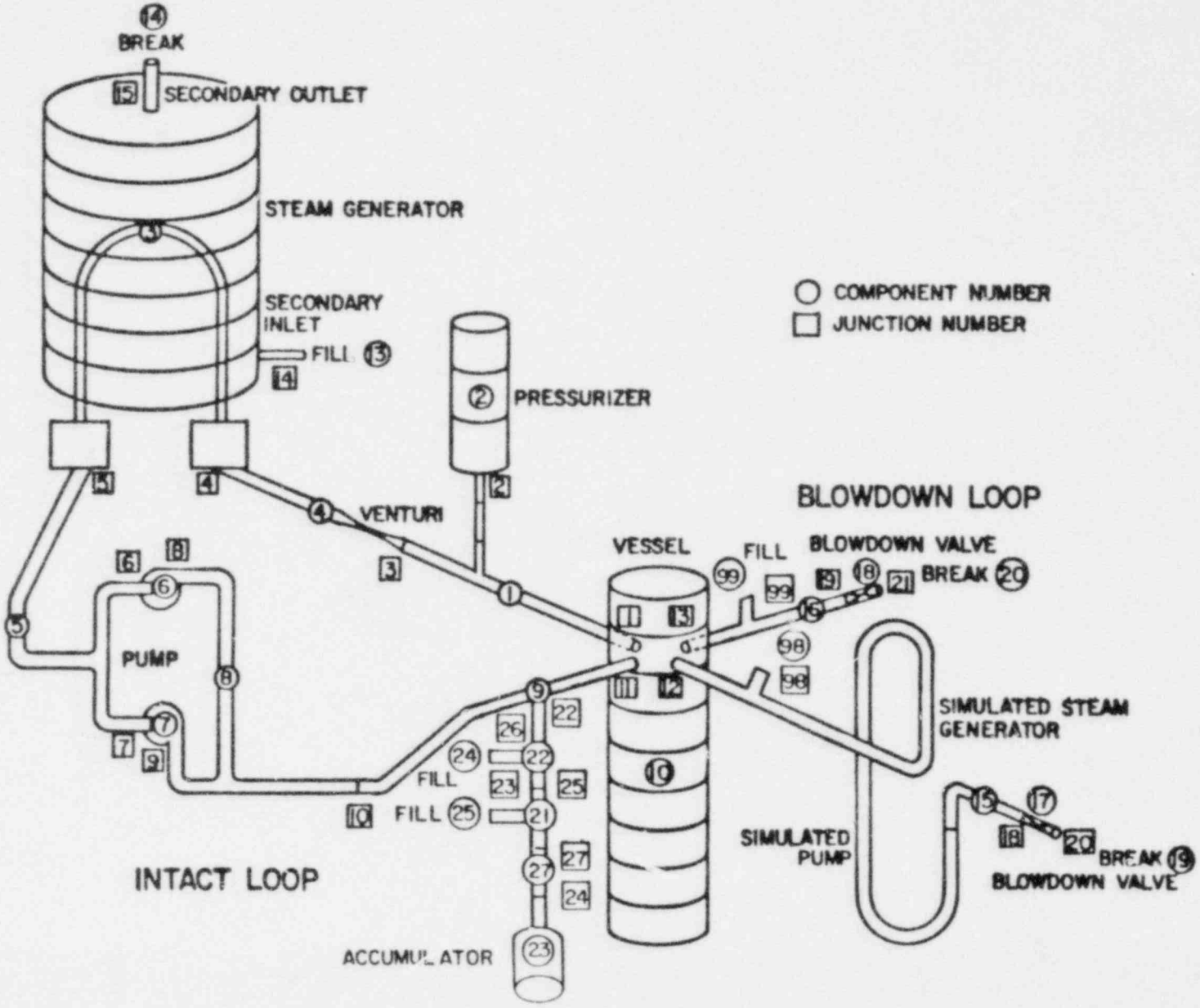

Fig. 36. LOFT large-break tests input schematic.

TABLE VIII

LOFT LARGE-BREAK LOCA TESTS
SUMMARY INITIAL CONDITIONS

	LOFT Test		
	L1-5	L2-2	L2-3
Core power (MW_t)	0	25	36
Maximum linear heat generation rate (kW/m)	0.0	26.4	39.4
System pressure (MPa)	15.55	15.50	15.06
Hot-leg temperature (K)	555	581	593
Core ΔT (K)	0	22	32
Mass flow (kg/s)	176	205	199

Figure 38 shows the density in the broken-loop cold leg. The data spikes between 20 and 30 s were the result of ECC bypass. The code predicted the voiding of the broken cold leg slightly late, and the calculated spikes caused by the ECC bypass were 20 s late. (There is a slight rise in the calculated density at the time of the initial spikes in the data; the calculated increase in the density can be interpreted as evidence of initial ECC bypass.) The broken-loop cold-leg mass flow is shown in Fig. 39. The trend of the data and the density both indicate that the flow saturated very early in the transient. The code apparently underpredicted the flow early, but there is no evidence of the underprediction in the pressure comparison.

The broken-loop hot-leg density and mass-flow comparisons are shown in Figs. 40 and 41. TRAC-P1A predicted both parameters very well. The pressure comparison (Fig. 37) and the two broken-loop flows (Figs. 39 and 41) collectively indicate that the code predicted the blowdown hydrodynamics very well.

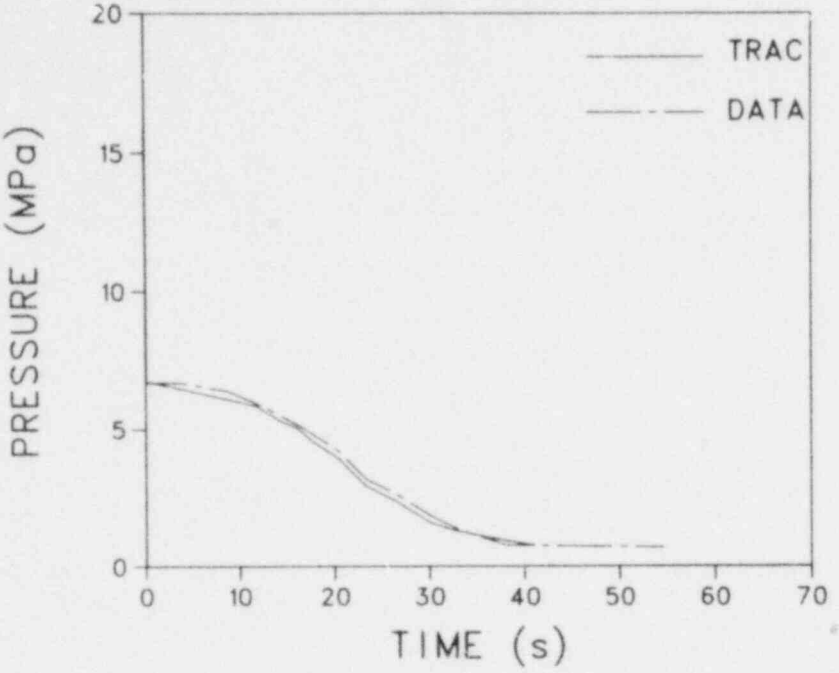

Fig. 37. LOFT test L1-5 intact-loop hot-leg pressure (DE-PR-2). Data uncertainty is ~250 kPa.

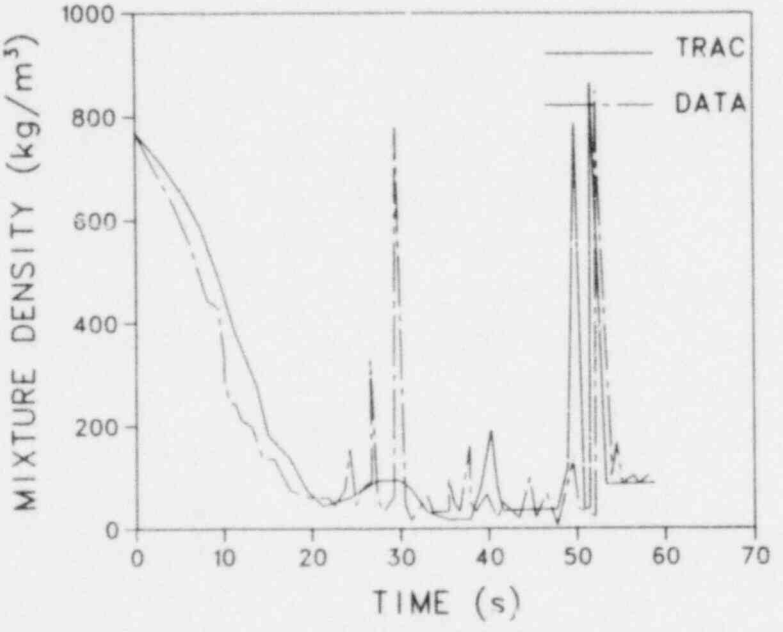

Fig. 38. LOFT test L1-5 broken-loop cold-leg density (DE-BL-105). Data uncertainty is ~20 kg/m^3.

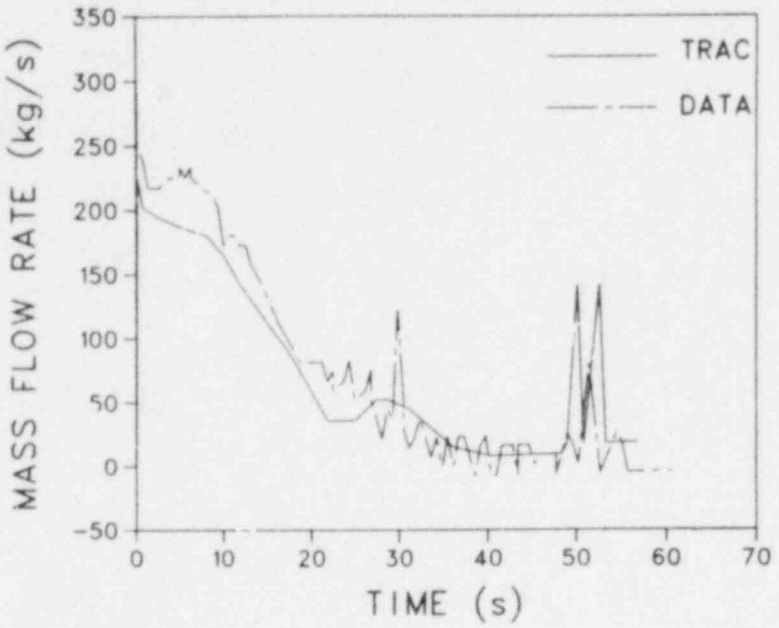

Fig. 39. LOFT test L1-5 broken-loop cold-leg mass flow (PdE-BL-2 and DE-BL-1).

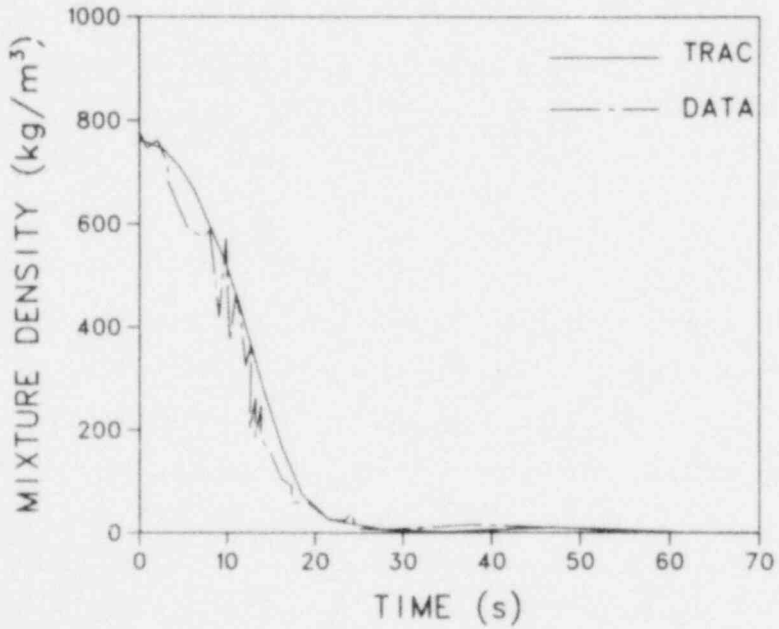

Fig. 40. LOFT test L1-5 broken-loop hot-leg density (DE-BL-205). The data uncertainty is ~20 kg/m^3.

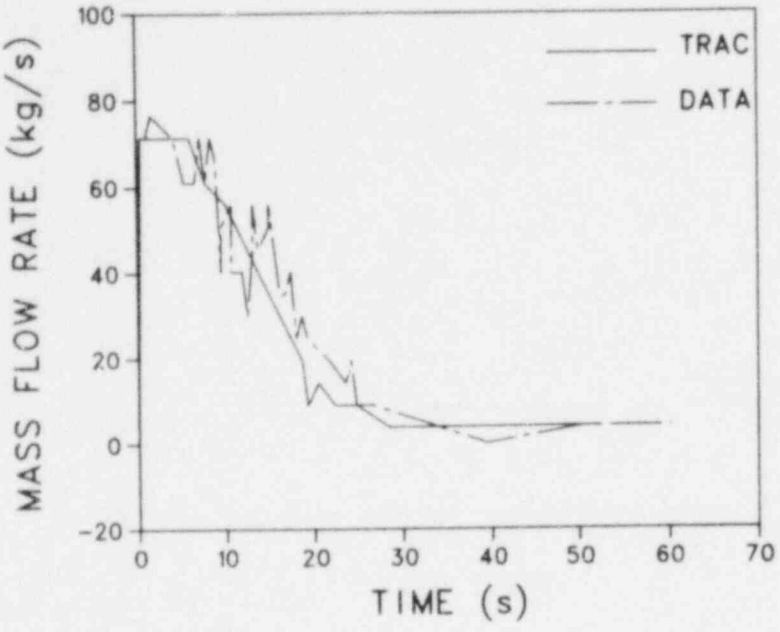

Fig. 41. LOFT test L1-5 broken-loop hot-leg mass flow (PdE-BL-1 and DE-BL-2).

Figure 42 shows a typical cladding temperature comparison. For the first 22 s both the code and the data followed saturation; after that time the calculated void fraction went to 1.0 and the temperature deviated from saturation. The thermocouple did not drv out until ~35 s. This comparison indicated that the calculated liquid inventory in the core region might have been low.

3.2. LOFT Test L2-2 Data Comparisons

Table VIII summarizes the initial conditions for test L2-2.[22] The initial calculation was a blind pretest prediction; however, a combination of significant differences between the anticipated and actual initial conditions for the test and an input error forced a new calculation. The second calculation was made after the test with actual initial conditions but before the release of the data. Again, the calculated steady-state conditions were within the data uncertainties of the measured conditions.

Figures 43-45 show, respectively, the system pressure, the broken-loop cold-leg flow, and the broken-loop hot-leg flow. The pressure comparison was very good, although there were two periods (~5 and 20 s) when the code slightly

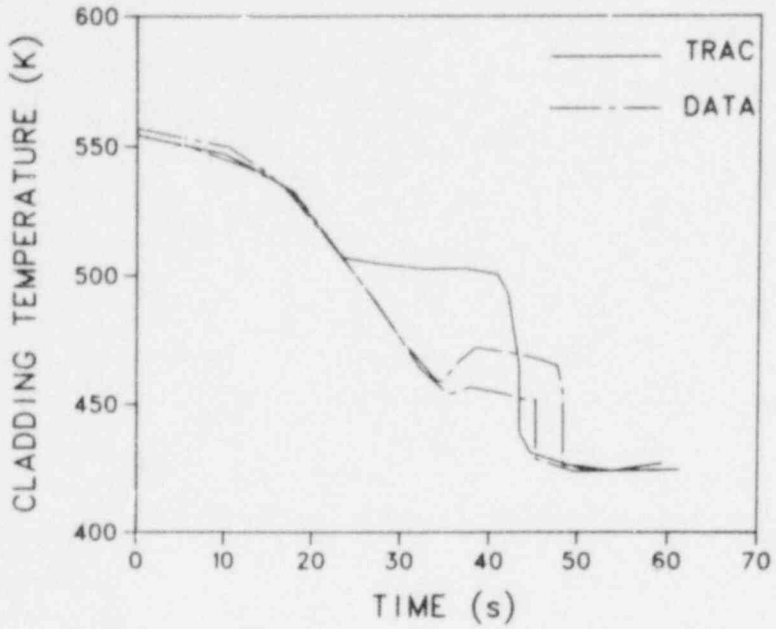

Fig. 42. LOFT test L1-5 cladding temperature (TE-5E08-049 and TE-5F03-024).

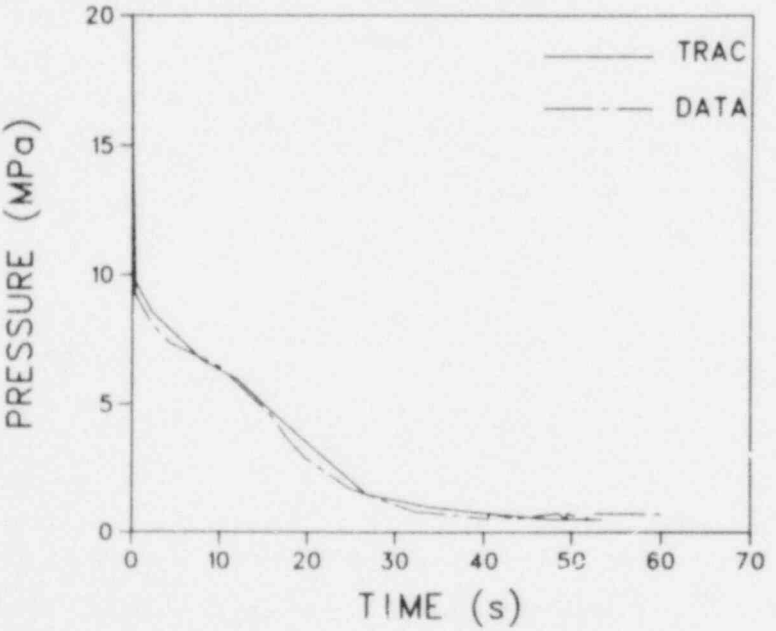

Fig. 43. LOFT test L2-2 vessel pressure measured at the downcomer stalk (PE-2ST-001A). The data uncertainty is ~250 kPa.

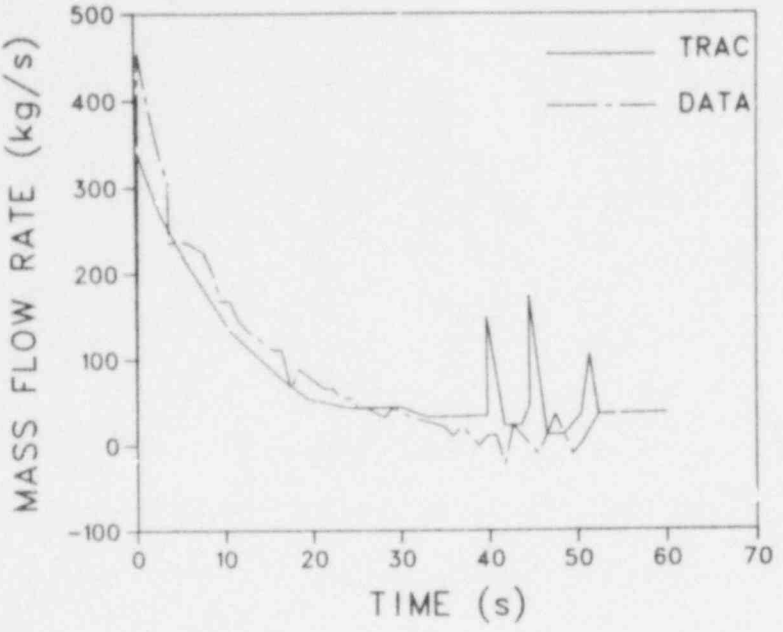

Fig. 44. LOFT test L2-2 broken-loop cold-leg flow (FR-BL-116). The data uncertainty is ~70 kg/s.

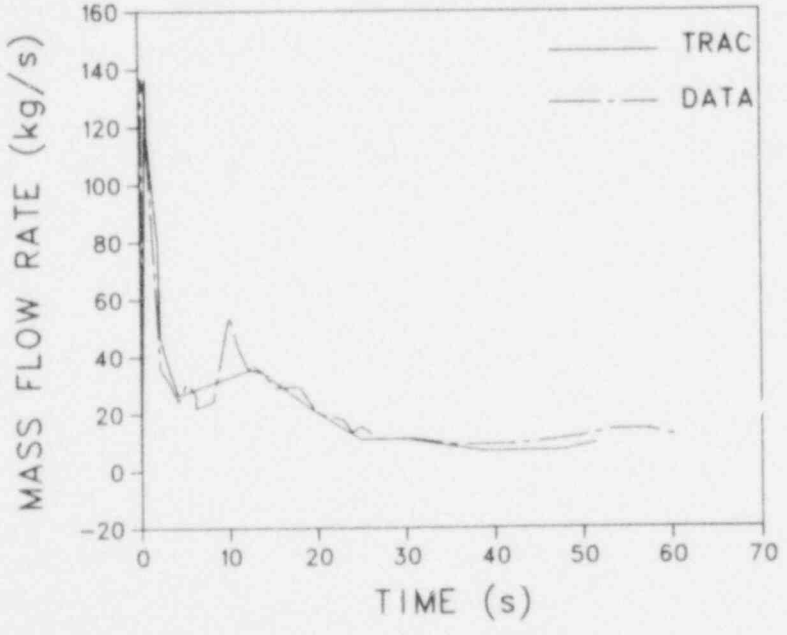

Fig. 45. LOFT test L2-2 broken-loop hot-leg flow (FR-BL-216). The data uncertainty is ~25 kg/s.

overpredicted the data. The broken-loop cold-leg mass flow was underpredicted early; the underprediction was caused by TRAC-P1A calculating near-equilibrium conditions in the nozzle just after the beginning of the transient, whereas the data did not saturate upstream of the break until ~4 s. After the data saturated, the mass-flow comparison was good. The arrival time of the ECC bypass into the broken cold leg was predicted well, but the magnitude of the calculated spikes associated with the ECC bypass was too large. The broken-loop hot-leg mass-flow comparison was good; the nonequilibrium effects initially were mitigated by the combination of a higher initial fluid temperature and the larger hydraulic resistance associated with the steam generator and pump simulators.

The accumulator injection flow, the intact-loop cold-leg fluid temperature, and the intact-loop hot-leg fluid temperature are shown in Figs. 46-48. The timing of the accumulator injection was calculated correctly. The peak accumulator flow was reasonably well predicted. The calculated initial spike, which was not reflected in the data, was caused by the liquid in the accumulator

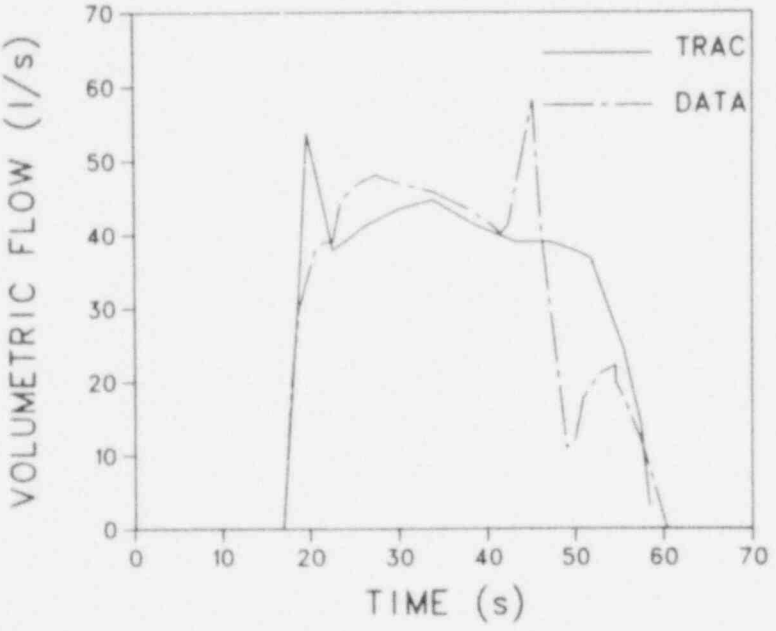

Fig. 46. LOFT test L2-2 accumulator flow (FT-P120-36-1). The data uncertainty is ~3.5 ℓ/s.

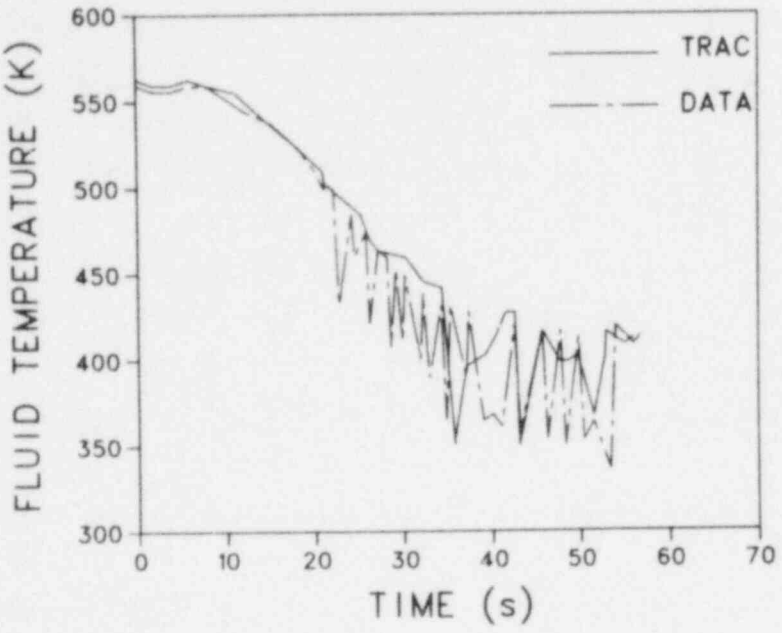

Fig. 47. LOFT test L2-2 intact-loop cold-leg fluid temperature (TE-PC-00i). The data uncertainty is ~6 K.

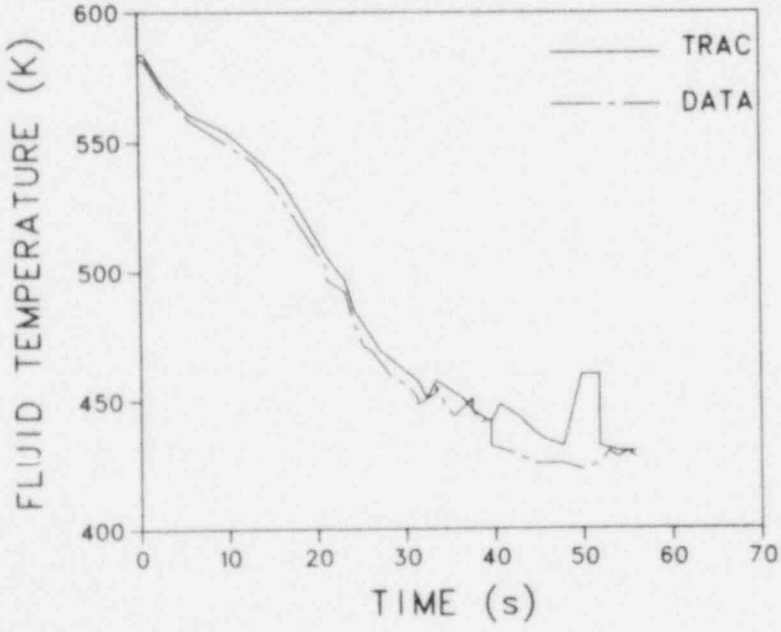

Fig. 48. LOFT test L2-2 intact-loop hot-leg fluid temperature (TE-PC-002). The data uncertainty is ~6 K.

injection line that was initialized at too high a temperature and subsequently voided during the depressurization transient before accumulator injection. The intact-loop cold-leg fluid-temperature comparison was good; the oscillations in the data that began at 21 s were caused by the cold accumulator water moving upstream to the measurement location. The code did not calculate the presence of the ECC water at the measurement location until 33 s. The intact-loop hot-leg fluid-temperature comparison was good; both the code and the data followed saturation until ~38 s when the code calculated the arrival of superheated vapor from the core.

Figures 49 and 50 show cladding temperature comparisons. Figure 49 is the comparison for the central core region (ring 1, core level 3); the code calculated the early critical heat flux (CHF) that is evident in the data but not the early rewet at 10 s. Therefore, after the peak cladding temperature was reached, the comparison degraded substantially. Figure 50 shows the cladding temperature comparisons at the midplane of the peripheral rods (ring 3, core level 3); for this comparison the code calculated properly all of the dryouts

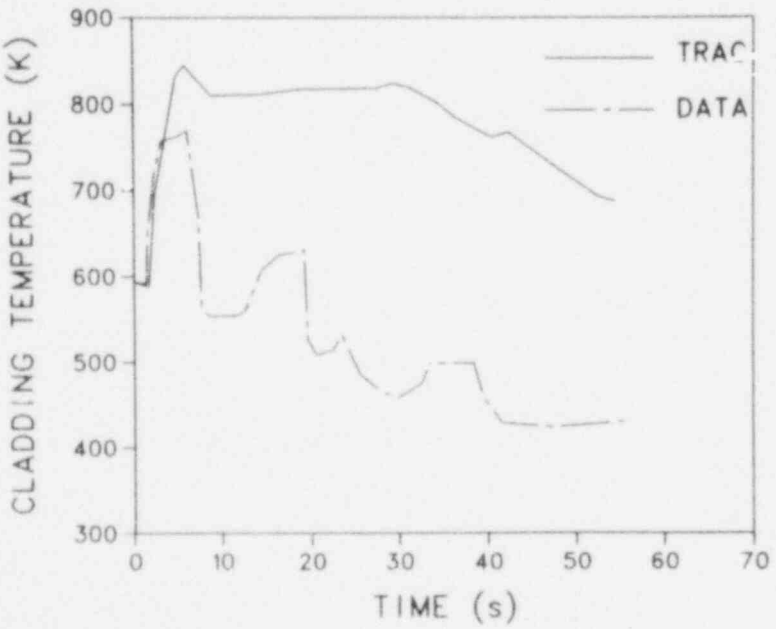

Fig. 49. LOFT test L2-2 cladding temperature in the high-powered region (TE-5G8-026). The data uncertainty is ~6 K.

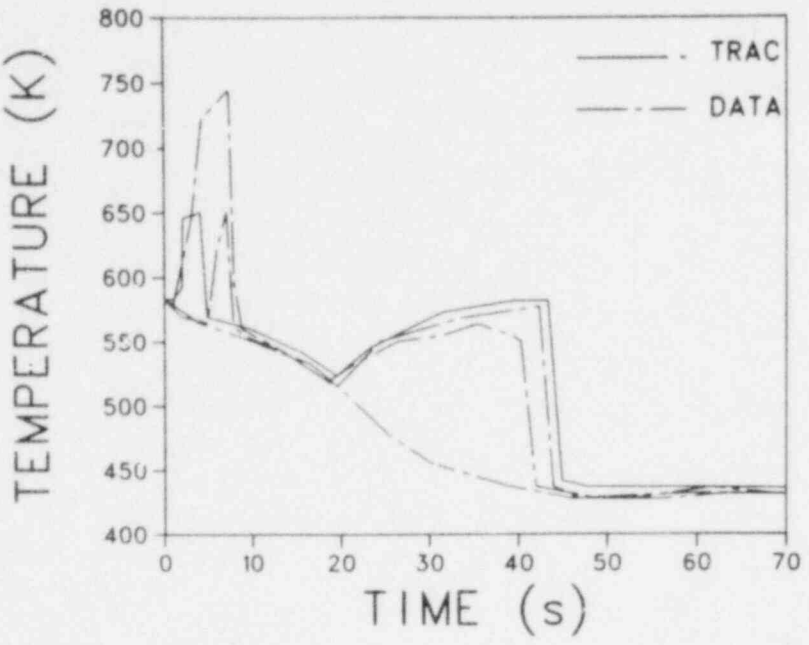

Fig. 50. LOFT test L2-2 cladding temperature at the midplane position for the peripheral rods (TE-4G14-030, TE-1B11-022, and TE-1B11-028). The data uncertainty is ~6 K.

and the rewets. This second temperature comparison is significant because it implies that the calculated hydraulics in the core periphery were proper for the rewet. The peak clad temperature in Fig. 49 was overpredicted but the timing of the initial dryout and rewet cycle (the rewet in the core periphery) was correct. The implication is that the stored energy in the rod is high.

3.3. LOFT Test L2-3 Data Comparisons

A pretest prediction was made for LOFT test L2-3. Table VIII summarizes the steady-state operating conditions for this test.[23] The calculated initial conditions for the pretest prediction were within the data uncertainties of the measured conditions, as the anticipated initial conditions were acceptably close to the actual initial conditions.

The upper-plenum pressure for test L2-3 is shown in Fig. 51. TRAC-P1A overpredicted the pressure during the first 40 s of the transient. The overprediction was significant only between 15 and 35 s, and the result was a small delay in beginning the accumulator injection.

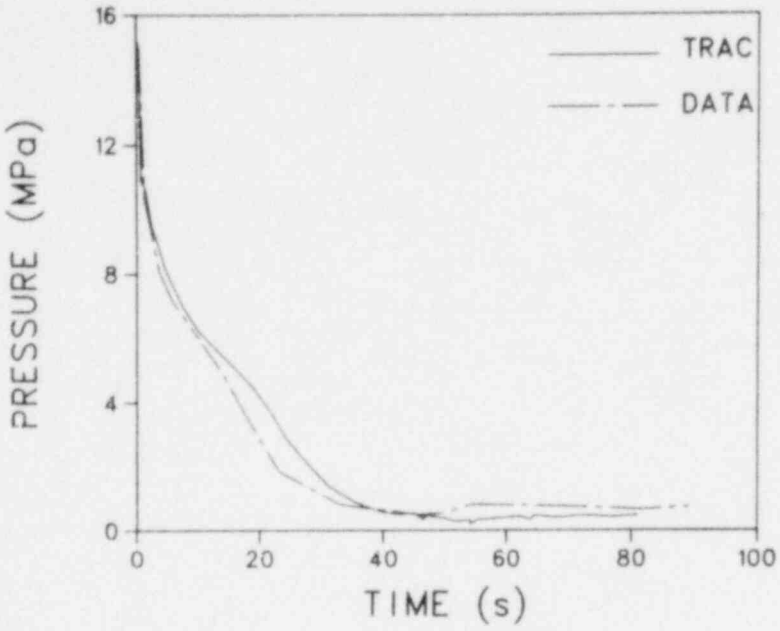

Fig. 51. LOFT test L2-3 upper-plenum pressure (PE-1UP-001A). The data uncertainty is ~200 kPa.

Figures 52 and 53 show the mixture density and mass flow in the broken-loop cold leg. Upstream of the break the broken-loop cold leg voided more slowly than in the data. The spikes from 25-55 s resulted from ECC bypass; the code predicted these spikes relatively well. The large, prolonged calculational spike in density between 60-80 s was not reflected in the data. The broken-loop cold-leg mass flow was underpredicted during the initial 5 s; this underprediction was the same problem that was seen in the L2-2 comparisons. After the break saturated in the test, the comparison was good.

Figures 54 and 55 show the broken-loop hot-leg density and mass flow. The code predicted the proper voiding of the broken-loop hot leg, although there was one calculated oscillation at 10 s (see Fig. 54) that was not reflected in the data. The mass flow in the broken hot leg, as in L2-2, was good.

The thermal-hydraulic comparisons for the intact-loop cold leg are shown in Figs. 56-60. The accumulator injection began 2 s late because of the overprediction of system pressure. The calculated peak accumulator flow compared well to data. The calculated integrated volumetric flow was greater than the measured integrated flow and indicated that too much ECC was injected

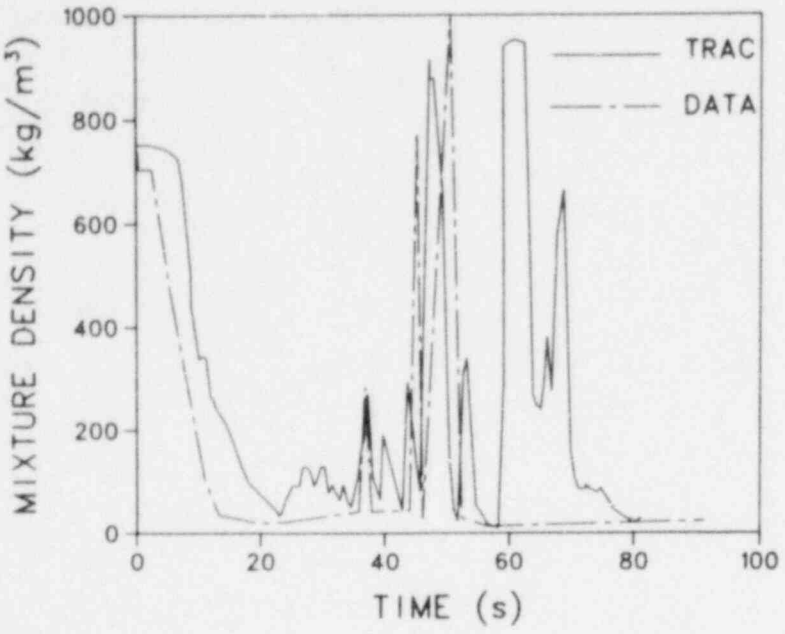

Fig. 52. LOFT test L2-3 broken-loop cold-leg density (DE-BL-105). The data uncertainty is ~130 kg/m^3.

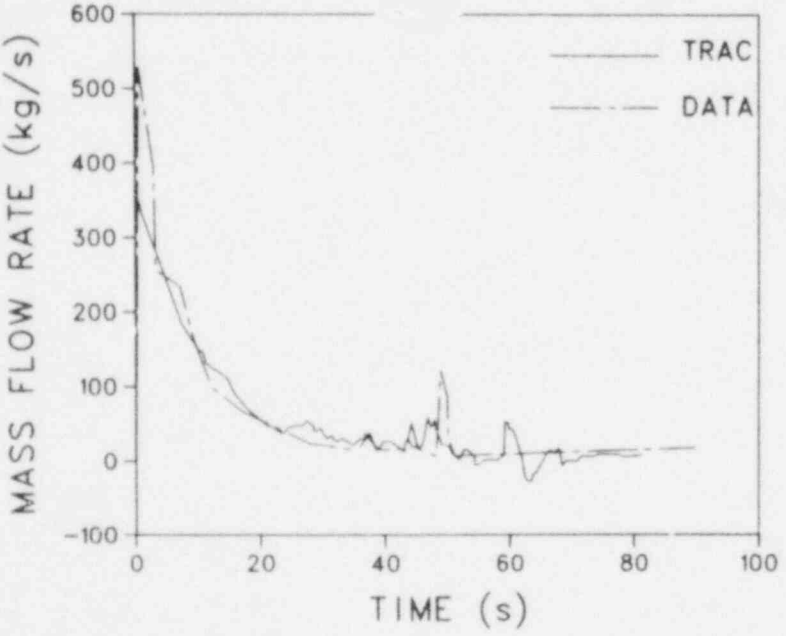

Fig. 53. LOFT test L2-3 broken-loop cold-leg mass flow (FR-BL-116). The data uncertainty is ~69 kg/s.

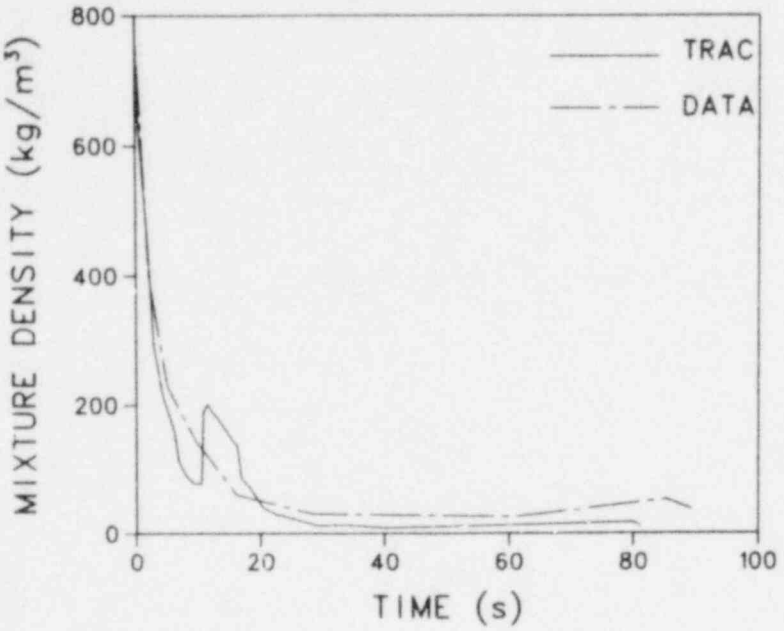

Fig. 54. LOFT test L2-3 broken-loop hot-leg density (DE-BL-205). The data uncertainty is ~150 kg/m^3.

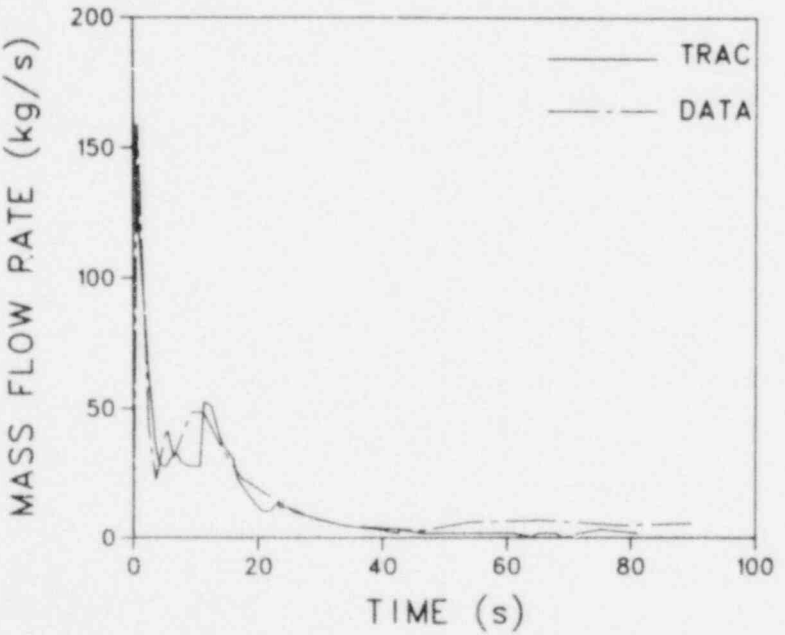

Fig. 55. LOFT test L2-3 broken-loop hot-leg mass flow (FR-BL-216). The data uncertainty is ~24 kg/s.

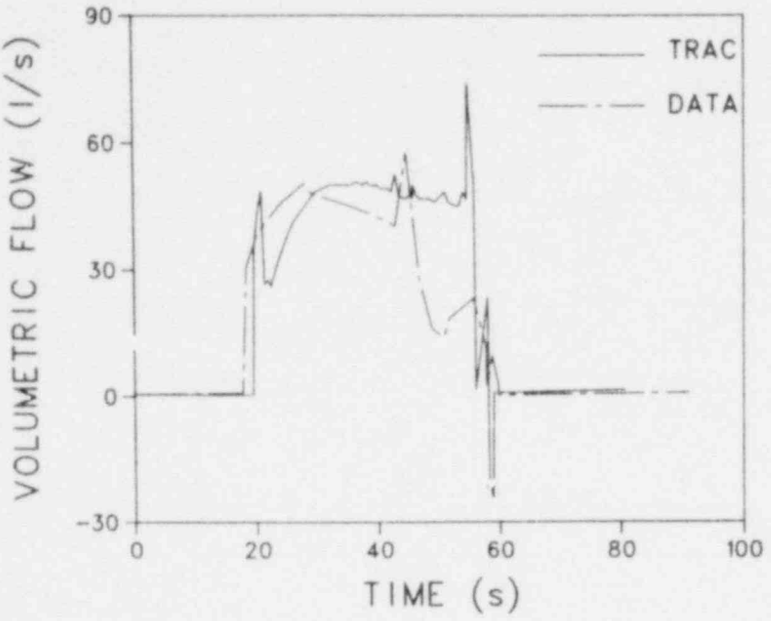

Fig. 56. LOFT test L2-3 accumulator discharge flow (FT-P120-36-1). The data uncertainty is ~1.25 ℓ/s.

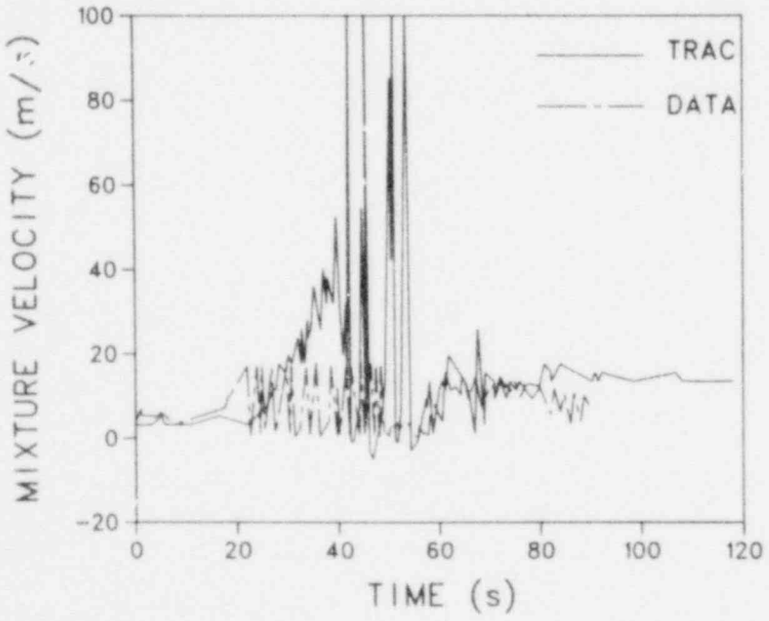

Fig. 57. LOFT test L2-3 intact-loop cold-leg mixture velocity (FE-PC-001). The data uncertainty is ~0.6 m/s.

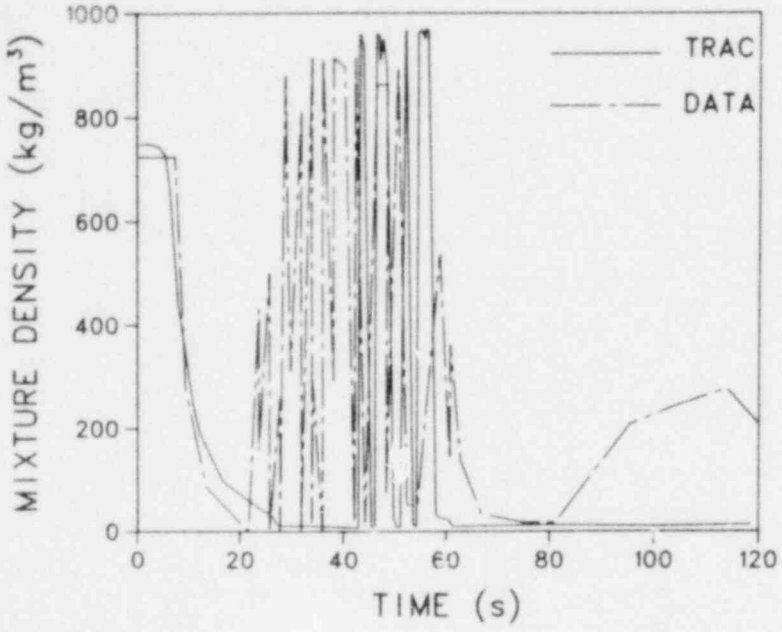

Fig. 58. LOFT test L2-3 intact-loop cold-leg density (DE-PC-105). The data uncertainty is ~160 kg/m^3.

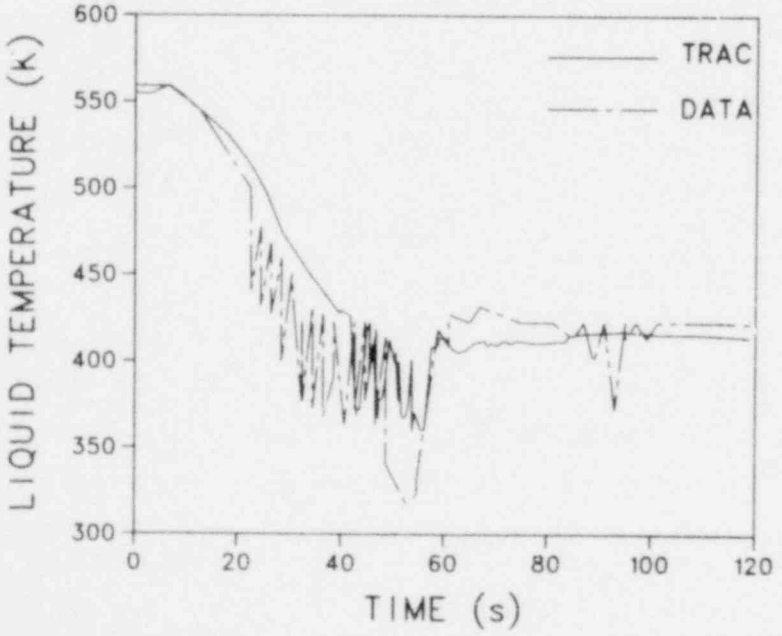

Fig. 59. LOFT test L2-3 intact-loop cold-leg fluid temperature (TE-PC-001). The data uncertainty is ~3 K.

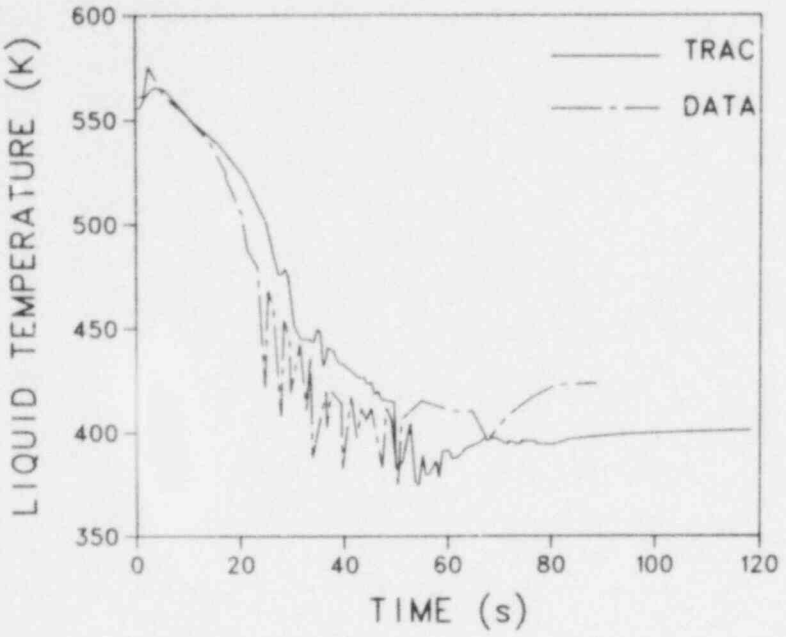

Fig. 60. LOFT test L2-3 downcomer fluid temperature (TE-2ST-014). The data uncertainty is ~5 K.

from the accumulator. The mixture-velocity comparison (Fig. 57) was good for the intact-loop cold leg. During the accumulator injection the calculated velocity increased substantially with some very large velocity spikes, but the data during this time was bouncing against the upper range limit on the meter. The cold-leg density (Fig. 58), upstream of the ECC injection location, indicated the presence of the ECC water by 22 s, whereas the code did not calculate the ECC at that location until 43 s. Based on the density comparison, it appears that the code permitted less upstream movement of the ECC. The liquid temperature comparison (Fig. 59) was similar to the density comparison with the data indicating subcooled liquid upstream of the injection point 20 s before the code. The fluid temperature in the vessel (Fig. 60) also indicated either more ECC or more liquid subcooling during the period of ECC injection than the code.

The intact-loop hot-leg thermal hydraulics are summarized in Figs. 61 and 62. The voiding behavior was calculated well, although there was a spike at 10 s that was not calculated sharply enough. The mixture-velocity comparison indicated that there were periods during the first 40 s when the code predicted

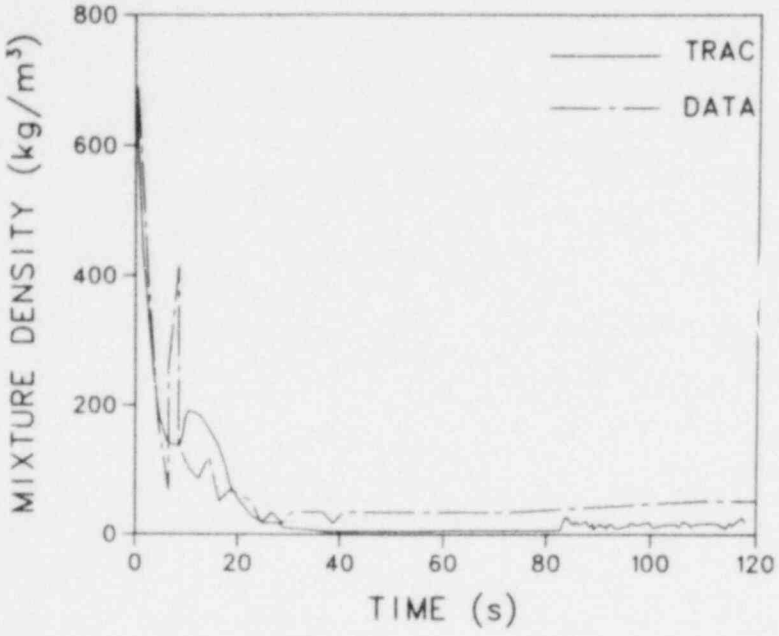

Fig. 61. LOFT test L2-3 intact-loop hot-leg density (DE-PC-205). The data uncertainty is ~150 kg/m^3.

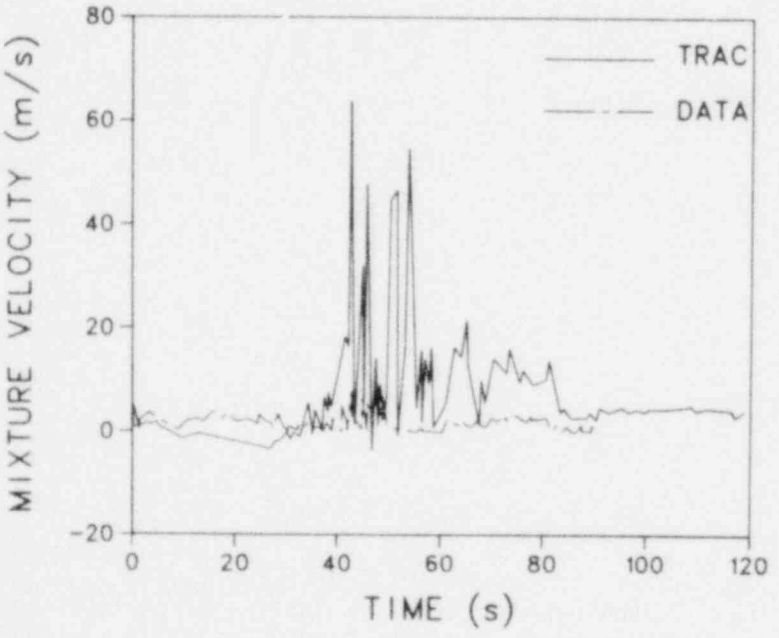

Fig. 62. LOFT test L2-3 intact-loop hot-leg mixture velocity (FE-PC-002). The data uncertainty is ~0.6 m/s.

the wrong flow direction. Between 40-60 s the code predicted high velocities that were not evident in the data; during this period the code predicted the quenching of portions of the core.

Figures 63-71 give the comparisons of the calculated cladding temperatures to the measured temperatures. For those figures with two data traces, the data were chosen to bracket all the applicable data. Not all of the figures will be discussed, but the nine figures did map the cladding behavior for core azimuthal segment 1. Early and sustained dryouts were calculated only for core level 3, rings 1 and 2. All other regions of the core were calculated to undergo repeated dryout/rewet cycles or substantially delayed dryouts. In certain cases the calculated delayed dryouts were not supported by the data. The code overpredicted the initial peak cladding temperature only in the central core region (level 3, ring 1). This thermal behavior indicated that the proper hydraulics existed in the core for rewets to occur. The lack of rewets in level 3, rings 1 and 2, must be interpreted either as a deficiency in the heat-transfer correlations or as an indication that, for whatever reason, the

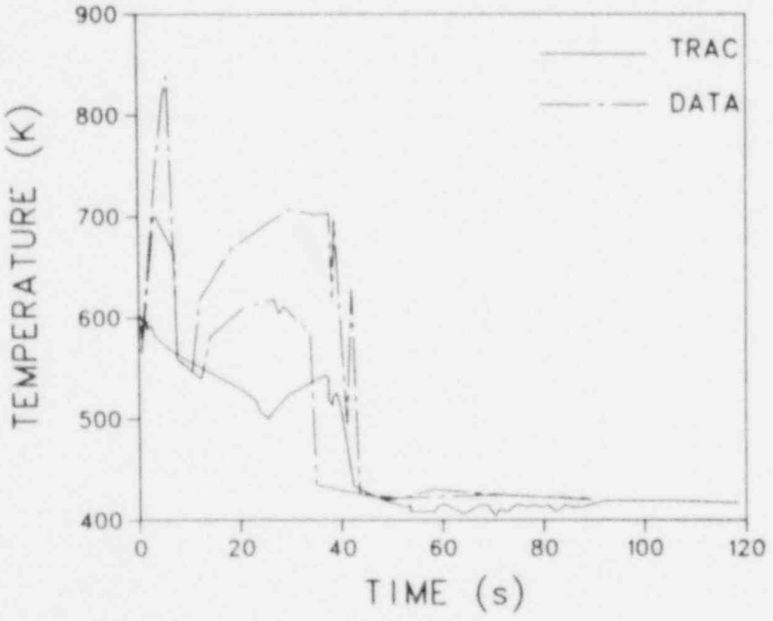

Fig. 63. LOFT test L2-3 cladding temperature, ring 1, core level 1 (TE-5H5-002 and TE-5F9-011). The data uncertainty is ~6 K.

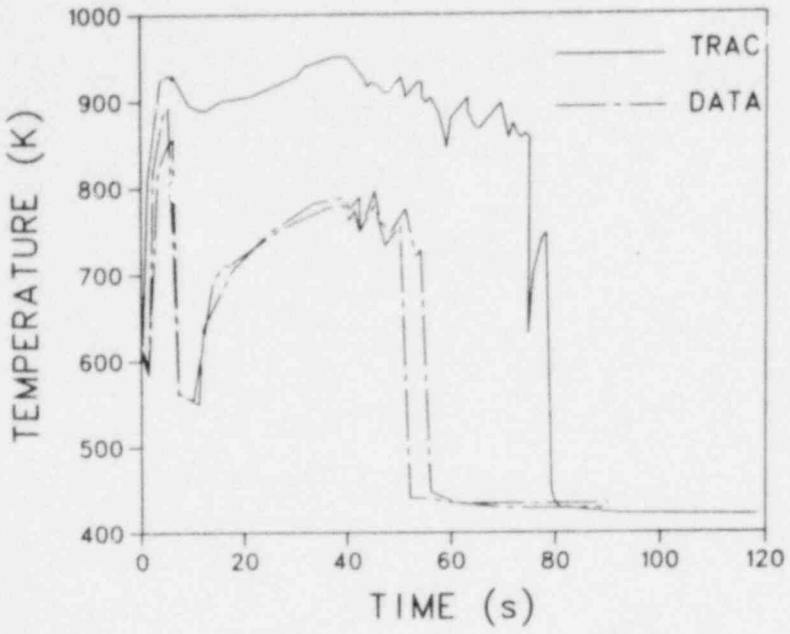

Fig. 64. LOFT test L2-3 cladding temperature, ring 1, core level 3 (TE-5F4-026 and TE-5I8-026). The data uncertainty is ~6 K.

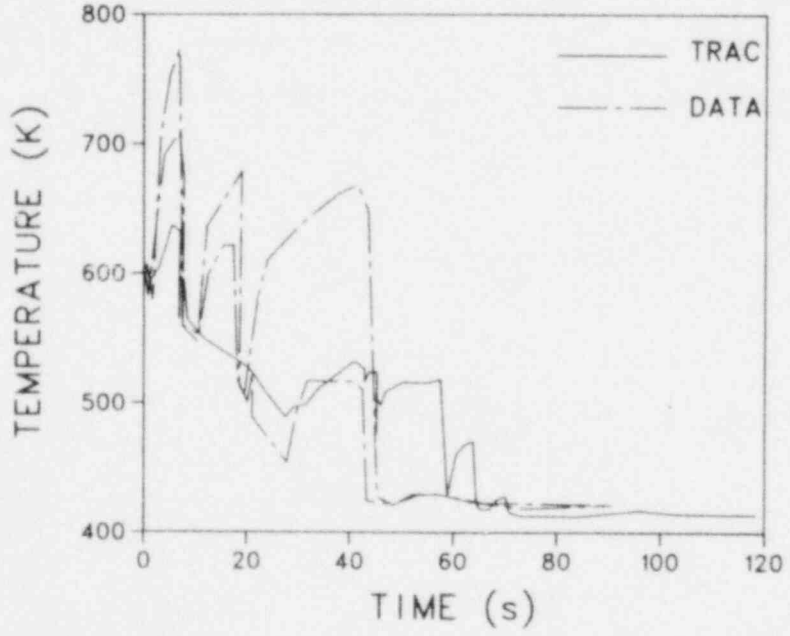

Fig. 65. LOFT test L2-3 cladding temperature, ring 1, core level 5 (TE-5J7-062 and TE-5H5-049). The data uncertainty is ~6 K.

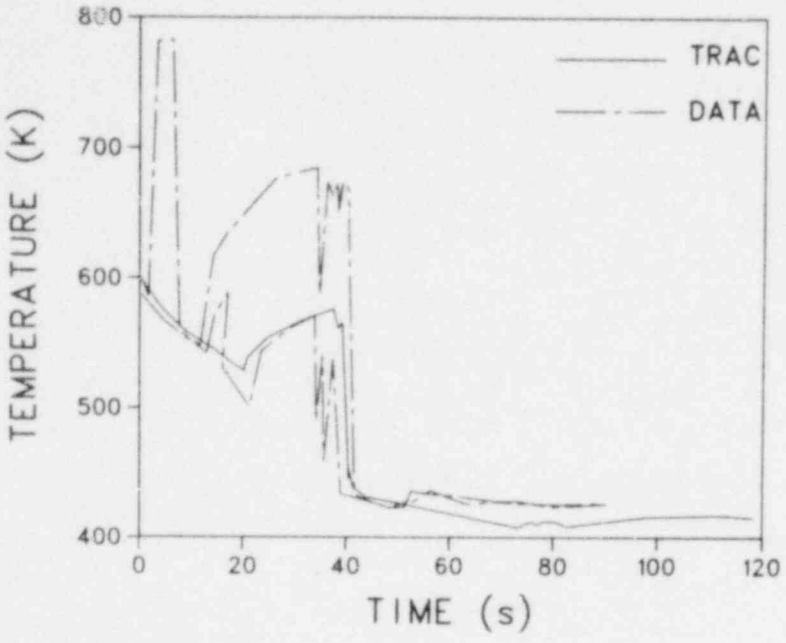

Fig. 6. LOFT test L2-3 cladding temperature, ring 2, core level 1 (TE-2G14-011 and TE-2E8-011). The data uncertainty is ~6 K.

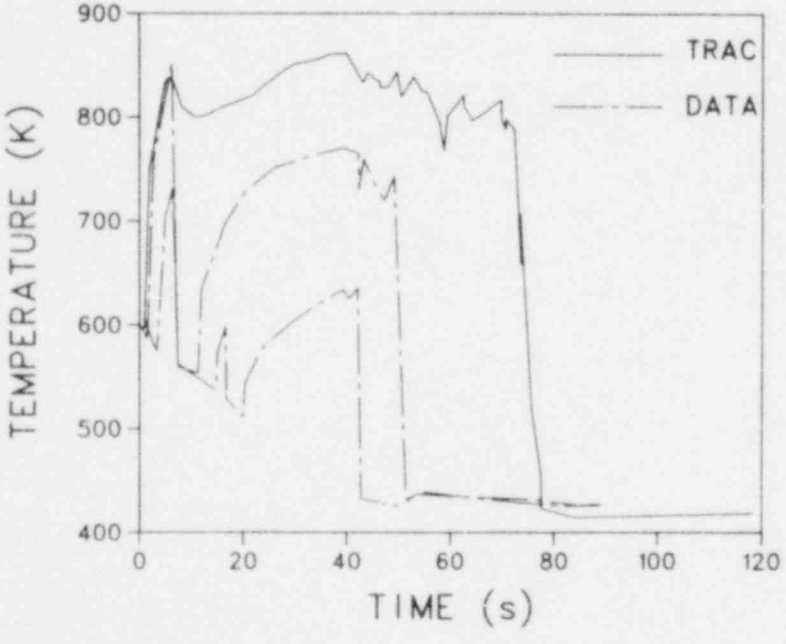

Fig. 67. LOFT test L2-3 cladding temperature, ring 2, core level 3 (TE-2H15-026 and TE-1B11-028). The data uncertainty is ~6 K.

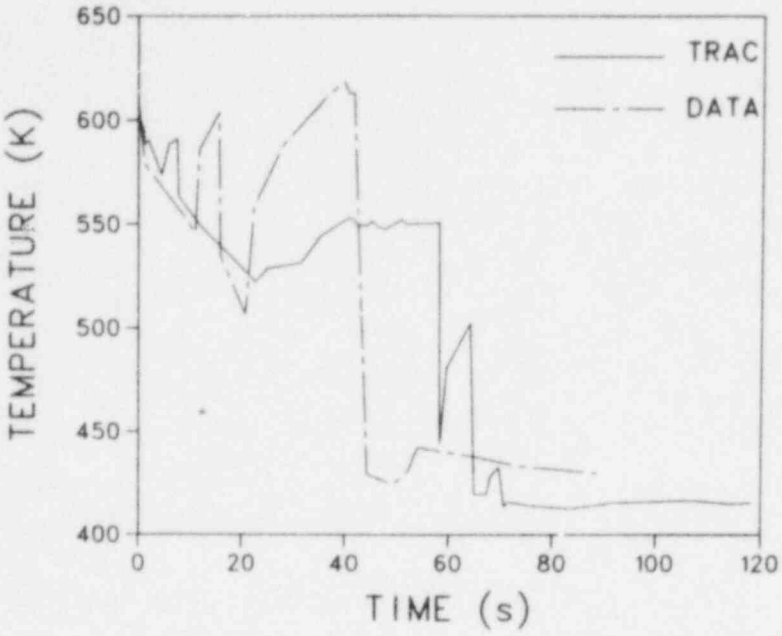

Fig. 68. LOFT test L2-3 cladding temperature, ring 2, core level 5 (TE-2H13-049). The data uncertainty is ~6 K.

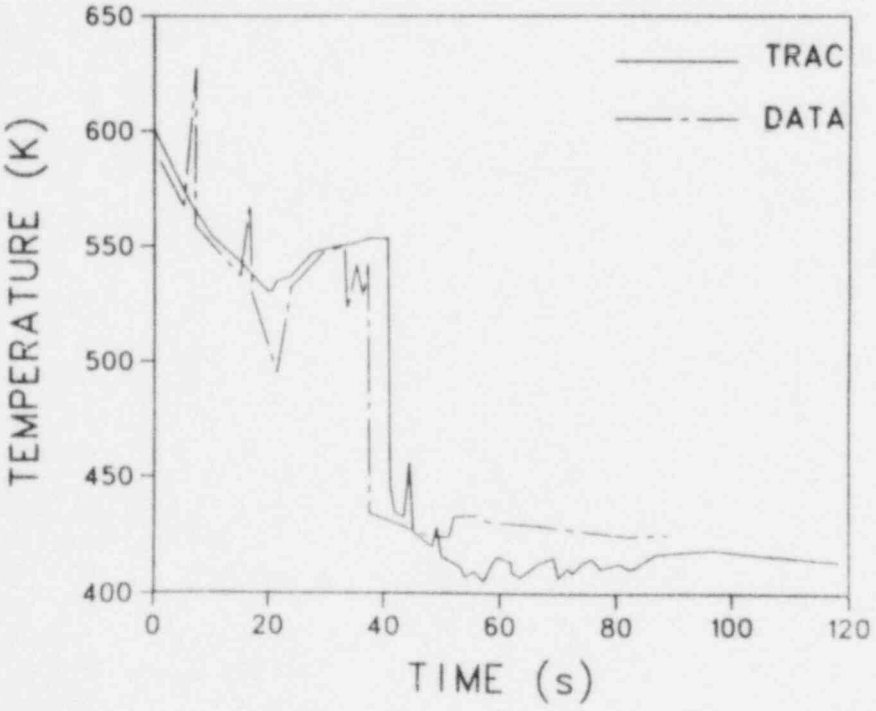

Fig. 69. LOFT test L2-3 cladding temperature, ring 3, core level 2 (TE-1F7-015). The data uncertainty is ~6 K.

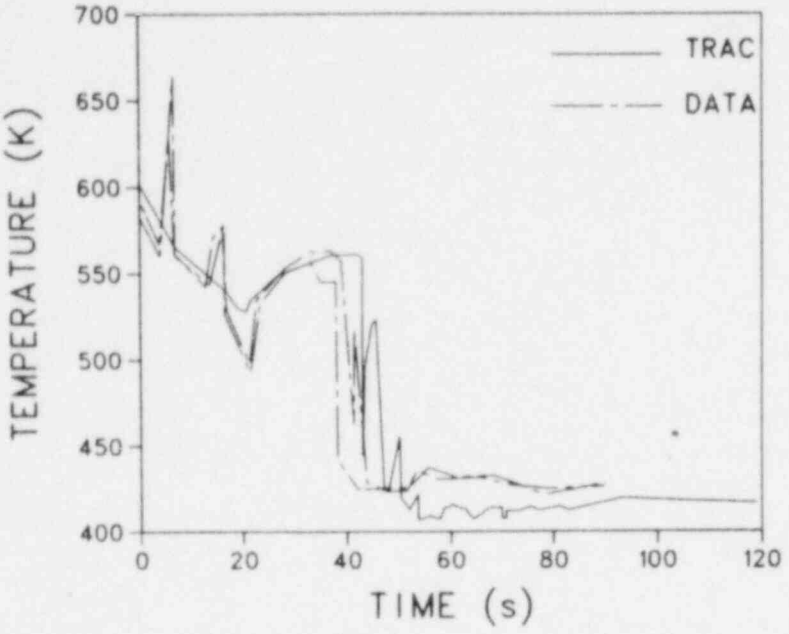

Fig. 70. LOFT test L2-3 cladding temperature, ring 3, core level 3 (TE-1F7-026 and TE-2H2-028). The data uncertainty is ~6 K.

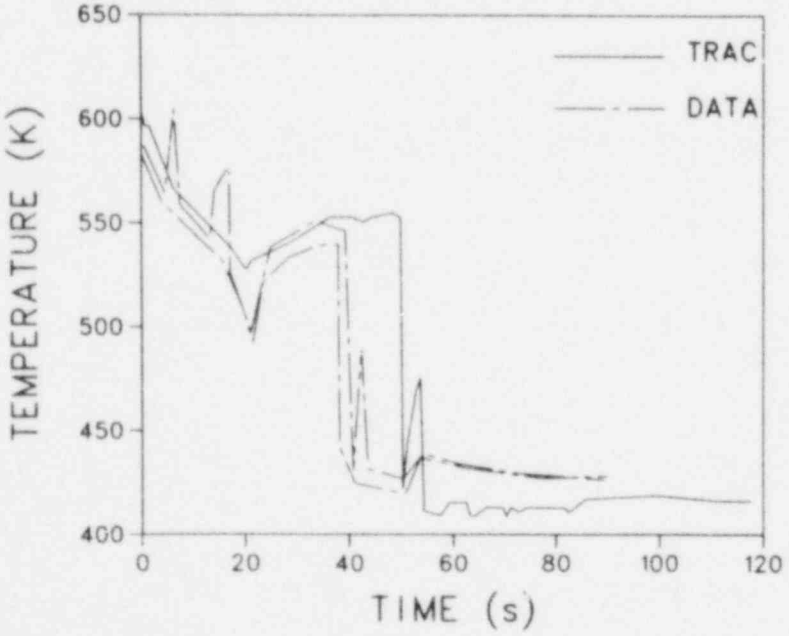

Fig. 71. LOFT test L2-3 cladding temperature, ring 3, core level 4 (TE-2H1-037 and TE-2I2-039). The data uncertainty is ~6 K.

cladding temperature had increased to the point that the cladding could not quench during the brief surge in core flow.

4. Conclusions and Observations

TRAC-P1A did predict very well the overall system thermal hydraulics. The only area in which the thermal-hydraulic calculation was unsatisfactory was the critical flow calculation in the broken cold legs when the upstream conditions were subcooled. Small errors in the flows in the broken legs could alter sufficiently the flows in the vessel to force unrealistic rewetting behavior or to prevent rewets from occurring. There was some evidence in the L2-3 cladding comparisons that the calculated rewetting behavior away from the central region of the core was more pronounced than in the data. The underpredictions of the broken-cold-leg flow for test L2-3 was probably responsible for the slight overprediction of the system pressure for that test.

The timing of the accumulator injections was predicted well, although in L2-3 the calculated delivery was 2 s late because of the pressure overprediction. The magnitude of the flows compared well with the data. Also, the code calculated the bypass and penetration consistent with the data. However, the code did not permit the ECC to back up in the intact cold leg as rapidly as did the test.

The cladding temperature comparisons were mixed. For L1-5 the code calculated an early dryout of the cladding, which might indicate that the code depleted the core liquid inventory more than the test, but the comparisons for tests L2-2 and L2-3 certainly did not indicate a low liquid inventory. The L2-2 cladding comparisons were the best of the three tests, with the code calculating the dryout/rewet behavior very well except at the high-powered region, where only the early dryout was calculated. The test L2-3 comparisons indicated that the rewet behavior was too pronounced and in certain cases measured dryouts were not predicted. In the high-powered region, the code only predicted the early dryout; which, together with the other comparisons, led to questions concerning how well the code was representing the core flows, the core liquid inventory, the stored energy in the fuel, and the heat-transfer correlations. The available data were insufficient to resolve (or even narrow) these questions. Relative to the stored energy in the fuel, the fuel in the high-powered region of the core should crack after several thermal cycles; this cracking would

result in degradation of both the fuel thermal conductivity and the fuel-rod gap. These fuel and gap changes should be modeled by the code. The LOFT Program should provide its best estimate of the fuel conditions before the test as a part of both the experiment specification and the data report.

Comparisons between the tests revealed that as the core power increased, the cold-leg break flow comparisons degraded. This degradation was caused by the larger subcooling in the broken cold leg resulting from the larger core temperature difference.

No other observations were made regarding the interrelationships of the three tests and the resulting comparisons that were clearly the result of differences in core power.

F. LOFT Small-Break LOCA Tests

After the Three Mile Island Unit 2 accident in March, 1979, the emphasis on LOCA testing shifted toward small-break testing. The LOFT Program responded to this change in emphasis very rapidly and in early summer ran the first small-break test (L3-0) at the LOFT facility. This test was initiated from isothermal conditions by lifting the power-operated relief valve (PORV). Subsequently, an entire small-break series of tests was planned and the second test of that series (L3-1) was conducted in November, 1979. This test was a single-ended cold-leg break. LASL produced blind pretest predictions for both of these small-break tests, although TRAC-PIA lacked specific modeling capabilities required for the small-break scenario.

1. Facility and Test Descriptions

Only minimal changes were made to the LOFT facility (see Sec. II.E.1). For test L3-0 the changes were limited to ensuring that the effluent from the PORV at the top of the pressurizer was properly directed into the pressure-suppresion tank. For test L3-1 a new break simulator with a break diameter of ~1.6 cm was installed into the break position in the broken-loop cold leg.

Test L3-0 was conducted from isothermal conditions (the residual decay heat in the core was ~4.2 kW). The PORV was opened, and the system was permitted to blow down. The pumps were tripped at time 0.0, and the quick-opening blowdown valves were opened at 2450 s to terminate the test.

Test L3-1 was conducted from full flow (480 kg/s) and full power (50 MW_t). Immediately before the test the reactor was scrammed to have the control rods fully inserted at time zero. The broken-loop cold-leg quick-opening blowdown valve was opened to simulate a single-ended cold-leg break. At the beginning of the transient the pumps were tripped and began to coast down; control actions also were taken to isolate the steam generator secondary. The ECC system (high- and low-pressure injections and the accumulator) operated in a normal fashion with normal set points.

2. TRAC-P1A Input Model Description

The input model description was based on the large-break input model (see Sec. II.E.2). Figure 72 shows the component schematic. The principal changes were that the vessel was more coarsely noded (8 axial levels, 2 rings, and 2 azimuthal segments for L3-0 and 9 axial levels, 2 rings, and 2 azimuthal segments for L3-1); also, the steam generator noding was simplified. For test L3-1 there were 24 components and a total of 124 hydraulic cells. For test L3-0 the pressurizer (component 8) was replaced by two pipe components and a break component to simulate the PORV flow. The input model for L3-0 contained 20 components and a total of 94 hydraulic cells.

3. Comparisons Between the Calculations and the Data

The comparisons for each test are discussed separately. For both tests the liquid inventory remained high throughout the parts of the transients that were analyzed and no cladding dryouts were calculated (or measured); the cladding temperatures followed saturation. For this reason cladding temperatures are not discussed.

3.1. LOFT Test L3-0 Data Comparisons

The system depressurization[24] is shown in Fig. 73. The drop in the data curve at 2450 s was the result of opening the quick-opening blowdown valves at that point; the analysis was terminated just before opening those valves. The pressure comparison was good through 800 s. After that time the code results and the data began to diverge. Figure 74, showing the calculated system initial mass, offered some insight to the problem. The system initial mass is a measure of how well the code conserves mass during the calculation; perfect mass conservation would result in a horizontal line. After 800 s the code began to gain mass; this was the same time frame in which the depressurization curves began to diverge. Basically, the mass error was probably responsible for the

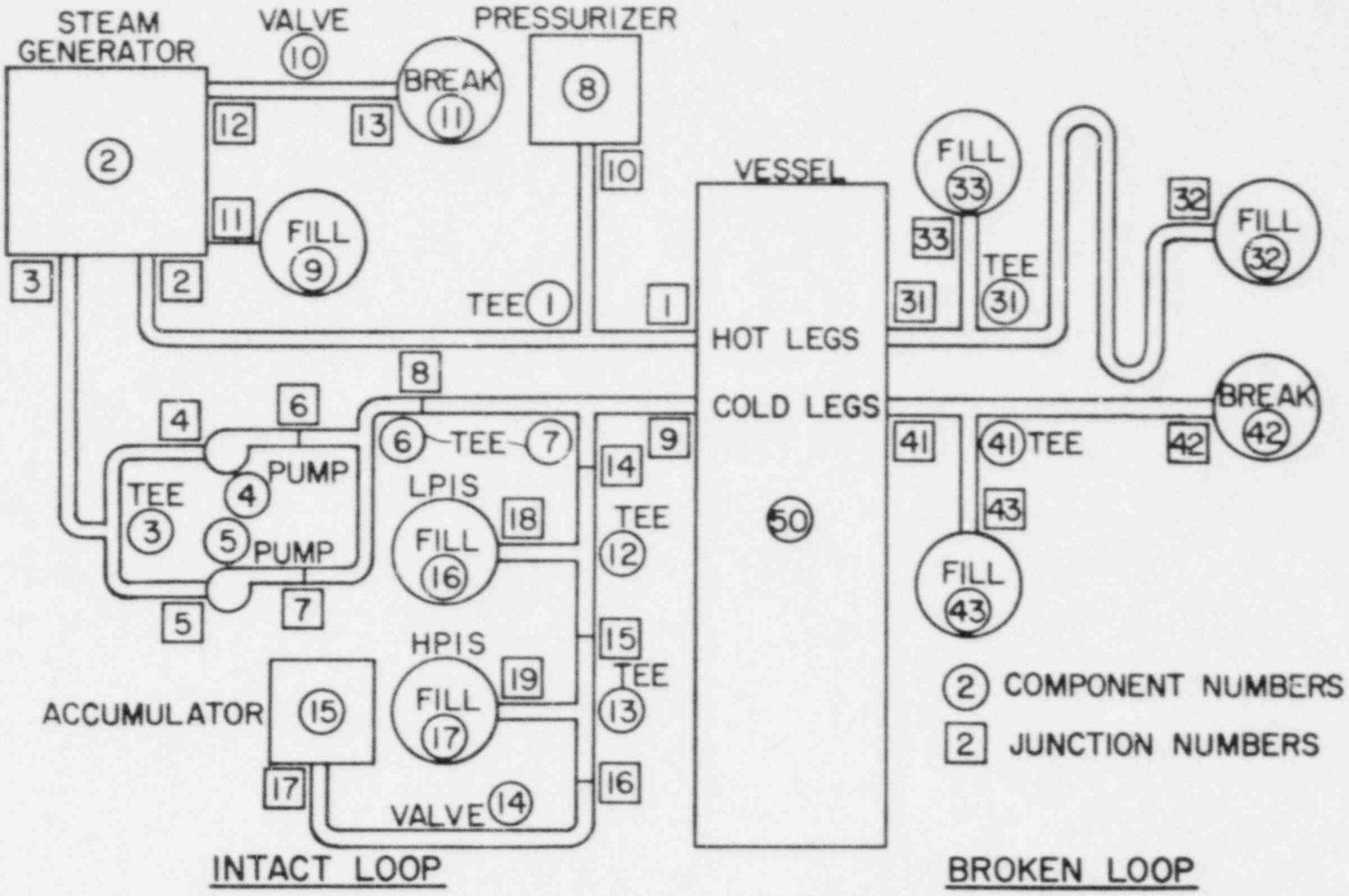

Fig. 72. LOFT small-break LOCA component schematic.

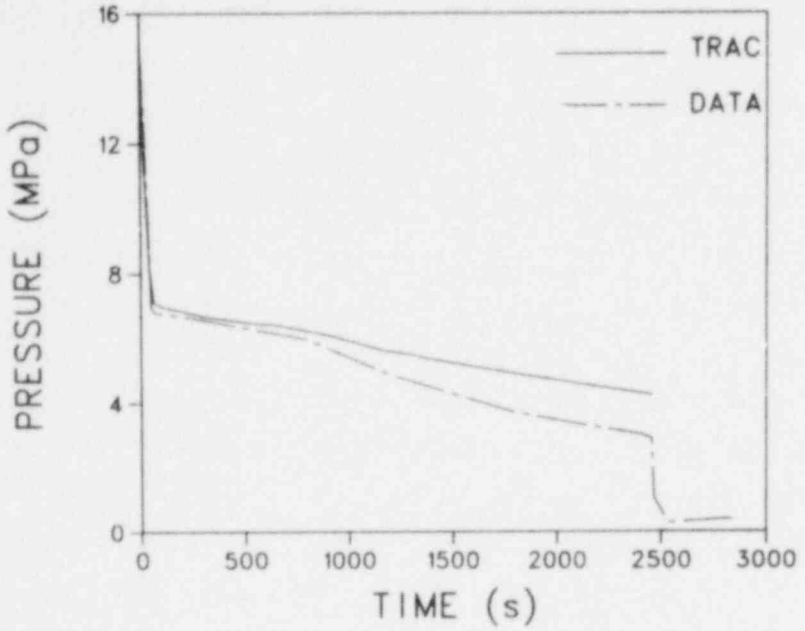

Fig. 73. LOFT test L3-0 system depressurization (PE-PC-004). The data uncertainty is ~250 kPa.

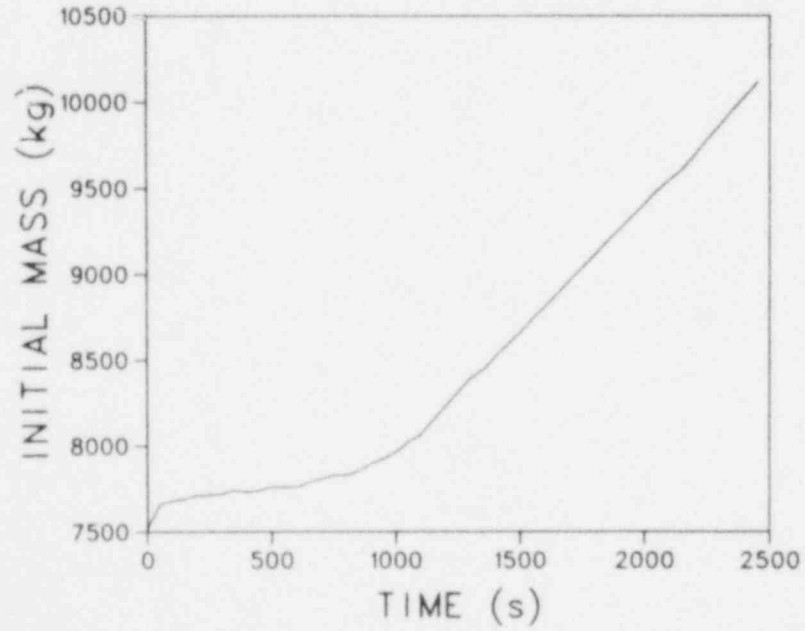

Fig. 74. LOFT test L3-0 system initial mass.

degradation in the depressurization comparison. The mass conservation errors will be resolved in TRAC-PD2. Primary system heat losses, which were not accounted for in the calculation, represent another possible cause of the degradation in the pressure comparison. All system temperature comparisons demonstrated the same characteristics as the depressurization comparison.
After the pumps slowed (~40 s), the system velocities (except through the pressurizer) were essentially zero. The mass flow through the pressurizer was critical to the calculation; the level swell in the pressurizer must be calculated correctly to obtain the correct flow. The depressurization comparisons during the initial 800 s of the transient indicated that the PORV flow was at least reasonable; however, a lack of flow data prevents comparison.

3.2. LOFT Test L3-1 Data Comparisons

The depressurization comparison for test L3-1[25] is shown in Fig. 75. The code overpredicted the pressure from the very beginning of the transient. The brief rise in the calculated pressure after 200 s was caused by the calculated natural circulation flow through the core becoming ineffective for removing

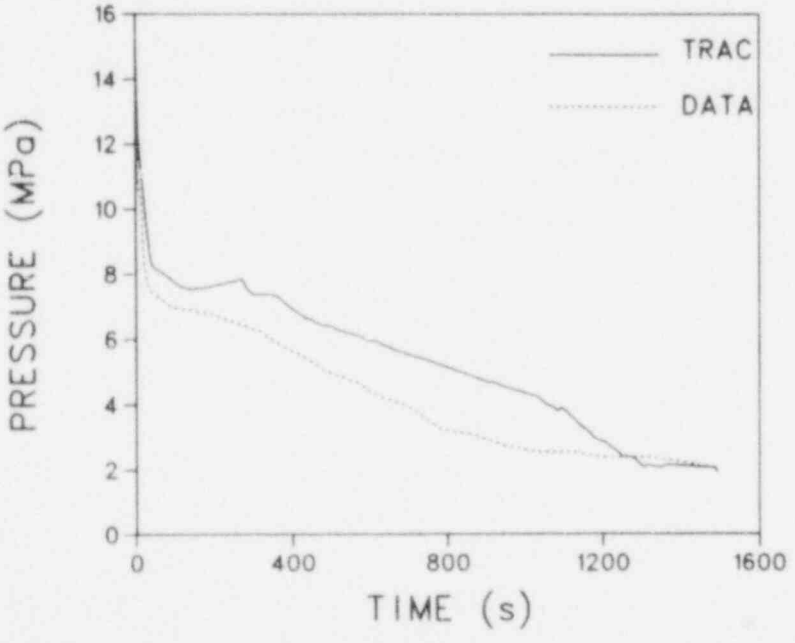

Fig. 75. LOFT test L3-1 intact-loop hot-leg pressure (PE-PC-002). The data uncertainty is ~250 kPa.

heat, which resulted in the core fluid heating. This pressure rise in the calculation was terminated when the loop seal (inlet piping to the intact-loop pumps) voided. However, the pressure rise was not apparent in the pressure data, and densitometers and differential pressure measurements in the loop seal indicated that the loop seal did not void. Therefore, we conclude that flow paths must exist, which were not modeled, to vent the vapor from the hot-leg side of the system to the break without requiring flow through the loop seal.

Figure 76 shows the flow at the break. The code substantially underpredicted the flow for the first 300 s. After that time the experimental system had saturated, and the flow was overpredicted because the system pressure was overpredicted. The initial underprediction was caused by the code calculating near-equilibrium conditions in the break nozzle (five hydraulic cells) when the upstream conditions were highly subcooled. The near-equilibrium conditions required the generation of vapor in the nozzle cells; the vapor caused a large decrease in the sonic velocity and, therefore, in the mass flow.

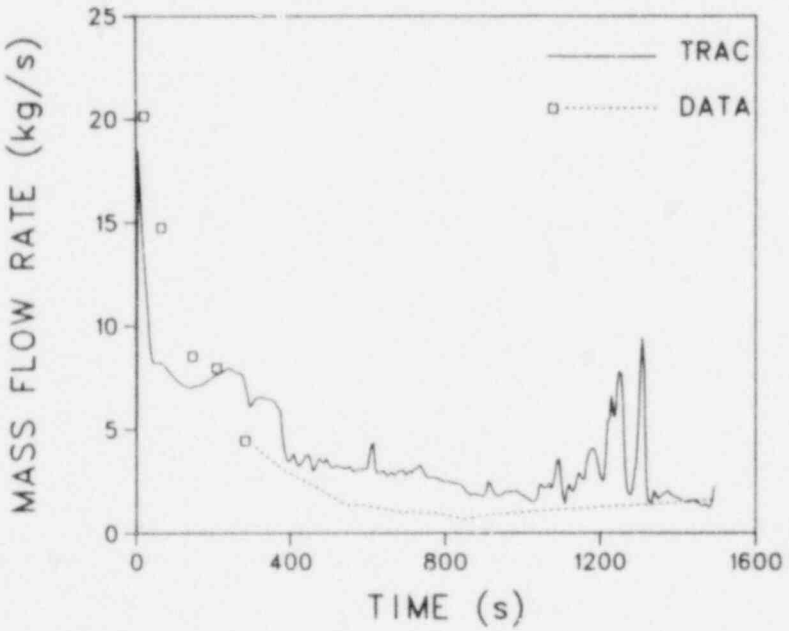

Fig. 76. LOFT test L3-1 broken-loop cold-leg flow (based on TTE-BL-1B and DE-BL-001B for the first 300 s; then based on level changes in the suppression tank). The data uncertainty is ~15%.

Figure 77 shows the results of a sensitivity calculation. The code was modified to prevent all vaporization in the break nozzle until the upstream void fraction was 0.005, at which point the usual constitutive relations in the code were invoked. A code error that permitted void fractions of 2-5% in highly subcooled conditions also was corrected. The figure shows the posttest results as a solid line and the pretest results as a chain dash line; the data are shown as discrete points. The comparison was much improved in the posttest analysis, although the calculation may have overpredicted the flow at 140 s. The transition to saturated critical flow (the normal mode in the code) was clearly too abrupt at a void fraction of 0.005. Figure 78 shows the effect of the code changes on the pressure comparisons. The pressure comparison was much improved during the initial 40 s in the posttest calculation. However, after 40 s, the posttest calculation was still overpredicting the data. Figure 79, the calculated system initial mass, indicated that the code was gaining appreciable mass during the entire transient, and this probably caused the pressure overprediction in the posttest calculation.

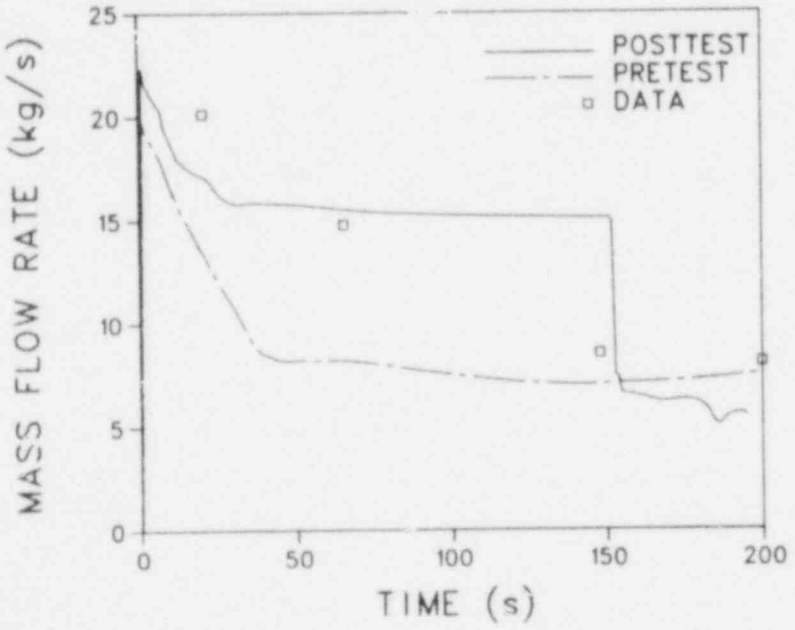

Fig. 77. LOFT test L3-1 short-term break flow (based on TTE-BL-1B and DE-BL-001B). The data uncertainty is ~15%.

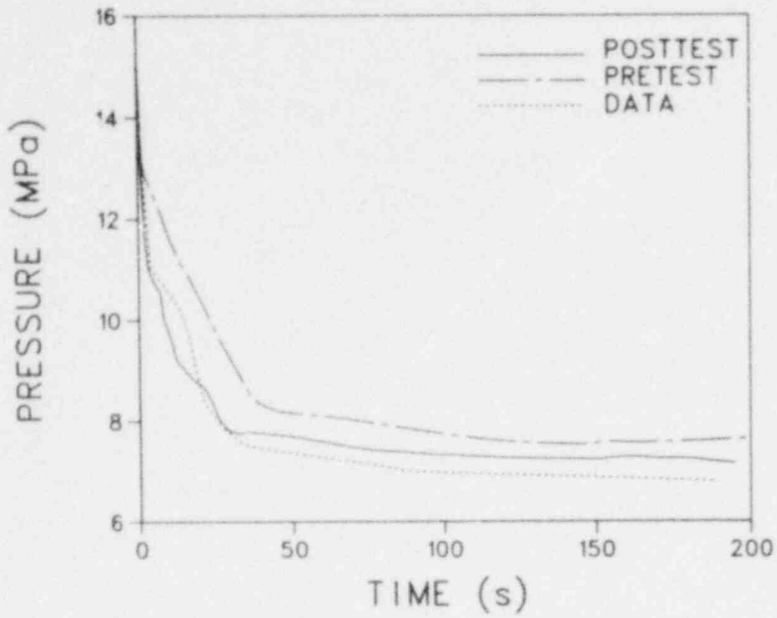

Fig. 78. LOFT test L3-1 short-term pressure comparison (PE-PC-001). The data uncertainty is ~250 kPa.

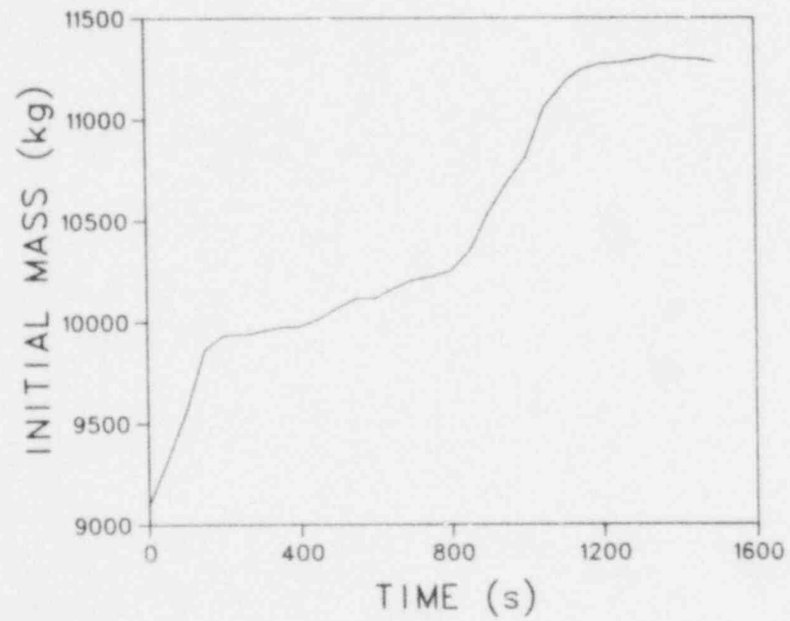

Fig. 79. LOFT test L3-1 calculated system initial mass.

4. Conclusions and Observations

Application of TRAC-P1A to small-break analyses emphasized certain problems in the code that were not that significant when the code was applied to large-break analysis. Mass conservation (or gaining mass) presented very real problems that are difficult to circumvent in long-term transients. For the TRAC-P1A code, the best approach to controlling mass conservation is to restrict the time-step size. The mass errors will be corrected in TRAC-PD2. The second problem for small-break applications was the critical flow calculations when the system conditions remained subcooled for extended periods. The approach here should be to renode the break coarsely (contrary to the large-break approach) with the fully implicit numerics and to force the first upstream interface to be a junction between components. Then, the flow may be adjusted using the additive friction (FRIC array) on input to yield flows that agree with some critical flow model. A critical flow model will be incorporated into TRAC-PF1. Other than these two problem areas, TRAC-P1A can predict the system behavior.

Another aspect of small-break analysis is that small bypass-flow paths (that may not be important for large-break analysis) must be represented.

III. SUMMARY AND CONCLUSIONS

The code calculated many things very well. The problems that have been described have stringently tested the predictive capability of the code. The code calculated mass flow for the large length-to-diameter ratio nozzles in Marviken very well. For the shorter nozzles where nonequilibrium effects were more important, the mass-flow comparisons were degraded because of the near-equilibrium calculation of the critical flow in TRAC-P1A. The critical flow problem also affected the LOFT L3-1 small-break comparisons, and was apparent in the L2-3 large-break comparisons, although the problem was not serious for that test. The problem solution requires improved constitutive relations that properly calculate liquid/vapor interactions when the fluid rapidly flows down a large pressure gradient (as in a nozzle). The alternative is to incorporate a critical flow model in the code.

The Battelle-Frankfurt comparisons indicated that the code can, when hydraulic losses are properly accounted for, calculate the pool level swell caused by depressurization. The comparisons for LOFT test L3-0 implied that the code calculated correctly the level swell in the pressurizer during the first 800 s of that transient, as the depressurization comparison was good.

The blowdown comparisons for Semiscale test S-07-6 and the large-break LOFT tests show that the code calculates the blowdown phases of the transients very well. In LOFT the refill phase of the transient also is calculated properly. In the Semiscale test, the refill calculation was poor because of an inability to calculate the flooding response of the pipe downcomer simulator (also demonstrated in the Dartmouth countercurrent flow comparisons) and the poor representation of the downcomer wall heat flux. This heat flux should be calculated directly by the code to maintain consistency with the fluid conditions in the downcomer. The wall heat flux calculation requires that a one-dimensional conduction calculation with multiple materials be incorporated in the code to represent the complex thermal structure of the downcomer pipe.

Finally, the LOFT and Semiscale comparisons demonstrate that additional information is necessary for the complete description of the facility and the data. In particular, minor flow paths need to be defined and the flows measured so that the information can be incorporated into the code input and the results assessed. In those cases where large heat fluxes from structural materials can

impact the calculation, sufficient instrumentation is needed to define the heat fluxes. For LOFT (and any other nuclear facility) it is important that the current state of the fuel rods be known so that the stored energy in the fuel can be properly accounted for and the appropriate conductivities used to remove the energy during the transient.

REFERENCES

1. "TRAC-P1A: An Advanced Best-Estimate Computer Program for PWR LOCA Analysis," Los Alamos Scientific Laboratory report NUREG/CR-0665, LA-7777-MS (May 1979).

2. J. C. Vigil and K. A. Williams, "TRAC-P1A Developmental Assessment," Los Alamos Scientific Laboratory report NUREG/CR-1059, LA-8056-MS (October 1979).

3. B. Holzer, T. Kanzleiter, and F. Steinhoff, "Specification of OECD Standard Problem No. 6: Determination of Water Level and Phase Separation Effects During the Initial Blowdown Phase," Battelle-Frankfurt, Frankfurt, FRG (February 1977).

4. L. Ericson, L. Gros d'Aillon, D. Hall, J. Ravnsborg, O. Sandervag, and H. Akesson, "The Marviken Full-Scale Critical Flow Tests Interim Report; Results from Test 1," Marviken report MX3-34 (March 1978).

5. L. Ericson, L. Gros d'Aillon, D. Hall, J. Ravnsborg, O. Sandervag, and H. Akesson, "The Marviken Full-Scale Critical Flow Tests Interim Report; Results from Test 2," Marviken report MX3-37 (April 1978).

6. L. Ericson, L. Gros d'Aillon, D. Hall, J. Ravnsborg, O. Sandervag, and H. Akesson, "The Marviken Full-Scale Critical Flow Tests Interim Report; Results from Test 4," Marviken report MX3-40 (May 1978).

7. L. Ericson, L. Gros d'Aillon, D. Hall, K. Kilpi, J. Ravnsborg, O. Sandervag, and J. Vidarsson, "The Marviken Full-Scale Critical Flow Tests Interim Report; Results from Test 7," Marviken report MX3-49 (August 1978).

8. L. Ericson, L. Gros d'Aillon, K. Kilpi, J. Ravnsborg, O. Sandervag, and J. Vidarsson, "The Marviken Full-Scale Critical Flow Tests Interim Report; Results from Test 13," Marviken report MX3-69 (December 1978).

9. L. Ericson, L. Gros d'Aillon, K. Kilpi, R. Schultz, O. Sandervag, and J. Vidarsson, "The Marviken Full-Scale Critical Flow Tests Interim Report; Results from Test 22," Marviken report MX3-87 (March 1979).

10. L. Ericson, L. Gros d'Aillon, K. Kilpi, O. Sandervag, R. Schultz, and J. Vidarsson, "The Marviken Full-Scale Critical Flow Tests Interim Report; Results from Test 24," Marviken interim report MX3-91 (May 1979).

11. "System Design Description for the Mod-3 Semiscale System," Idaho National Engineering Laboratory (July 1978).

12. V. Esparza, K. E. Sackett, and K. Stanger, "Experiment Data Report for Semiscale Mod-3 Integral Blowdown and Reflood Heat Transfer Test S-07-6 (Baseline Test Series)," EG&G Idaho report NUREG/CR-0467, TREE-1226 (January 1979).

13. J. M. Cozzuol, "Quick Look Report for Semiscale Mod-3 Test S-07-6 Baseline Test Series," EG&G Idaho report WR-S-78-020 (October 1978).

14. EG&G Idaho letter, D. J. Olson to R. E. Tiller, DJO-153-78, "Investigation of Downcomer Mass Depletion in Semiscale," (December 1978).

15. H. J. Richter and T. W. Lovell, "The Effect of Scale on Two-Phase Countercurrent Flow Flooding in Vertical Tubes," Final Report on Contract No. AT(49-24)-0329, Thayer School of Engineering, Dartmouth College (August 1978).

16. G. B. Wallis, One-Dimensional Two-Phase Flow, (McGraw-Hill, New York 1969).

17. M. M. Giles, "A TRAC Analysis of the INEL Air-Water Test Series," Idaho National Engineering Laboratory report RE-A-78-247 (October 1978).

18. C. W. Solbrig, J. H. McFadden, R. W. Lyczkowski, and E. D. Hughes, "Heat Transfer and Friction Correlations Required to Describe Steam-Water Behavior in Nuclear Safety Studies," AIChE Symposium Series, No. 174, 74, pp. 100-128 (1978).

19. K. A. Williams and D. R. Liles, "TRAC Calculations of ECC Bypass Phenomena in a 1/15-Scale Experimental Facility," Trans. Am. Nucl. Soc., 28, p. 391 (June 1978).

20. D. L. Reeder, "LOFT System and Test Description (5.5 Ft. Nuclear Core 1 LOCEs)," EG&G Idaho report NUREG/CR-0247, TREE-1208 (July 1978).

21. M. S. Jacoby, "Experiment Data Report for LOFT Nonnuclear Test L1-5 (Isothermal Test with Core 1 Installed)," EG&G Idaho report NUREG/CR-0265, TREE-NUREG-1215 (June 1978).

22. M. McCormick-Barger, "Experiment Data Report for LOFT Power Ascension Test L2-2," EG&G Idaho report NUREG/CR-0492, TREE-1322 (February 1979).

23. P. G. Prassinos, B. M. Galusha, and D. B. Engelman, "Experiment Data Report for LOFT Power Ascension Experiment L2-3," EG&G Idaho report NUREG/CR-0792, TREE-1326 (July 1979).

24. P. G. Prassinos, B. M. Galusha, and D. B. Jarrell, "Experiment Data Report for LOFT Nonnuclear Small-Break Experiment L3-0," EG&G Idaho report NUREG/CR-0959, TREE-1390 (August 1979).

25. P. D. Bayless, J. B. Marlow, and R. H. Averill, "Experiment Data Report for LOFT Nuclear Small-Break Experiment L3-1," EG&G Idaho report NUREG/CR-1145, EGG-2007 (January 1980).

DISTRIBUTION

	Copies
Nuclear Regulatory Commission, R4, Bethesda, Maryland	388
Technical Information Center, Oak Ridge, Tennessee	2
Los Alamos National Laboratory, Los Alamos, New Mexico	50
	440

☆ U.S. GOVERNMENT PRINTING OFFICE: 1981-0-777-022/3

Available from

GPO Sales Program
Division of Technical Information and Document Control
US Nuclear Regulatory Commission
Washington, DC 20555

and

National Technical Information Service
Springfield, VA 22161